

## **ABSTRACT - PROVENANCE OF KALAHARI SAND: PALEOWEATHERING AND RECYCLING IN A LINKED FLUVIAL-EOLIAN SYSTEM**

We here review what is known about the dunefields and fluvial systems of the Kalahari Basin in terms of geological setting and Quaternary dynamics and set out what has been hypothesized about the provenance of Kalahari sand so far. Previous work has tackled this problem by applying a limited number of techniques (mostly sediment textures and heavy minerals) to parts of the large dryland. The generally highly quartzose mineralogy of the dunes and their compositional variability have been only broadly evaluated and several sedimentological issues have thus remained controversial, including the relative role played by fluvial processes *versus* aeolian reworking of older sediments and weathering controls. This reveals a need for a systematic provenance study that considers the entire basin. For this reason, we here combine original petrographic, heavy-mineral, and detrital-zircon geochronology data with previously published clay-mineral, geochemical, and geochronological information in order to present the first comprehensive provenance study of the vast Kalahari sand sea.

Our multi-proxy dataset comprises 100 samples, collected across the Kalahari Basin from 11°S (NW Zambia) to 28°S (NW South Africa) and from 15°E (Angola) to 28°30'W (Zimbabwe). Kalahari dune sand mostly consists of monocrystalline quartz associated with durable heavy minerals and thus drastically differ from coastal dunefields of Namibia and Angola, which are notably richer in feldspar, lithic grains, and chemically labile clinopyroxene. The western Kalahari dunefield of southeastern Namibia is distinguished by its quartz-rich feldspatho-quartzose sand, indicating partly first-cycle provenance from the Damara Belt and Mesoproterozoic terranes. Within the basin, supply from Proterozoic outcrops is documented locally. Composition varies notably at the western and eastern edges of the sand sea, reflecting partly first-cycle fluvial supply from crystalline basements of Cambrian to Archean age in central Namibia and western Zimbabwe. Basaltic detritus from Jurassic Karoo lavas is dominant in dunes near Victoria Falls.

Bulk-sediment petrography and geochemistry of northern and central Kalahari sands, together with heavy-mineral and clay-mineral assemblages, indicate extensive recycling via aeolian and ephemeral-fluvial processes in arid climate of sediment strongly weathered during previous humid climatic stages in subequatorial Africa. Distilled homogenized dune sand composition thus reverberates the echo of paleo-weathering passed on to the present landscape through multiple episodes of fluvial and aeolian recycling.

Intracratonic sag basins such as the Kalahari contain vast amounts of quartz-rich polycyclic sand that may be tapped by coastal rivers aggressively eroding backwards during rejuvenation stages associated with rift propagation. Such an event may considerably increase the sediment flux to the ocean, fostering the progradation of river-fed continental-embankments, as documented by augmented accumulation rates coupled with upward increasing mineralogical durability in the post-Tortonian subsurface succession of the Zambezi Delta.

# Provenance of Kalahari Sand: Paleoweathering and recycling in a linked fluvial-aeolian system

Eduardo Garzanti<sup>1\*</sup>, Guido Pastore<sup>1</sup>, Abi Stone<sup>2</sup>, Shlomy Vainer<sup>3</sup>, Pieter Vermeesch<sup>4</sup>,  
Alberto Resentini<sup>1</sup>

<sup>1</sup> *Laboratory for Provenance Studies, Department of Earth and Environmental Sciences, University of Milano-Bicocca, 20126 Milano, Italy*

<sup>2</sup> *Department of Geography, The University of Manchester, M13 9PL, United Kingdom*

<sup>3</sup> *Institute of Earth Surface Dynamics, University of Lausanne, 1015 Lausanne, Switzerland*

<sup>4</sup> *London Geochronology Centre, Department of Earth Sciences, University College London, London, WC1E 6BT, UK*

Email: [eduardo.garzanti@unimib.it](mailto:eduardo.garzanti@unimib.it) (Garzanti), [g.pastore2@campus.unimib.it](mailto:g.pastore2@campus.unimib.it) (Pastore),  
[abi.stone@manchester.ac.uk](mailto:abi.stone@manchester.ac.uk) (Stone), [shlomy.vainer@mail.huji.ac.il](mailto:shlomy.vainer@mail.huji.ac.il) (Vainer),  
[p.vermeesch@ucl.ac.uk](mailto:p.vermeesch@ucl.ac.uk) (Vermeesch), [alberto.resentini@unimib.it](mailto:alberto.resentini@unimib.it) (Resentini),

\* Corresponding author

*Keywords:* Kalahari Basin; Sand petrography; Heavy minerals; Detrital-zircon geochronology; Dryland landscape evolution; Drainage changes; Dynamic topography; Sediment-routing connectivity; Southern Africa.

1  
2  
3  
4  
5  
6  
7  
8  
9  
10  
11  
12  
13  
14  
15  
16  
17  
18  
19  
20  
21  
22  
23  
24  
25  
26  
27  
28  
**ABSTRACT.** We here review what is known about the dunefields and fluvial systems of the  
Kalahari Basin in terms of geological setting and Quaternary dynamics and set out what has been  
hypothesized about the provenance of Kalahari sand so far. Previous work has tackled this problem  
by applying a limited number of techniques (mostly sediment textures and heavy minerals) to parts  
of the large dryland. The generally highly quartzose mineralogy of the dunes and their  
compositional variability have been only broadly evaluated and several sedimentological issues  
have thus remained controversial, including the relative role played by fluvial processes *versus*  
aeolian reworking of older sediments and weathering controls. This reveals a need for a systematic  
provenance study that considers the entire basin. For this reason, we here combine original  
petrographic, heavy-mineral, and detrital-zircon geochronology data with previously published  
clay-mineral, geochemical, and geochronological information in order to present the first  
comprehensive provenance study of the vast Kalahari sand sea.

29  
30  
31  
32  
33  
Our multi-proxy dataset comprises 100 samples, collected across the Kalahari Basin from 11°S  
(NW Zambia) to 28°S (NW South Africa) and from 15°E (Angola) to 28°30'W (Zimbabwe).

34  
35  
36  
37  
38  
39  
40  
41  
42  
43  
44  
45  
46  
47  
48  
49  
50  
51  
52  
53  
Kalahari dune sand mostly consists of monocrystalline quartz associated with durable heavy  
minerals and thus drastically differ from coastal dunefields of Namibia and Angola, which are  
notably richer in feldspar, lithic grains, and chemically labile clinopyroxene. The western Kalahari  
dunefield of southeastern Namibia is distinguished by its quartz-rich feldspatho-quartzose sand,  
indicating partly first-cycle provenance from the Damara Belt and Mesoproterozoic terranes. Within  
the basin, supply from Proterozoic outcrops is documented locally. Composition varies notably at  
the western and eastern edges of the sand sea, reflecting partly first-cycle fluvial supply from  
crystalline basements of Cambrian to Archean age in central Namibia and western Zimbabwe.  
Basaltic detritus from Jurassic Karoo lavas is dominant in dunes near Victoria Falls.

54  
55  
56  
57  
58  
59  
60  
61  
62  
63  
64  
65  
Bulk-sediment petrography and geochemistry of northern and central Kalahari sands, together with  
heavy-mineral and clay-mineral assemblages, indicate extensive recycling via aeolian and  
ephemeral-fluvial processes in arid climate of sediment strongly weathered during previous humid

1 climatic stages in subequatorial Africa. Distilled homogenized dune sand composition thus  
2 reverberates the echo of paleo-weathering passed on to the present landscape through multiple  
3  
4 episodes of fluvial and aeolian recycling.  
5  
6

7 Intracratonic sag basins such as the Kalahari contain vast amounts of quartz-rich polycyclic sand  
8  
9 that may be tapped by coastal rivers aggressively eroding backwards during rejuvenation stages  
10  
11 associated with rift propagation. Such an event may considerably increase the sediment flux to the  
12  
13 ocean, fostering the progradation of river-fed continental-embankments, as documented by  
14  
15 augmented accumulation rates coupled with upward increasing mineralogical durability in the post-  
16  
17 Tortonian subsurface succession of the Zambezi Delta.  
18  
19  
20  
21  
22  
23  
24  
25  
26  
27  
28  
29  
30  
31  
32  
33  
34  
35  
36  
37  
38  
39  
40  
41  
42  
43  
44  
45  
46  
47  
48  
49  
50  
51  
52  
53  
54  
55  
56  
57  
58  
59  
60  
61  
62  
63  
64  
65

*The Central Kalahari is not a true desert. It has none of the naked, shifting sand dunes that typify the Sahara and other great deserts of the world. In some years the rains may exceed twenty — once even forty — inches, awakening a magic green paradise.”*

Mark Owens, Cry of the Kalahari

## 1. Introduction

The intracratonic Kalahari sag basin hosts several dunefields that, largely inactive at present, represent the largest sand sea on Earth. The compositional signatures of such a vast expanse of aeolian sand and their provenance have not been systematically studied so far, and yet encrypted in them lies a bounty of information on the geological, geomorphological, and environmental history of the region. Formed as a consequence of the multistep break-up of Gondwana, the Kalahari Basin presently occupies the core of southern Africa, which experienced dynamic uplift in the Cenozoic and is currently cut across by the southwestward-propagating East African rift system (Haddon and McCarthy, 2005; De Wit, 2007). Complex landscape evolution during the Pleistocene and Holocene was punctuated by a high-frequency alternation of arid and humid climatic stages and consequent repeated changes in hydrology, drainage patterns, and interaction of fluvial and aeolian processes (Burrough et al., 2009a; Moore et al., 2012; Matmon et al., 2015). Decrypting the Kalahari sedimentary archive is an essential step to improve our understanding not only of the evolution of tropical southern Africa but also of the interplay between tectonic and climatic forces that mould the Earth’s surface. Clarifying the control exerted by key climate variables on arid landscapes can, in turn, help test the robustness of numerical models simulating dunefield dynamics and improve model simulations that are used to predict the impact of future climate change on dune remobilisation (e.g., Thomas et al., 2005; Mayaud et al., 2007).

This article first considers what is known about the Kalahari Basin and its hydrological systems and dunefields, including an overview of their Quaternary history. The geology of the region is then outlined in the wider context of southern Africa, before reviewing what was currently known about the provenance of the dunefields and potential fluvial feeder systems. To date, much of the

24 information on provenance has been inferred from likely palaeowind directions (e.g. [Thomas, 1987](#))  
1  
25 or by applying a limited number of techniques (mostly sediment textures and heavy minerals) to  
3  
26 some parts of this vast basin. Several sedimentological issues have thus remained controversial,  
4  
6 including the relative role played by fluvial processes *versus* aeolian reworking and the origin of  
7  
8 weathering. Quantitative petrographic data were obtained only on a few dune sands in the north and  
9  
10  
11  
12  
13 west, and detrital-zircon ages only on fluvial sands in the north ([Gärtner et al., 2014](#); [Garzanti et al.,](#)  
14  
15  
16 [2014a](#)).

17  
18 For this reason, we collate new results from bulk-petrography, heavy-mineral, and detrital-zircon  
19  
20  
21  
22  
23 U–Pb geochronology analyses on 100 aeolian-dune and river sand samples collected across 17  
24  
25  
26  
27  
28 degrees of latitude from Zambia to South Africa and 13 degrees of longitude from Angola to  
29  
30  
31  
32  
33 Zimbabwe. A set of statistical techniques was applied to this multi-proxy dataset to adequately  
34  
35  
36  
37  
38 illustrate the compositional variability of aeolian sand across the Kalahari Basin, reveal meaningful  
39  
40  
41  
42  
43 mineralogical patterns, identify the original sediment sources, and gain insight on sand dispersal  
44  
45  
46  
47  
48 pathways. In particular, this paper investigates signs for inheritance from past climatic conditions,  
49  
50  
51  
52  
53 buffering of environmental signals through linked fluvial and aeolian systems, and progressive  
54  
55  
56  
57  
58 compositional homogenization and concentration of most durable minerals acquired through  
59  
60  
61  
62  
63 multiple cycles of erosion, transport, deposition, and diagenesis. The new provenance data are  
64  
65  
66  
67  
68 integrated and reviewed in terms of what is known about fluvial-aeolian interactions,  
69  
70  
71  
72  
73 palaeoweathering, and drainage evolution in the Kalahari. Understanding the complexities of  
74  
75  
76  
77  
78 sediment transport systems, and particularly how sediment-routing connectivity regulates the  
79  
80  
81  
82  
83 transmission of environmental signals from source areas to depositional sinks over spatial and  
84  
85  
86  
87  
88 temporal scales, is essential for a realistic interpretation of the stratigraphic record ([Romans et al.,](#)  
89  
90  
91  
92  
93 [2016](#); [Allen, 2017](#); [Caracciolo, 2020](#)).

## 2. The Kalahari Basin

50 The intracratonic Kalahari sag basin comprises the largest continuous sand sea on Earth, which  
 1 extends for over  $2.5 \cdot 10^6$  km<sup>2</sup> (Fig. 1). The interior of the Kalahari is an elevated plateau with flat  
 251 topography (average altitude 1200 m), delimited by relatively steep escarpments down to the  
 3 Atlantic Ocean in the west and to the Indian Ocean in the east. Kalahari Group sediments, including  
 452 basal gravel and conglomerate, sandstone with calcrete, and unconsolidated sand stretch north from  
 6 the Orange River in South Africa (~29°S) to the Democratic Republic of Congo (~6°S; Haddon and  
 753 McCarthy, 2005).

154 The landscape across the Kalahari is varied, encompassing spatially discrete dunefields dominated  
 11 by linear dunes, the Okavango alluvial fan (delta) and wetlands in northern Botswana, and aligned  
 155 drainage and pans (Lancaster, 1981; Thomas and Shaw, 1991; Shaw and Goudie, 2002; Goudie and  
 13 Viles, 2015). The erg is traversed by rivers that were initially mostly endorheic but were  
 14 progressively captured from both sides by rivers eroding headwards from the coast (e.g., Moore and  
 155 Larkin, 2001). Development of endorheic drainage and expansion of a landlocked sand sea in this  
 16 arid tropical region was favored by multiple phases of tectonic activity in bordering areas since the  
 17 Mesozoic, promoted by asthenosphere upwelling during the rifting stage and maintained during the  
 18 passive-margin stage by flexuring associated with sediment loading of the continental terrace, or  
 19 rejuvenated by isostatic processes or buoyancy forces in the mantle (Moucha and Forte, 2011;  
 20 Blenkinsop and Moore, 2013).

### 2.1. Climate

459 Climate in southern Africa results from the disturbance by a great land mass of quasi-stationary  
 46 anticyclones over the Atlantic and Indian Oceans, corresponding to the descending limb of the  
 47 Hadley Cell (Schulze, 1972). A major influence is exerted by the Intertropical Convergence Zone  
 481 and associated Tropical Rain Belt (Nikulin and Hewitson, 2019), by the Congo Air Boundary, and  
 49 by temperate frontal systems within the southern hemisphere westerlies in the west and south. The  
 50 Indian Ocean is a major source of water vapor for the subcontinent via easterly winds (Fig. 2A), and



77 climatic changes within southern Africa have been linked to the variability of Indian Ocean surface  
 1 temperature (Partridge, 1993; Tyson and Preston-Whyte, 2000; Washington and Preston, 2006;  
 278 3 Vigaud et al, 2009). The South Indian Convergence Zone may extend its influence to the  
 4 579 6 subcontinent via synoptic systems known as Tropical Temperate Troughs, which connect the mid-  
 780 8 latitudes to the tropics (Cook, 2000; Todd et al., 2002).

9 81 Oceanic currents also affect climate in the continental interiors (Walker, 1990). The warm Agulhas  
 10 11 1282 13 current flows southward along the coast of Mozambique, allowing humid air masses to enter the  
 14 1583 16 continent from the Indian Ocean, thus causing heavy rains onto orographic barriers (e.g.  
 1784 18 Drakensberg Mountains of Lesotho) and a marked westward decrease in precipitation across  
 19 2085 21 southern Africa (Reason, 2001) (Fig. 2B, 2C). The Agulhas current is retro-deflected at 16-20°E  
 2286 23 longitude when encountering the cold Benguela current (Lutjeharms and Van Ballegooyen, 1988),  
 2487 25 which displaces Antarctic water along the Atlantic coast of South Africa, Namibia, and southern  
 26 2788 28 Angola, causing low sea-surface temperatures, low humidity of southerly winds, and very little rain  
 2989 30 through the year (Rogers and Bremner, 1991).

31 3290 33 Rainfall occurs mainly during winter in the southwestern corner of the continent and during summer  
 3491 35 in the rest of the region. The aridity center is situated in southern Botswana and climate becomes  
 3692 37 sub-humid and less seasonal northward, annual rainfall increasing from 150 mm in the southwest to  
 38 3993 40 4194 42 400 mm in Zimbabwe.

43 4495 45 The wind regime in the Kalahari is more complex than expected in areas of linear dune  
 4696 47 development (Fig. 2A), being influenced by the seasonal fluctuation of the high-pressure cells  
 48 4997 50 (Tyson and Preston-Whyte, 2000). The dry winter season is characterized by southeasterly winds  
 5198 52 associated with the South Atlantic anticyclone (Bultot and Griffith, 1972). In the summer, winds  
 53 5499 55 blow mainly from the north in the eastern Kalahari and from the west in the western Kalahari  
 5600 57 (Nicholson, 1996). The southwestern Kalahari is dominated by southwesterly winds (Wiggs et al.  
 58 5901 60 1996).

## 61 62 63 64 65 2.2. Hydrology

104  
105  
2  
3  
106  
4  
5  
107  
6  
7  
108  
8  
9  
10  
109  
11  
12  
13  
110  
14  
15  
16  
111  
17  
18  
19  
20  
21  
22  
23  
24  
25  
26  
27  
28  
29  
30  
31  
32  
33  
34  
35  
36  
37  
38  
39  
40  
41  
42  
43  
44  
45  
46  
47  
48  
49  
50  
51  
52  
53  
54  
55  
56  
57  
58  
59  
60  
61  
62  
63  
64  
65

Three major rivers flow from humid Angola and western Zambia across the northern Kalahari: the Cunene, the Okavango, and the Zambezi (Fig. 1). The Cunene, sourced in Angolan highlands uplifted recently in the Plio-Quaternary (Klöcking et al., 2020; Vainer et al., 2021), runs along the westernmost edge of the sand sea drained by the Caculuvar and Mucope tributaries (Fig. 1A; Shaw and Goudie, 2002). Once endorheic and emptying into what is today Etosha Pan (Miller et al., 2010), the Cunene was captured by a headward eroding coastal stream and its youthful terminal tract now debouches into the Atlantic Ocean (Goudie and Viles, 2015 p.14-15).

The Okavango is the main endorheic river of the Kalahari. Fed from humid Angola, where the southward migration of the Congo Air Boundary brings heavy rains between December and March (annual rainfall  $\leq 1400$  mm), the flood wave takes until August to filter through the anastomosing channels and swamps of the Okavango, the largest wetland in southern Africa and the largest inland delta on Earth (McCarthy and Ellery, 1998). Sedimentation of fine sand dominates the upper delta, whereas chemical sedimentation in the form of calcrete and silcrete prevails in the lower delta (McCarthy and Metcalfe, 1990). Finally reunited in the Boteti River, the drastically reduced flood waters traverse another stretch of the Kalahari, ending endorheically in the Makgadikgadi Pan. The main source of water for the pan is the ephemeral Nata River, sourced in Zimbabwe to the east.

The Zambezi and its major Cuando tributary (named Kwando, Linyanti, and next Chobe after entering the Okavango Graben in the Caprivi strip) also flow across the northern Kalahari. Downstream of Victoria Falls, the Zambezi plunges into deep gorges carved in Karoo basalt, heading towards the Indian Ocean (Moore et al., 2007). The Gwai River drains the eastern edge of the sand sea in Zimbabwe, along with its tributaries once directed westwards toward the central Kalahari (Thomas and Shaw, 1988).

In Namibia, three ephemeral rivers draining into the Kalahari flow only in case of exceptionally heavy and continuous precipitation. The Omatako in the north is an Okavango tributary, the Rietfontein dries up in central Botswana as a former tributary of the fossil Okwa River (Fig. 2A), and the Nossob in the south joins the Molopo River. The occasional floods in the Nossob and

131 Molopo are absorbed along the way and recharge groundwater aquifers with water losses up to 90%  
 132 and 80%, respectively (van Veelen et al., 2009). The flow of the Nossob and Auob (its major  
 133 western tributary) typically ceases between 24°S and 25°S, respectively, and the Molopo seldom  
 134 flows west of 23°40'E (Nash, 2015). Extreme events with continuous river flow have a return  
 135 period of between 20 and 50 years (Nash and Endfield, 2002), when the Molopo may reach the  
 136 Orange River thus becoming exorheic. The Kuruman, the major Molopo tributary in South Africa, is  
 137 also dry except for flash floods, but has permanent flow over its first 10 km owing to its famous  
 138 dolomite spring source (*Die Oog*, the 'Eye of the Kalahari'), which has yielded a constant ~750  
 139 m<sup>3</sup>/hour flux during the last two centuries at least (Shaw et al., 1992).

140 The southern and western Kalahari rivers are misfit streams within wider, flat-bottomed channels  
 141 reaching 0.5 to 1.8 km in width (Bullard and Nash, 2000). They contain gorge-like sections with  
 142 varying steepness (typical incision depth ~25 m) and support groundwater processes (sapping and  
 143 deep weathering; Shaw and deVries, 1988; Bullard and Nash, 1998; Stone, 2021a).

144 Pans (endorheic basins that temporarily host water and deposit mostly salt and clay) are widespread  
 145 in the Kalahari, found in depressed areas where an integrated fluvial system is lacking and surface  
 146 geology is suitable (soluble duricrusts or regions with deflatable loose silt and sand). They occur in  
 147 many interdune corridors of the linear dunefields and in higher concentration along the western  
 148 watershed of the southern dunefield (Goudie and Thomas, 1985; Lancaster, 1986; Lancaster, 1978).

### 149 2.3. *Dunefields*

150 The five dunefields identified in the Kalahari Basin (NWK, northwestern; NEK, northeastern; EK,  
 151 eastern; WK, western; SK southern; Fig. 2A) are all dominated by linear dunes (Thomas and Shaw,  
 152 1991; Shaw and Goudie, 2002). Other morphologies include topographically-constrained dunes  
 153 occurring at hill and mountain fronts (Tyson, 1999) and lunette dunes fringing the widespread pans  
 154 (Telfer and Thomas, 2006; Hürkamp et al., 2011). There are also areas with sand sheets (e.g., south-  
 155 western Kalahari; Bateman et al., 2003) and areas of degraded dune patterns resembling barchanoid

158 ridges on the eastern edge of the western Kalahari near the Botswana/Namibia border ([McFarlane et](#)  
1  
159 [al., 2005](#); [Stone, 2021a](#)).

160 Kalahari dunefields may have started to accumulate in the early Pleistocene ([Partridge, 1993](#);  
2  
161 [Miller, 2014](#); [Vainer et al., 2018a](#)). In the western Kalahari, dunes superimposed over a megafan are  
3  
162 inferred to be younger than the 4-Ma-old fossils that lie below the sand ([Miller, 2008](#); [Miller et al.,](#)  
4  
163 [2010](#)), whereas dunes in the east lie below Middle Stone Age artifacts, constraining the youngest  
5  
164 possible age for sand deposition ([McFarlane and Segadika, 2001](#)). In the southern Kalahari, [Vainer](#)  
6  
165 [et al. \(2018a\)](#) simulated a range of scenarios of sand exposure and burial based on cosmogenic  
7  
166 nuclides and luminescence constrains and suggested there may have been 22 overturning cycles  
8  
167 since sand was available for aeolian distribution, at 1.5-2.2 Ma and/or 4.2-5.2 Ma (in agreement  
9  
168 with [Miller, 2014](#)).

169 Reworking of the initially produced sand occurred throughout the Quaternary, and burial ages for  
10  
170 the most recent of any dune recycling and accumulation episodes are determined by luminescence  
11  
171 dating (see compilation spanning ~190 ka for the INQUA Dune Atlas by [Thomas and Burrough,](#)  
12  
172 [2016](#)). Finite luminescence ages for basal sediments of linear dunes range from  $1.1\pm 0.1$  ka to  $104\pm 8$   
13  
173 ka (including samples in saturation, i.e. at the upper limit of the dating technique, which can be  
14  
174 extended if integrated with cosmogenic-nuclide dating; [Vainer and Ben Dor, 2021](#)).

175 Today, precipitation levels, vegetation cover, and insufficient wind energy hamper aeolian activity  
15  
176 even in the driest area of the erg, excepting some blowing sand on dune crests in the western and  
16  
177 southern Kalahari ([Wiggs et al., 1995](#); [Bhattachan et al., 2013](#)). The cover of grasses and savannah  
17  
178 bush increases on a broad north-south gradient, with increasing concentrations of woodland north of  
18  
179 ~21°S ([Van Rensburg, 1971](#); [Thomas and Shaw, 1991](#)). Therefore, Kalahari dunes are currently  
19  
180 largely inactive, sometimes pedogenically modified and in places extensively degraded, with a  
20  
181 higher proportion of silt and clay than normally found in active dune fields ([Thomas, 1984](#); [Wiggs](#)  
21  
182 [et al. 1995](#); [McFarlane et al., 2005](#)). The extent of this alteration by slope and locally tectonic  
22  
183 processes ([McFarlane and Eckardt, 2007](#)) increases northwards and eastwards as the woodland  
23  
24  
25  
26  
27  
28  
29  
30  
31  
32  
33  
34  
35  
36  
37  
38  
39  
40  
41  
42  
43  
44  
45  
46  
47  
48  
49  
50  
51  
52  
53  
54  
55  
56  
57  
58  
59  
60  
61  
62  
63  
64  
65

184 vegetation cover increases, and in western Zambia eroded dune crests largely stabilized by  
 1  
 185 vegetation may rise only ~5 m from the vegetated interdunes (O'Connor and Thomas, 1999).  
 3  
 4  
 186 The trend of linear dunes changes from ESE/WNW to E/W and then to ENE/WSW from west to  
 6  
 187 east in the northern Kalahari (NWK, NEK, and EK), it is NE/SW south of Makgadikgadi and  
 8  
 188 NW/SE to NNW/SSE in the southern Kalahari (WK and SK). These patterns have been ascribed to  
 10  
 189 wind circulation around, and shifts in the position of, the southern African anticyclone (Lancaster,  
 13  
 190 1979, 1981; Thomas, 1984). However, the accompanying idea that there were discrete periods of  
 15  
 191 formation for each dunefield has been overturned by the large number of compiled luminescence  
 18  
 192 ages, indicating multiple accumulation phases in each region over the last ~190 ka.  
 20  
 193 Five different classes of linear dunes are identified in the southern Kalahari (WK, SK; Bullard et al.,  
 23  
 194 1995; Bullard and Nash, 1998): 1) simple and discontinuous; 2) simple and continuous; 3)  
 25  
 195 compound with common Y-junction branches; 4) compound with more-obtuse angles between  
 27  
 196 branches; and, 5) no preferred orientation and discontinuous. The tallest and most closely spaced  
 30  
 197 dunes are found in the southeast of this region, as shown by detailed morphometric analysis using  
 32  
 198 ASTER global digital-elevation-model data (White et al., 2015). This violates the often-reported  
 35  
 199 relationship of bigger dunes with wider spacing, suggesting that these dunes have experienced a  
 37  
 200 reduction in sediment supply through time and/or post-depositional modification (Kiss et al., 2009;  
 40  
 201 White et al., 2015).

#### 202 203 2.4. Duricrusts

204  
 205 Duricrusts that act as cement and stabilize sand's potential movement are widespread below, within,  
 49  
 206 and above Kalahari sands, covering most of the surface in the southern part of the basin (Botha,  
 51  
 207 2000). Studies based on their mineralogy, micromorphology, bulk geochemistry, isotopic signature,  
 54  
 208 chronology, and geomorphological context have suggested several formation mechanisms  
 56  
 209 dependent on hydrology and climate. Semi-arid to arid conditions under alternating dry and humid  
 58  
 210 stages are generally considered as suitable for their precipitation (Kampunzu et al., 2007; Ringrose

211 et al., 2009), but their paleoenvironmental interpretation is not straightforward (Summerfield, 1983;  
 1  
 212 Nash and McLaren, 2003).

213 As chemical precipitates forming under saturation of the hosting solution through a combination of  
 2  
 3  
 4  
 5  
 6  
 7  
 8  
 9  
 10  
 11  
 12  
 13  
 14  
 15  
 16  
 17  
 18  
 19  
 20  
 21  
 22  
 23  
 24  
 25  
 26  
 27  
 28  
 29  
 30  
 31  
 32  
 33  
 34  
 35  
 36  
 37  
 38  
 39  
 40  
 41  
 42  
 43  
 44  
 45  
 46  
 47  
 48  
 49  
 50  
 51  
 52  
 53  
 54  
 55  
 56  
 57  
 58  
 59  
 60  
 61  
 62  
 63  
 64  
 65

214 lateral and vertical transfer mechanisms, duricrusts are not restricted to chronological stratigraphy  
 215 and occur in both vadose and phreatic environments. Alternating conditions promote changes in pH  
 216 that commonly result in mixed compositions of cements, which range from pure carbonate to pure  
 217 silica and may include Fe-oxy-hydroxides and clays (Shaw and Nash, 1998; Nash et al., 2004;  
 218 Kampunzu et al., 2007; Vainer et al., 2018a). Multi-phase accumulation through repeated  
 219 dissolution and re-precipitation occurs at varied sunsurface and surficial settings, including  
 220 paleolakes, pans, and marginal pools (McCarthy and Ellery, 1995; Ringrose et al., 2002; Thomas et  
 221 al., 2003), valley-fills (Nash and McLaren, 2003), and pedogenic profiles (Watts, 1980), where flora  
 222 and fauna may be involved in their generation.

223 Varied formation settings and processes, with consequently diverse textures ranging from dispersed  
 224 powder to nodular and hardpan, has led to different classification criteria (Goudie, 2020). These  
 225 consider geomorphological and hydrological conditions as well as macro- and micromorphological  
 226 characteristics including size, structure, mineralogy, porosity, biological components, secondary  
 227 filling and coating, and chronological relationships between the precipitating phases (Nash and  
 228 Shaw, 1998; Nash and McLaren, 2003).

229 In the Kalahari, indurated layered carbonate characterizes weathering profiles in NW Botswana and  
 230 could be widespread throughout the basin but covered by unconsolidated sand (McFarlane et al.,  
 231 2010). Precipitation shortly after clastic deposition when aquifer levels dropped, from solutions  
 232 migrating laterally from dolomitic rocks, was inferred based on Sr isotopic ratios (Vainer et al.,  
 233 2018a). A source other than underlying bedrock for the cementing agents was similarly inferred for  
 234 duricrusts in southern and central Botswana based on geochemical differences with the underlying  
 235 bedrock (Nash et al., 2004).

236 U-Pb dating of carbonates deposited in a mega-fan environment in the Etosha sub-basin reaches  
 1  
 237 back to the early Eocene (Houben et al., 2020), much earlier than the establishment of dunefields in  
 3  
 4  
 238 the Kalahari. Because of intrinsic difficulties in radiometric dating of calcrete (Burrough et al.,  
 6  
 239 2009a), the age of duricrusts is mainly constrained by the association with fossils and artefacts,  
 8  
 240 indicating formation since the early Pleistocene and throughout the Quaternary (Haddon, 2005).  
 10  
 11  
 241 Over the last decades, luminescence dating has allowed to establish when quartz grains within  
 13  
 14  
 242 calcrete were last exposed to light, confirming duricrust formation spanning at least from the middle  
 15  
 16  
 243 and late Pleistocene (Ringrose et al., 2002) to the Holocene (Burrough et al., 2009a).  
 18

#### 244 2.5. Quaternary climate change

245  
 246  
 247 In the Kalahari dryland, Quaternary environmental and climatic changes are documented in a range  
 24  
 25  
 248 of archives, including sand dunes, former lake shorelines, pan deposits and fringing lunette dunes,  
 27  
 249 fluvial sediments, tufa carbonates, speleothems, groundwater and rock shelter deposits (animal and  
 29  
 30  
 250 human middens and rock art), each containing different proxies (table 1 in Stone, 2021b). The  
 32  
 33  
 251 Quaternary dynamics of aeolian-fluvial interactions can be put into context by combining these  
 34  
 35  
 252 different archives. Given the size and current climatic heterogeneity of the Kalahari Basin it is  
 36  
 37  
 253 pragmatic to consider three broad sub-regions: i) northern (including the NWK, NEK and EK  
 39  
 40  
 254 dunefields); ii) southern (including the WK and SK dunefields); and, iii) eastern, with no major  
 41  
 42  
 255 dunefield.

43  
 44  
 256 Over the past ~150 ka, at least seven wetter intervals are identified in these sub-regions, which are  
 46  
 47  
 257 not paced consistently with precession and whose onset and end do not align with global marine  
 49  
 50  
 258 oxygen isotope stages. Some appear to be widespread but others display opposing meridional  
 51  
 52  
 259 trends. Data compiled from the INQUA Dune Atlas by Thomas and Burrough (2016) indicate  
 54  
 55  
 260 relatively continuous dune accumulation across most of the Kalahari over the past 190 ka, with only  
 56  
 57  
 261 a few gaps (174-107 ka, 96-87 ka, and 38-42 ka) possibly ascribed to a lack of preservation. The  
 58  
 59  
 262 implication of this dataset of ~400 ages is that the pattern of episodic dune formation and aridity

263 proposed by [Stokes et al. \(1998\)](#) is an artefact driven by low sampling density across space and to  
 1  
 264 only shallow depths within a dynamic and heterogeneous landscape ([Stone and Thomas, 2008](#)).  
 3  
 4  
 265 A first wetter interval at ~140 to 120 ka is seen in the northern sub-region, when diverse isolated  
 6  
 266 basins became interconnected in mega-lake Makgadikgadi ([Burrough et al., 2009b](#)), and by  
 8  
 267 speleothem growth (133±27 ka; [Brook et al., 1998](#)). In the southern sub-region, presence of  
 10  
 1268 palygorskite suggests semi-arid climate from 156±11 to 121±6 ka ([Lukich et al., 2019; 2020](#)). After  
 13  
 14  
 269 local deposition at >183 ka ([Stone and Thomas, 2008](#)), there is no preserved evidence of linear-  
 15  
 16  
 270 dune accumulation between ~174 and 107 ka in the southern Kalahari, but for a mottled sandstone  
 18  
 19  
 271 unit dated by luminescence as between 160 and 108 ka ([Bateman et al., 2003](#)).  
 20  
 21  
 272 A second wetter interval between ~112 and 90 ka is recorded by mega-lake Makgadikgadi phases  
 23  
 24  
 273 (105±4 ka and 92±2 ka; [Burrough et al., 2009b](#)) and speleothem growth (112±5 to 108±7 ka and  
 25  
 26  
 274 93±6 ka; [Brook et al., 1998](#)). Evidence for dune accumulation is lacking in the southern sub-region  
 28  
 29  
 275 during this period. A third wetter interval between ~80 and 70 ka is recorded at Etosha Pan  
 30  
 31  
 276 ([Hipondoka et al., 2014](#)) but not in the mega-lake Makgadikgadi system.  
 32  
 33  
 277 In contrast, a fourth interval between ~63 and 43 ka is documented by a mega-lake Makgadikgadi  
 35  
 36  
 278 phase at 64±2 ka and by speleothem growth (~61 ka; [Brook et al., 1998](#); ~51-43, [Holmgren et al.,](#)  
 37  
 38  
 279 [1995](#); 58-46 ka, [Holzkämper et al., 2009](#); from 56.8±0.4 to 43±7 ka, [Pickering et al., 2007](#)). The  
 40  
 41  
 280 southern sub-region recorded semi-arid conditions at 55±3 ka ([Lukich et al., 2020](#)) and dunes  
 42  
 43  
 281 continued to accumulate ([Thomas and Burrough, 2016](#)). A following drier interval is documented in  
 45  
 46  
 282 the eastern sub-region by a lack of speleothem growth between ~43 and 21 ka ([Holmgren et al.,](#)  
 47  
 48  
 283 [1995](#)) and groundwater record ([Kulongski et al., 2004](#)). However, wetter conditions are locally  
 49  
 50  
 284 testified between ~43 and 30 cal ka B.P. ([Schüller et al., 2018](#)). Dunes accumulated consistently,  
 52  
 53  
 285 suggesting sufficient windiness and perhaps inadequate moisture availability to keep vegetation  
 54  
 55  
 286 cover below a limiting threshold.  
 57  
 58  
 287 A fifth wetter interval is documented in the northern sub-region at 39±2 ka and 27±1 ka by two  
 59  
 60  
 288 mega-lake Makgadikgadi phases ([Burrough et al., 2009](#)) and at 36-32 and 27-22 ka ([Thomas et al.,](#)  
 62  
 63  
 64  
 65



289 2003). In the southern sub-region, evidence includes aquifer recharge at ~36-33 ka (Stute and  
 1 Talma, 1998), speleothem growth at ~33 ka (Brook et al., 2010), and pan-floor flooding at  $32\pm 5$  ka  
 290 (Telfer et al., 2009). In contrast, dry conditions are documented locally (~30-25 cal ka B.P.;  
 2 3 4  
 291 Schüller et al., 2018) and dunes continued to accumulate in the southern sub-region (Thomas and  
 5 6  
 292 Burrough, 2016). Wetter conditions started later in the eastern sub-region, as indicated by  
 7 8  
 293 speleothem growth from 27-21 ka (Holmgren et al., 1995), 24.3-12.7 ka (Holmgren et al., 2003),  
 9 10 11  
 294 and  $16.5\pm 0.2$  ka (Pickering et al., 2007).  
 12 13 14 15

16 A sixth wetter interval between ~23 and 16 ka is documented as a mega-lake Makgadikgadi phase  
 17 18  
 296 (17±2 ka; Burrough et al., 2009b) and as lake phases at Etosha Pan (23-21 and 18-16 ka; Hipondoka  
 19 20  
 297 et al., 2014). In the southern sub-region, fluvial units were dated as 23 ka and 18 ka in the lower  
 21 22  
 298 Molopo basin (Hürkamp et al., 2011), pan flooding as ~20 ka (Telfer et al., 2009), and speleothem  
 23 24  
 299 growth as 32-17 ka (Brook et al., 2010). In contrast, drier conditions are indicated at  $22\pm 1$  ka by a  
 25 26  
 300 hardpan unit indicating a strongly negative moisture balance (Lukich et al., 2020) and locally at  
 27 28  
 301 ~19.5-18 cal ka B.P. (Schüller et al., 2018).  
 29 30 31 32

33 A seventh wetter interval is recorded in the northern sub-region at 16-12 ka (Thomas et al., 2003)  
 34 35  
 303 and in the southern sub-region at 15-13 cal ka B.P. (Schüller et al., 2018). This episode is not  
 36 37  
 304 documented in the mega-lake Makgadikgadi system and dunes continued to accumulate in the  
 38 39  
 305 southern sub-region (Thomas and Burrough, 2016).  
 40 41 42

43 At the start of the Holocene, wetter conditions are indicated by a mega-lake Makgadikgadi phase at  
 44 45  
 307  $8\pm 5$  ka (Burrough et al., 2009b), speleothem growth at ~8.2 ka (Brook et al., 1998), and an absence  
 46 47  
 308 of age evidence for dune activity from ~8 ka in the northeastern Kalahari (Thomas and Burrough,  
 48 49  
 309 2016). In contrast, only episodic flash-flood events are documented in the lower Molopo from ~9.5  
 50 51  
 310 to 6.5 ka (Schüller et al., 2018) and dunes were active in the southern-sub-region during this time  
 52 53  
 311 (Thomas and Burrough, 2016). Speleothem growth ceased before the Holocene in the eastern sub-  
 54 55  
 312 region (Holmgren et al., 1995) but continued from ~ 5 ka onwards in the north (Brook et al., 1998).  
 56 57 58 59 60 61 62 63 64 65

314 A wet phase is recorded at ~5.5 cal ka B.P. in the south (Schüller et al., 2018), whilst dune activity  
 1 continued in the southern sub-region (Thomas and Burrough, 2016).  
 3  
 4

### 3. Overview of previous work on the provenance of Kalahari sands

318  
 9  
 1019 Provenance of Kalahari sands has not been investigated thoroughly by a multi-technique approach  
 11 so far. Previous surveys recognized the highly quartzose composition of aeolian sands but their  
 12  
 1320 compositional variability has been only broadly evaluated, and the origin of Kalahari dunefields  
 14  
 1521 was mostly ascribed to either reworking of older sediments (e.g., Du Toit, 1954; Baillieul, 1975;  
 16  
 1722 Thomas, 1987) or dominant fluvial processes (e.g., De Ploey et al., 1968; Verboom, 1974; Moore  
 18  
 1923 and Dingle, 1998). Petrographic, mineralogical, geochemical, and geochronological results from  
 20  
 2124 aeolian and river sediments collected in the Kalahari Basin and illustrated in Garzanti et al. (2014a,  
 22  
 2325 2014b) complement the new dataset obtained in this study and will be summarized and discussed  
 24  
 2526 later on.  
 26  
 2727  
 28  
 29  
 30

31  
 3228 The earliest heavy-mineral study of Kalahari sands was carried out by Poldervaart (1957), who  
 33  
 3429 identified tourmaline as a ubiquitous component, associated with zircon increasing eastwards at the  
 35  
 36380 expense of staurolite and kyanite. In his survey across Botswana, Baillieul (1975) distinguished four  
 37  
 3839 different types of Kalahari sands according to their texture, composition, and origin: 1) pure quartz  
 39  
 4041 sand reworked from older longitudinal dunes in northwestern Botswana; 2) finer-grained feldspar-  
 42  
 4344 bearing sand largely derived from recycling of the feldspatho-quartzose Neoproterozoic Ghanzi  
 45  
 46344 Sandstone in central-western Botswana; 3) pure quartz sand inferred to be recycled from Upper  
 47  
 484935 Triassic/Lower Jurassic sandstones of the Karoo Supergroup in central to southwestern Botswana  
 49  
 5051 (Boocock & Van Straaten, 1962); and, 4) various sands of fluvial origin in eastern Botswana,  
 52  
 53547 locally containing micas or basaltic rock fragments and largely derived from diverse exposed  
 55  
 56338 bedrocks. Thomas (1987) emphasized the remarkable homogeneity of textural and compositional  
 57  
 58539 features, held to testify an overriding importance of aeolian activity across the Kalahari.  
 59  
 60  
 61  
 62  
 63  
 64  
 65

340 In their textural and mineralogical study of the Kalahari Erg in NW South Africa, central Botswana  
 1  
 341 and NE Namibia, [Schlegel et al. \(1989\)](#) distinguished between sand collected from the crest of  
 3  
 342 modern aeolian dunes and 'mixed sands' collected in interdune areas or close to semi-periodical  
 4  
 343 rivers or pans. They found that tourmaline and staurolite are most abundant in dune-crest samples,  
 6  
 344 whereas garnet, zircon, amphibole, pyroxene, rutile, sillimanite, andalusite, and opaque oxides  
 8  
 345 (magnetite, ilmenite, and hematite) are more abundant in the 'mixed' samples. In South Africa,  
 10  
 346 dunes resulted to yield subrounded to very well-rounded tourmaline, staurolite, kyanite, and opaque  
 11  
 347 oxides. In Botswana and Namibia, more heterogeneous suites consist of mostly well rounded  
 12  
 348 tourmaline with subordinate staurolite, epidote, and zircon. Heavy minerals were observed to be  
 13  
 349 denser, less spherical and less rounded in 'mixed samples', garnet commonly occurring as broken  
 14  
 350 angular fragments. Main source rocks were held to be Nama and Karoo Group siliciclastics in South  
 15  
 351 Africa and Botswana  
 16  
 352 In their textural and mineralogical study of central Botswana cover sands, [Moore and Dingle \(1998\)](#)  
 17  
 353 failed to find a correspondence between the variability of sediment textures and wind patterns, and  
 18  
 354 thus inferred a dominance by fluvial processes. Ephemeral streams and sheetwash were inferred to  
 19  
 355 produce heavy-mineral enrichment in coarser proximal sands passing to finer sediments with fewer  
 20  
 356 heavy minerals in distal settings. Tourmaline (mainly in the southwest), staurolite (mainly in the  
 21  
 357 north), and kyanite were confirmed as the most common heavy minerals.  
 22  
 358 More recently, [Haddon and McCarthy \(2005\)](#) recognized the major role played by both fluvial and  
 23  
 359 aeolian process and identified local reworking from older deposits as a major source of Kalahari  
 24  
 360 sand. In a most recent study, [Vainer et al. \(2018b\)](#) used detrital mineralogy, elemental  
 25  
 361 geochemistry, and Sr, Nd and Pb isotopic ratios to detect provenance changes through a complete  
 26  
 362 Quaternary section of Kalahari Group sediments in South Africa. Provenance from distant Angolan  
 27  
 363 highlands *via* a trans-Kalahari palaeodrainage system was inferred for the basal part of the section,  
 28  
 364 overlain by strata containing detritus derived locally from volcano-sedimentary rocks of the  
 29  
 365 Archean Kaapvaal Craton exposed in the east and south. The more recent aeolian sands indicated  
 30  
 31  
 32  
 33  
 34  
 35  
 36  
 37  
 38  
 39  
 40  
 41  
 42  
 43  
 44  
 45  
 46  
 47  
 48  
 49  
 50  
 51  
 52  
 53  
 54  
 55  
 56  
 57  
 58  
 59  
 60  
 61  
 62  
 63  
 64  
 65

366 instead sediment supply from Paleoproterozoic source rocks in the west and northwest. Chemical  
 1 proxies suggested that weathering intensity was typical of humid areas for the basal part of the  
 367 3 section at a time of relatively dense hominin occupation of the area, but limited to groundwater  
 4 368 alteration and precipitation of duricrusts in the overlying strata.  
 6 369

9 370 Based on geochemical data, sediments of the Okavango Basin were considered to represent a  
 10 11 mixture of detritus derived from Proterozoic basement rocks exposed in Angola, Namibia, and NW  
 1371 13 Botswana with locally recycled aeolian sand and calcareous soils (Huntsman-Mapila et al., 2005).  
 14 372 Using elemental geochemistry complemented by Nd, Sr, and Pb isotopes, Vainer et al. (2021)  
 15 16 outlined a more complex provenance pattern, with detritus derived from multiple sources including  
 1373 18 the Angola Shield in the northwest, the Archean Kasai Craton in the north, Mesoproterozoic  
 1974 20 granitoids of the Choma-Koloma Block in the east, and the Ghanzi-Chobe and Damara Belts in the  
 21 2275 west, with possible contribution also from the Lufilian Belt and Karoo basalts.  
 23 2476

25 26 377 Gärtner et al. (2014) used U-Pb detrital-zircon geochronology and zircon morphology from sand  
 28 2978 carried by the Cunene, Okavango, Cuando, and Uppermost Zambezi Rivers to pin-point the  
 30 31 379 protosources of sediment recycled from and fed into the Kalahari Basin. They suggested that most  
 32 33 sediment originated from the Lufilian and Kibaran Belts with westward increasing input from the  
 34 380 Damara Belt. Zircons derived from the Angola Block were detected only in the Cunene and  
 35 36 381 westernmost part of the Okavango drainage basins.  
 37 38 382  
 39 40  
 41 383  
 42 43  
 44 384

#### 45 385 4. Geology of southern Africa

47 386 Southern Africa was amalgamated through multiple tectono-magmatic events dating back to the  
 48 4987 Archean and culminated with the Neoproterozoic Pan-African orogeny (Fig. 3; Hanson, 2003). The  
 50 51 388 Archean core consists of the Kaapvaal and Zimbabwe Cratons, welded by the Limpopo Belt. The  
 52 53 389 Kaapvaal Craton, progressively amalgamated between 3.7 and 2.7 Ga, was stabilized by 2.6 Ga, and  
 54 55 390 eventually intruded by the Bushveld Complex at 2.06 Ga (Eglington and Armstrong, 2004). The  
 56 57 391 Zimbabwe Craton, comprising 3.5-2.95 Ga gneisses non conformably overlain by volcanic and  
 58 59 392  
 60 61  
 62 63  
 64 65

393 sedimentary rocks and 2.7 Ga greenstone belts, was eventually sealed by the Great Dyke Swarm at  
1  
394 ~2.6 Ga (Kusky, 1998; Jelsma and Dirks, 2002). The ~200 km-wide Limpopo Belt includes high-  
3  
4  
395 grade orthogneisses, retrograde amphibolite-facies metasedimentary rocks, and granitoids with  
6  
396 ages clustering at 3.3-3.2, 2.7-2.6, and 2.1-2.0 Ga (Zeh et al., 2007).

397 This composite Archean core grew progressively during Proterozoic orogenic cycles that generated  
10  
11  
1398 the discontinuously exposed mid-Paleoproterozoic Magondi-Okwa-Kheis Belt in the west and the  
13  
14  
399 latest Mesoproterozoic Namaqua–Natal Belt in the south. In the northwest, the Angola Block  
15  
16  
400 represents instead the southern part of the Congo Craton, cored by largely mid-Paleoproterozoic (~2  
18  
19  
401 Ga) mid-crustal granitoid gneisses (De Carvalho et al., 2000; McCourt et al., 2013; Jelsma et al.,  
20  
21  
402 2018).

2403 Stabilization of the Proto-Kalahari Craton by 1.75 Ga was followed by intraplate magmatism at 1.4-  
25  
26  
404 1.35 Ga and again at 1.1 Ga (Hanson et al., 2006). Amalgamation of the Kalahari Craton was  
27  
28  
405 completed by 1.0 Ga (Jacobs et al., 2008), when the Namaqua–Natal Belt was generated by arc  
30  
31  
406 accretion and continental collision. This orogen extends from SW Namibia to NE South Africa and  
32  
33  
407 includes Paleoproterozoic basement and up to high-grade metasedimentary rocks intruded by  
35  
36  
408 voluminous granitoids dated at 1.2-1.0 Ga (Eglington, 2006). The thick Stenian volcano-  
37  
38  
409 sedimentary Sinclair Group of southern Namibia underwent only low-grade deformation and was  
40  
410 intruded by numerous granitoids (Becker et al., 2006).

411 Cratonic southern Africa was finally welded to the Congo Craton in the north during the major  
45  
46  
412 Neoproterozoic Pan-African orogeny, testified by the Damara–Lufilian–Zambezi Belt stretching  
47  
48  
413 from coastal Namibia in the west and across Botswana and southern Zambia to connect with the  
49  
50  
414 Mozambique Belt in the east (Frimmel et al., 2011; Goscombe et al., 2020). The Damara Belt in  
52  
53  
415 Namibia includes 2.0-1.2 Ga basement gneisses overlain by Neoproterozoic metasediments intruded  
54  
55  
416 by 570-460 Ma granitoids (Miller, 2008). A 3 km-thick succession of Neoproterozoic to Cambrian  
57  
58  
417 sandstone, mudrock and limestone was deposited in the foreland basin of the Damara Orogen in  
59  
60  
418 southern Namibia (Nama Group; Blanco et al., 2011). The Lufilian Arc consists of metasedimentary  
62  
63  
64  
65

419 and metaigneous rocks hosting Cu-Co-U and Pb-Zn mineralizations ([Kampunzu and Cailteux,](#)  
1  
420 [1999](#); [Eglinger et al. 2016](#)). The Zambezi Belt contains a volcano-sedimentary succession deformed  
3  
4  
421 under amphibolite-facies conditions at 0.9–0.8 Ga ([Hanson 2003](#)), whereas eclogite-facies  
6  
422 metamorphism dated as 592 Ma constrains the timing of subduction and thrust emplacement as 550-  
8  
423 530 Ma ([Hargrove et al., 2003](#); [John et al., 2004](#)).

11  
424 Initial disruption of the Gondwana supercontinent was recorded by the several km-thick Upper  
13  
14  
425 Carboniferous to Lower Jurassic Karoo Supergroup, covering almost two-thirds of southern Africa.  
15  
16  
426 Basin subsidence in the southern retroarc basin was induced by subduction of paleo-Pacific  
18  
19  
427 lithosphere, while transtensional stress propagated southwards from the Neotethyan rift in the north  
20  
21  
428 ([Catuneanu et al., 2005](#)). The Karoo succession begins with diamictite, turbidite, and coal-bearing  
23  
24  
429 fluvio-deltaic strata, followed by braidplain sandstone, mudrock, and aeolian sandstone ([Johnson et](#)  
25  
26  
430 [al., 1996](#)). Permian sandstones contain andesitic-dacitic volcanic detritus ([Johnson, 1991](#)) and  
28  
29  
431 interlayered tuffs yielding ages mainly between 270 and 260 Ma ([Lanci et al., 2013](#); [McKay et al.,](#)  
30  
31  
432 [2016](#)). Karoo sedimentation was terminated by flood-basalt eruptions recorded throughout southern  
32  
33  
433 Africa around 183 Ma ([Svensen et al., 2012](#); [Greber et al., 2020](#)). A vast network of dolerite dykes  
35  
36  
434 and sills suggests that tholeiitic lavas originally covered an area of ~2.5 million km<sup>2</sup>.

38  
435 The passive margins surrounding Africa developed after rifting of the Indian and Atlantic Oceans in  
40  
41  
436 the Late Jurassic and Early Cretaceous, respectively. Widespread intrusion of pipe-like bodies,  
42  
43  
437 including diamond-bearing kimberlites, took place in the Cretaceous to Paleogene ([Moore et al.,](#)  
45  
46  
438 [2008](#)).

47  
48  
439 In the Kalahari Basin, stretching ~2200 km in the hinterland from the Congo to South Africa, up to  
50  
51  
440 450 m-thick sediments were deposited since the Late Cretaceous ([Haddon and McCarthy, 2005](#)).  
52  
53  
441 The Plio-Pleistocene consists of gravel, clay, and aeolian sand with calcrete and silcrete ([Thomas](#)  
54  
55  
442 [and Shaw, 1990](#); [Vainer et al., 2018b](#)). In the Quaternary, the region was reached by along-axis  
57  
58  
443 propagation of the East African rift, through a network of unconnected basins extending from Lake  
59  
60  
61  
62  
63  
64  
65

444 Tanganyika to the Okavango Graben and central Namibia farther west ([Modisi et al., 2000](#); [Kinabo](#)  
 445 [et al., 2007](#); [Vainer et al., 2021](#)).

446

## 447 5. Methods

448

449 In this provenance study, we have analysed 57 dune sand samples collected across the vast Kalahari  
 450 sand sea in the frame of diverse research projects ([Stone and Thomas, 2008](#); [Matmon et al., 2018](#);  
 451 [Burrough et al., 2019](#); [Stone et al., 2019](#); [Wittman et al., 2020](#); [Vainer et al., 2021](#)). Another 43 sand  
 452 samples collected from exposed sandbars or dry riverbeds in Angola, Botswana, Zambia,  
 453 Zimbabwe, Namibia and South Africa, and previously studied with similar and complementary  
 454 methodological approaches ([Garzanti et al., 2014a, 2018a, 2021a](#)), were considered to monitor  
 455 changes in sediment composition associated with fluvial-aeolian interactions. Full information on  
 456 sampling sites is provided in [Appendix Table A1](#) and Google Earth™ file [Kalahari.kmz](#).

457

### 458 5.1. Petrography

459

460 Petrographic composition of each sand sample was determined by counting  $\geq 400$  points in thin  
 461 section by the Gazzi-Dickinson method ([Ingersoll et al., 1984](#)). Sands are classified by their main  
 462 components exceeding 10% QFL (e.g., in a feldspatho-quartzose sand  $Q > F > 10\% \text{ QFL} > L$ ).  
 463 Among feldspatho-quartzose sands, feldspar-rich ( $Q/F < 2$ ) and quartz-rich ( $Q/F > 4$ ) compositions  
 464 are distinguished; pure quartzose sand has  $Q > 95\% \text{ QFL}$  ([Garzanti, 2016, 2019](#)). Cross-hatched  
 465 microcline is called for simplicity microcline\*. Rock fragments were classified by protolith  
 466 composition and metamorphic rank ([Garzanti and Vezzoli, 2003](#)). The complete petrographic  
 467 dataset is provided in [Appendix Table A2](#).

468

### 469 5.2. Transparent heavy minerals

470

471 From the bulk sample or from a wide size-range obtained by wet sieving, heavy minerals were  
 472 separated by centrifuging in Na-polytungstate ( $2.90 \text{ g/cm}^3$ ) and recovered after partial freezing of

473  
474  
475  
476  
477  
478  
479  
480

the test tube with liquid nitrogen. The dense fraction thus obtained was weighed, split with a micro-riffle box, and mounted on a glass slide with Canada balsam for counting. About 200 to 250 transparent heavy minerals were either counted by the area method or point-counted at suitable regular spacing to obtain real volume percentages (Galehouse, 1971).

Transparent-heavy-mineral concentration ranges from extremely poor ( $tHMC < 0.1$ ), very poor ( $0.1 \leq tHMC < 0.5$ ), poor ( $0.5 \leq tHMC < 1$ ) and moderately poor ( $1 \leq tHMC < 2$ ), to moderately rich ( $2 \leq tHMC < 5$ ), rich ( $5 \leq tHMC < 10$ ), very rich ( $10 \leq tHMC < 20$ ), and extremely rich ( $20 \leq tHMC < 50$ ) (Garzanti and Andò, 2007, 2019). The sum of the percentages of zircon, tourmaline, and rutile (collectively called ZTR minerals throughout the text) expresses the mineralogical durability of the suite (ZTR index of Hubert, 1962; Garzanti, 2017). The “Amphibole Color Index” ACI varies from 0 in detritus from lower-grade metamorphic rocks yielding exclusively blue/green amphibole to 100 in detritus from granulite-facies or volcanic rocks yielding exclusively brown amphibole or oxyhornblende (Andò et al., 2014). Transparent-heavy-mineral assemblages are called “tHM suites” throughout the text and significant minerals are listed systematically in order of abundance (high to low). The complete heavy-mineral dataset is provided in Appendix Table A3.

### 5.3. Detrital geochronology

Detrital zircons were identified by Automated Phase Mapping (Vermeesch et al., 2017) with a Renishaw inVia™ Raman microscope on the heavy-mineral separates of 42 samples, concentrated with standard magnetic techniques and directly mounted in epoxy resin without any operator selection *via* hand picking. U-Pb zircon ages were determined at the London Geochronology Centre using an Agilent 7900 LA-ICP-MS (laser ablation-inductively coupled plasma-mass spectrometry) system, employing a NewWave NWR193 Excimer Laser operated at 10 Hz with a 25  $\mu\text{m}$  spot size and  $\sim 2.5 \text{ J/cm}^2$  fluence. No cathodo-luminescence imaging was conducted. The laser spot was always placed blindly in the middle of zircon grains in order to treat all samples equally and avoid bias in intersample comparison (“blind-dating approach” illustrated and discussed in Garzanti et al.,



2018b). No common Pb correction was applied. The mass spectrometer data were converted to isotopic ratios using GLITTER 4.4.2 software (Griffin et al., 2008) employing Plešovice zircon (Sláma et al., 2008) as a primary age standard and GJ-1 (Jackson et al., 2004) as a secondary age standard. A NIST SRM612 glass was used as a compositional standard for U and Th concentrations. GLITTER files were post-processed in R using IsoplotR 2.5 (Vermeesch, 2018). We used  $^{206}\text{Pb}/^{238}\text{U}$  and  $^{207}\text{Pb}/^{206}\text{Pb}$  as preferred ages for zircons younger and older than 1100 Ma, respectively. Additionally, we calculated concordia ages as the maximum likelihood intersection between the concordia line and the error ellipse of  $^{207}\text{Pb}/^{235}\text{U}$  and  $^{206}\text{Pb}/^{238}\text{U}$  ages (Ludwig, 1998). The discordia cutoff was set as +6.8 and -2.3 based on the Aitchison distance from the measured log ratio and the concordia line (Vermeesch, 2021). A total number of 5459 ages were obtained, 3433 of which (62.9%) were used for statistical analysis. The complete geochronological dataset is provided in Appendix B.

#### 5.4. Graphical/statistical tools

The statistical tools applied to the analysed sand samples include Multidimensional Scaling (MDS; Kruskal and Wish, 1978; Vermeesch, 2013). This multivariate ordination technique takes a dissimilarity matrix as input and produces a map of samples as output, in which similar samples plot close together and dissimilar samples plot far apart. For detrital zircon U-Pb age spectra, a dissimilarity matrix can be constructed using the Kolmogorov-Smirnov statistic (i.e., the maximum vertical difference between two cumulative distribution functions; Feller, 1948).

To illustrate heavy-mineral data we used the compositional biplot (Gabriel, 1971), a statistical/graphical display that allows discrimination among multivariate observations (points) while shedding light on the mutual relationships among multiple variables (rays). The length of each ray is proportional to the variance of the corresponding variable in the dataset. If the angle between two rays is close to  $0^\circ$ ,  $90^\circ$  or  $180^\circ$ , then the corresponding variables are correlated, uncorrelated, or inversely correlated, respectively.

527  
 1  
 528  
 2  
 3  
 529  
 4  
 5  
 530  
 6  
 7  
 531  
 8  
 9  
 10  
 532  
 11  
 12  
 533  
 13  
 14  
 534  
 15  
 16  
 535  
 17  
 18  
 19  
 536  
 20  
 21  
 537  
 22  
 23  
 24  
 538  
 25  
 26  
 539  
 27  
 28  
 29  
 540  
 30  
 31  
 541  
 32  
 33  
 542  
 34  
 35  
 36  
 543  
 37  
 38  
 544  
 39  
 40  
 41  
 545  
 42  
 43  
 546  
 44  
 45  
 547  
 46  
 47  
 48  
 548  
 49  
 50  
 51  
 549  
 52  
 53  
 550  
 54  
 55  
 56  
 551  
 57  
 58  
 552  
 59  
 60  
 553  
 61  
 62  
 63  
 64  
 65

## 6. Mineralogy of river sands

The Caculuar and Mucope tributaries of the Cunene River, draining the western edge of the Kalahari Erg in Angola (Fig. 1A), carry pure quartzose sand with a few K-feldspar grains. The extremely poor, zircon-rich tHM suite includes epidote, tourmaline, and minor andalusite, staurolite and rutile (Table 1). The Okavango and Cuando Rivers, which are sourced in Angola and drain the northern Kalahari towards the Caprivi Strip and Botswana, carry pure quartzose sand (Fig. 4I) with extremely poor, tourmaline-zircon-epidote-staurolite-kyanite-rutile tHM suites.

Sand carried by the upper Zambezi River in Zambia is also pure quartzose (Fig. 4K) with a poor tHM suite dominated by ZTR minerals with common kyanite, staurolite, and minor epidote. Clinopyroxene appears downstream of Ngonye Falls, increases towards Victoria Falls, and becomes rapidly predominant along the gorges downstream.

Zambezi tributaries in Zimbabwe include the Matetsi, which carries quartzo-lithic basalticlastic sand (Fig. 4M) with extremely rich tHM suites containing clinopyroxene exclusively, and the Gwai, which carries feldspatho-quartzose sand (Fig. 4O) with a poor tHM suite containing amphibole, subordinate epidote and garnet, and minor clinopyroxene, kyanite, and sillimanite. The Shangani, a Gwai tributary (Fig. 1A), carries quartzose sand with basaltic rock fragments, a few plagioclase grains, and a moderately rich tHM suite dominated by clinopyroxene.

In northern and central Namibia, the Omatako carries feldspatho-quartzose sand with K-feldspar >> plagioclase and a very poor tourmaline-amphibole-garnet tHM suite. The Okakongo (a northern tributary of the Swakop River draining towards the Atlantic Ocean) carries feldspar-rich feldspatho-quartzose sand (Fig. 4A) with moderately rich hornblende-dominated tHM suite. The Rietfontein carries pure quartzose sand (Fig. 4C) with a very poor staurolite-tourmaline tHM suite.

The White Nossob and Black Nossob (western and eastern branches of the Nossob River) carry feldspatho-quartzose sand containing granitoid and high-rank metamorphic rock fragments (Fig. 4E) with a moderately poor amphibole-garnet-staurolite-epidote tHM suite, and quartz-rich

554 feldspatho-quartzose sand containing low-rank metasedimentary rock fragments with a moderately  
 1  
 555 poor staurolite-epidote-garnet-zircon tHM suite, respectively.  
 3

556 The Molopo River, which drains the southern Kalahari, carries quartz-rich feldspatho-quartzose  
 6  
 557 sand with common monocrystalline quartz displaying abraded overgrowths, plagioclase > K-  
 8  
 558 feldspar, and a few shale/slate or quartzose sedimentary and metasedimentary rock fragments (Fig.  
 10  
 559 4G). The moderately poor tHM suite includes epidote, amphibole, ZTR minerals, garnet,  
 13  
 560 clinopyroxene, and minor staurolite and kyanite.  
 15

## 562 7. Mineralogy of dune sands

563  
 564 Dune sand is quartz-rich over most the vast Kalahari Basin: out of the 57 studied samples, 31 are  
 23  
 565 pure quartzose, 12 quartzose, and 10 quartz-rich feldspatho-quartzose (Fig. 5). Throughout the  
 26  
 566 northern Kalahari, in Angola, northeastern Namibia, Caprivi Strip, northern Botswana, and western  
 28  
 567 Zambia, sand consists virtually exclusively of monocrystalline quartz commonly showing rounded  
 31  
 568 to subrounded outline and abraded overgrowths (Fig. 4L). Dune sand in the Caprivi Strip contains  
 33  
 569 abundant red iron-oxide particles.  
 35

570 Pure quartzose sand also characterizes the eastern edge of the Kalahari in Zimbabwe as well as the  
 38  
 571 central part of the sand sea from eastern Namibia to southeastern Botswana. In all these regions, K-  
 40  
 572 feldspar prevails among the few feldspar grains, lithics are rare or lacking, and tHM assemblages  
 43  
 573 are very poor to extremely poor and dominated by ZTR minerals. Staurolite is widespread, most  
 45  
 574 common in the Ghanzi area (Fig. 4D) and generally associated with kyanite and minor andalusite.  
 48  
 575 Kyanite increases progressively southwards in westernmost Zambia and is most abundant to the  
 50  
 576 west of the Cuando/Zambezi confluence, where it is associated with minor garnet. Epidote is  
 52  
 577 common south of the Okavango inland delta, where a few amphibole grains occur. Garnet is rare or  
 55  
 578 lacking altogether (Table 1).  
 57

579 Basaltic detritus including rock fragments, plagioclase and clinopyroxene is significant in dune sand  
 1  
 580 NW of Victoria Falls, and dominant in litho-quartzo-feldspathic dune sand close to the Zambezi  
 3  
 4  
 581 gorges downstream (Fig. 4N).

582 In western Zimbabwe, dune sand is markedly enriched in feldspars. In the NW near Masuma, sand  
 8  
 9  
 583 is feldspatho-quartzose (Fig. 4P) with plagioclase > K-feldspar, quartz-rich siltstone/sandstone and  
 10  
 11  
 584 medium-rank metamorphic rock fragments, biotite, and a moderately rich garnet-epidote tHM suite.

14  
 15  
 585 In the SE near Bulawayo, sand is quartzo-feldspathic with K-feldspar > plagioclase and a poor  
 16  
 17  
 586 amphibole-epidote suite. In eastern Botswana around the Makgadikgadi Pan, dune sand is  
 18  
 19  
 587 quartzose, with K-feldspar > plagioclase and very poor tHM suitentwetwes with common epidote,  
 20  
 21  
 588 ZTR minerals, amphibole and/or clinopyroxene, and minor kyanite, garnet and staurolite.

23  
 24  
 589 Polycrystalline quartz, a few felsic volcanic, and quartz-rich siltstone/sandstone rock fragments are  
 25  
 26  
 590 locally significant. Calcareous grains including common ooids occur in mounds on the surface of  
 27  
 28  
 591 the Ntwetwe (western Makgadikgadi) Pan (Fig. 4J; McFarlane and Long, 2015).

31  
 32  
 592 Straddling the Botswana/South Africa border, dune sand is quartzose to pure quartzose (Fig. 4H)  
 33  
 34  
 593 with K-feldspar > plagioclase, and very poor tHM suites dominated by ZTR minerals with locally  
 35  
 36  
 594 common epidote or staurolite. The Koppieskraalpan dune is quartz-rich feldspatho-quartzose with a  
 37  
 38  
 595 few basaltic rock fragments, plagioclase > K-feldspar, and a moderately rich tHM suite including  
 40  
 41  
 596 dominant clinopyroxene and subordinate garnet.

43  
 44  
 597 In the western Kalahari, SW of the Nossob River, dune sand is relatively homogeneously quartzose  
 45  
 46  
 598 to quartz-rich feldspatho-quartzose with K-feldspar >> plagioclase (Fig. 4F). The mostly poor and  
 47  
 48  
 599 epidote-dominated tHM suite includes ZTR minerals and staurolite. Amphibole with minor  
 50  
 51  
 600 clinopyroxene are significant in the northern Hardap region, staurolite with subordinate kyanite  
 52  
 53  
 601 most common in SW Namibia, and garnet common in South Africa.

55  
 56  
 602 In northern Namibia, mineralogy is more varied. The Okahandja dune is feldspar-rich feldspatho-  
 57  
 58  
 603 quartzose (Fig. 4B) with plagioclase > K-feldspar, up to high-rank metasedimentary rock fragments,  
 59  
 60  
 604 common biotite, and a moderately rich tHM suite dominated by hornblende with clinopyroxene,  
 62  
 63  
 64  
 65

605 ZTR minerals, apatite and epidote. In the central region, dune sand is quartzose to pure quartzose,  
 1  
 606 with K-feldspar >> plagioclase and poor tHM suites including mainly ZTR minerals, epidote,  
 3  
 607 kyanite associated with either staurolite or garnet, and locally clinopyroxene. Quartzose sandstone  
 4  
 6 and shale rock fragments may occur. In northwesternmost Botswana, the Qangwa dune is quartz-  
 6  
 608 rich feldspatho-quartzose with plagioclase > K-feldspar and a moderately poor, epidote-dominated  
 8  
 609 tHM suite including ZTR minerals.  
 10  
 11  
 12  
 13

611

15

612

17

613

19

614

20

21

615

23

616

24

25

26

617

28

618

29

30

31

619

33

620

34

35

36

621

38

622

39

40

41

623

42

43

624

44

45

625

46

47

48

626

49

50

627

51

52

53

628

54

55

629

56

57

630

58

59

60

61

62

63

64

65

## 8. Ages of detrital zircons

The U-Pb age spectra of detrital zircons (Fig. 6) allow us to discriminate among protosources (i.e. original crystalline source rocks) of different ages, whereas the proportion of first-cycle *versus* even multiply recycled zircon grains can be only qualitatively evaluated for each sample based on petrographic composition and heavy-mineral concentration.

Five age ranges recur among the analysed samples, corresponding to main orogenic episodes in southern Africa (Hanson, 2003; Dirks et al. 2009; Andersen et al., 2016, 2018): I) Damara-Lufilian (0.45-0.65 Ga, Ordovician-Cryogenian; peak at 581 Ma) II) Namaqua-Irumide (1.0-1.1 Ga, Stenian; peak at 1056 Ma); III) Sinclair-Kibaran (1.2-1.4 Ga, Ectasian; peak at 1312 Ma); IV) Eburnean (1.8-2.05 Ga, Orosirian; peak at 1893 Ma); V) Limpopo (2.5-2.8 Ga, Neoproterozoic; peak at 2720 Ma). Younger ages include a minor ‘Karoo’ cluster (220-320 Ma, Triassic-Pennsylvanian; peak at 266 Ma) and some Lower Cretaceous ages (120-135 Ma) associated with magmatism related to South Atlantic rifting (e.g., Trumbull et al., 2004). Even younger grains (59-70 Ma, Paleocene-latest Cretaceous), associated with post-rift alkaline magmatism (Moore et al., 2008), sporadically occur in Botswana.

Data obtained in this study are compared with previously obtained radiometric ages on diverse crustal domains across southern Africa compiled from numerous literature sources (Fig. 7). The age compilation is summarized in Table 2 and presented in full in Appendix C. Further extensive

631 information on bedrock ages in the region are contained in [Gärtner et al. \(2014\)](#) and [Goscombe et](#)  
 1  
 632 [al. \(2020\)](#).

633  
 634 *8.1. River sands*

635  
 636 The zircon-age spectrum in sand of the Mucope River, draining entirely within the northwestern  
 10  
 637 Kalahari dunefield in Angola, displays a unimodal Orosirian peak at ~1.96 Ga, identifying the  
 11  
 12  
 638 Eburnean Angola Block as the main protosource. Minor clusters reflect the Karoo and Damara  
 13  
 14  
 15  
 639 thermal events ([Fig. 6](#)).

16  
 17  
 18  
 19  
 20  
 21  
 22  
 23  
 24  
 25  
 26  
 27  
 28  
 29  
 30  
 31  
 32  
 33  
 34  
 35  
 36  
 37  
 38  
 39  
 40  
 41  
 42  
 43  
 44  
 45  
 46  
 47  
 48  
 49  
 50  
 51  
 52  
 53  
 54  
 55  
 56  
 57  
 58  
 59  
 60  
 61  
 62  
 63  
 64  
 65

640 Detrital-zircon U-Pb age patterns are similar in Okavango and upper Zambezi sands, both  
 641 characterized by sharp Ediacaran and Stenian peaks, with a few Calymmian-aged zircons, a major  
 642 Orosirian cluster, and a minor Neoproterozoic cluster ([Garzanti et al., 2014a, 2021a](#)). These rather  
 643 homogeneous zircon-age signatures across the northern part of the Kalahari Basin reflect extensive  
 644 recycling of sediment originally derived from mostly Damara and Irumide protosources.

645  
 646 *8.2. Dune sands*

647  
 648 Pure quartzose dune sand in the Okavango region, from the inland delta to the Makgadikgadi Pan,  
 649 yielded multimodal zircon-age spectra characterized by Ediacaran, Stenian, and Orosirian peaks.  
 650 Similar spectra, with more Cryogenian to Stenian ages and less Paleoproterozoic to Neoproterozoic  
 651 ages, are displayed by pure quartzose dune sand all along the upper Zambezi valley, reflecting more  
 652 Damaran and Irumide, and somewhat less Eburnean protosources.

653 In Zimbabwe, similar age spectra with major Ediacaran and Stenian peaks, subordinate Orosirian  
 654 and minor Neoproterozoic clusters characterize pure quartzose sand at the eastern edge of the  
 655 Kalahari Basin. Instead, the feldspatho-quartzose Masuma dune yielded a few Stenian, Orosirian-  
 656 Rhyacian, and Archean zircon ages, whereas Archean-aged zircons occur in quartzo-feldspathic  
 657 dune sand near Bulawayo.

658 In Botswana south of Makgadikgadi Pan, Paleozoic ages increase slightly and Orosirian ages  
 659 decrease. Farther south, the quartzose Mokgomane dune near Gaborone is singled out by the

660 common Neoproterozoic to Mesoproterozoic zircons, whereas Stenian and subordinate Cryogenian zircons  
 1  
 661 increase progressively westwards in pure quartzose to quartz-rich feldspatho-quartzose dune sand  
 3  
 662 along the Molopo River course.  
 4  
 6

663 In Namibia, Ordovician to Ediacaran and Cambrian to Ediacaran ages predominate in quartzose and  
 8  
 664 feldspar-rich feldspatho-quartzose dune sand, respectively, reflecting prominent Damara  
 10  
 665 protosources. Along a SW/NE traverse in northern Namibia, pure quartzose dune sand yielded  
 13  
 666 multimodal, Permo-Triassic, Cambrian to Ediacaran, Stenian, Orosirian and minor Neoproterozoic  
 15  
 667 clusters. The quartz-rich feldspatho-quartzose Qangwa dune located near the Aha Hills in NW  
 18  
 668 Botswana is singled out by its nearly unimodal spectrum with early Tonian age peak at 956 Ma  
 20  
 669 (Fig. 6).  
 21  
 22  
 23

670 Along a W/E traverse between Windhoek in central Namibia and the Ghanzi Ridge in Botswana,  
 25  
 671 pure quartzose dune sand yielded mainly Orosirian, Statherian, and Stenian zircon ages in the west,  
 26  
 27  
 28  
 672 mainly Stenian to Ectasian ages in the center, and mainly Cambrian to Ediacaran ages in the east.  
 30  
 673 Quartzose to quartz-rich feldspatho-quartzose sand in the western Kalahari yielded mostly  
 31  
 32  
 33  
 674 Mesoproterozoic (Ectasian and subordinately Stenian) zircon ages and no ages younger than 500  
 35  
 675 Ma, indicating mainly Sinclair and Namaqua protosources (Fig. 6).  
 36  
 37  
 38

## 676 40 677 **9. Provenance of Kalahari dune sand** 41

678  
 42  
 43  
 679 In most of the Kalahari Basin, including the NWK and NEK dunefields in Angola, Namibia and  
 45  
 680 Zambia, much of Botswana, and part of the EK dunefield in Zimbabwe, dune sand is dominated by  
 46  
 48  
 681 monocrystalline quartz associated with very poor tHM suites including durable ZTR minerals,  
 50  
 682 staurolite, and kyanite (Figs. 8, 9, and 10). Such a homogenized mineralogical signature reveals  
 51  
 52  
 53  
 683 extensive recycling of older quartzose sandstones through time. A local exception is the quartz-rich  
 55  
 684 feldspatho-quartzose sand of the Qangwa dune collected near the Aha Hills, containing a  
 56  
 57  
 58  
 685 moderately poor, epidote-dominated tHM suite with zircon grains yielding mostly Tonian-Stenian  
 60  
 686 ages (peak between 900 and 950 Ma), indicating recycling of the Neoproterozoic Ghanzi Group  
 61  
 62  
 63  
 64  
 65

687 (Baillieu, 1975; Hall et al., 2018); a few Statherian-Orosirian ages suggest minor protosources in  
 1  
 688 the Angola Block to the north (McCourt et al., 2013).

689 At the other extreme, dunes situated near exposures of either crystalline basement or Karoo basalts  
 6  
 690 at the opposite margins of the Kalahari in central Namibia and Zimbabwe reveal mainly first-cycle  
 8  
 691 provenance with limited mixing with recycled aeolian sand of the erg (Fig. 10). Litho-quartzo-  
 10  
 692 feldspathic composition with dominant plagioclase, clinopyroxene, and mafic volcanic rock  
 13  
 693 fragments derived from Karoo lavas characterizes dune sand near the basaltic gorges carved by the  
 14  
 694 Zambezi River downstream of Victoria Falls, where less than a fourth of the bulk sediment is  
 16  
 695 represented by aeolian monocrystalline quartz (i.e., less than in local right-bank Zambezi tributaries  
 19  
 696 draining into the Karoo volcanic rocks; cf. Figs. 4M and 4N).

697 The dune located on the Zimbabwe Craton near Bulawayo (Fig. 3) is singled out by its quartzo-  
 25  
 698 feldspathic composition with high-rank metamorphic rock fragments, amphibole-epidote tHM suite,  
 26  
 699 and Archean-aged zircon grains, reflecting largely first-cycle provenance from local cratonic  
 28  
 700 basement. The feldspatho-quartzose Masuma dune yielded a moderately rich garnet-dominated  
 31  
 701 tHM suite with subordinate epidote and most zircon grains dated between 2.0 and 3.4 Ga, indicating  
 32  
 702 largely local provenance from the metamorphic basement of the Dete/Kamativi Inlier belonging to  
 33  
 703 the Paleoproterozoic Magondi Belt (Glynn et al., 2020).

704 On the opposite western side of the Kalahari, the Okahandja dune has feldspar-rich feldspatho-  
 42  
 705 quartzose composition with moderately rich amphibole-dominated tHM suite and mainly Cambrian-  
 43  
 706 Ediacaran zircon grains, indicating provenance dominantly from amphibolite-facies metamorphic  
 45  
 707 rocks exposed in the inland branch of the Damara orogen (Jung et al., 2007).

708 Consistently quartz-rich feldspatho-quartzose to quartzose composition and poor tHM suite  
 52  
 709 including common epidote associated with ZTR minerals and staurolite characterize sand in the  
 53  
 710 western Kalahari dunefield, where detrital-zircon ages are mostly Mesoproterozoic (Ectasian to  
 54  
 711 Stenian with peak around 1.3 Ga and subordinately late Paleoproterozoic with peak around 1.8 Ga).  
 55  
 712 Dune sand is inferred to have been largely derived from arc-related low-grade metasedimentary and  
 57  
 58  
 59  
 60  
 61  
 62  
 63  
 64  
 65



713 magmatic rocks of the Rehoboth terrane in the northwest (Becker et al., 2006) and from Damara,  
 1  
 714 Nama, and Karoo sedimentary and metasedimentary rocks. Clinopyroxene occurs in the northern  
 3  
 715 Hardap region, reflecting minor contribution from locally exposed Karoo basalts. Petrographic  
 4  
 6  
 716 composition is similar in the adjacent western SK dunefield, where garnet notably increases and  
 8  
 717 detrital-zircon ages are mainly Stenian (peak around 1.07 Ga), indicating extensive recycling of the  
 9  
 10  
 11  
 12  
 13  
 14  
 15  
 16  
 17  
 18  
 19  
 20  
 21  
 22  
 23  
 24  
 25  
 26  
 27  
 28  
 29  
 30  
 31  
 32  
 33  
 34  
 35  
 36  
 37  
 38  
 39  
 40  
 41  
 42  
 43  
 44  
 45  
 46  
 47  
 48  
 49  
 50  
 51  
 52  
 53  
 54  
 55  
 56  
 57  
 58  
 59  
 60  
 61  
 62  
 63  
 64  
 65

## 10. Fluvial-aeolian interactions and multistep recycling

The mineralogical composition of dunes and its variability across a sand sea reflect the relative importance of fluvial and aeolian processes and the degree of their interplay. Sand seas largely fed by river systems are typically characterized by partly first-cycle detritus including various amounts of diverse types of rock fragments, feldspars and heavy minerals, generally allowing identification of a single dominant source, as for the Namib Erg (Garzanti et al., 2012). The opposite end member is represented by dunefields where sand is dominantly generated *in situ* from disaggregation of locally exposed rocks with high sand-generation potential (e.g., quartz-rich sandstones) and next reworked and homogenized by winds during several sedimentary cycles. In these cases, sand

740 typically bears a distilled homogenous composition consisting almost exclusively of mostly  
 1  
 741 rounded monocrystalline quartz associated with an extremely poor tHM suite dominated by durable  
 3  
 742 ZTR minerals, as for the Sahara Desert ([Pastore et al., 2021](#)).

743 The geographic distribution of such contrasting desert types is mainly controlled by precipitation in  
 8  
 744 adjacent highlands fuelling fluvial discharge. In hyper-arid tropical deserts dominated by aeolian  
 10  
 745 dynamics, such as the Sahara or the Great Nafud in Arabia, river action may be weakened to the  
 13  
 746 point that fluvial supply to the dunes becomes insignificant. Conversely, dry river valleys are  
 15  
 747 invaded by pure quartzose sand, thus erasing all local sources of mineralogical heterogeneity  
 18  
 748 ([Garzanti et al., 2013, 2015a](#) p.46). Fluvial sources are instead readily identified for dunefields  
 20  
 749 accumulated in drylands at the foot of high mountain areas, as in central Asia or Argentina (e.g.,  
 23  
 750 [Rittner et al., 2016; Garzanti et al., 2019a, 2020, 2021b](#)).

751 The Kalahari Basin — which extends over twenty degrees of latitude, is characterized by a  
 28  
 752 pronounced increase in precipitation from the southwest to the subequatorial north, and has seen  
 30  
 753 repeated changes in climatic conditions through the recent and less recent past — provides both  
 33  
 754 end-member examples, as well as a series of intermediate situations. Sand mineralogy is rather  
 35  
 755 homogeneously pure quartzose in the relatively humid north (NWK, NEK, and EK dunefields), but  
 38  
 756 presents peculiar feldspar-rich or even lithic-rich compositions at both western and eastern margins  
 40  
 757 of the erg, where detrital modes with more abundant and varied tHM suites indicate largely first-  
 42  
 758 cycle supply from local rivers ([Fig. 10](#)).

759 Intermediate is the case of the WK dunefield in SE Namibia, where sand is quartz-rich but with a  
 47  
 760 significant amount of mostly K-feldspar, a few lithic fragments, and an up to moderately poor tHM  
 50  
 761 suite including not only epidote and staurolite but also amphibole and pyroxene locally, reflecting  
 52  
 762 deflation of fluvially transported sediments (cf. [Figs. 4E and 4F](#)).

763 In the NWK and NEK dunefields, as in Botswana, the coexistence of pure quartzose sand both in  
 57  
 764 rivers (Mucope, Okavango, Cuando, upper Zambezi, Rietfontein) and adjacent dunes (cf. [Figs. 4C](#)  
 59  
 765 and [4K](#) with [4D](#) and [4L](#)) makes it hard to discern how much of the river sand has ended up in the  
 62  
 63  
 64  
 65

dunes and, *vice versa*, how much of the river sand has been supplied by erosion and reworking of the dunes. Overall, most of the sand in all of the above-mentioned rivers must have been ultimately derived from reworking of Kalahari Group sediments, as most reliably assessed for Angolan rivers (e.g., Mucope and Cuando) that drain entirely within the erg. It is noteworthy that both river and dune sands along the final Chobe tract of the Cuando River get notably enriched in kyanite. This reveals mixing with sand originally fed by the upper Zambezi and reworked by the Cuando from the toe of the alluvial fan previously built by the Zambezi across the Okavango rift, between Lake Liambezi in the west and the Chobe depression in the east (Lake Caprivi of [Shaw and Thomas, 1988](#)).

In the opposite case, feldspar-rich or lithic-rich dune sand with similar mineralogy as river sediments nearby points to partly first-cycle origin and chiefly fluvial supply, followed by wind deflation and accumulation at the erg's margins with limited mixing with aeolian quartz (cf. [Figs. 4A, 4M, and 4O](#) with [4B, 4N, and 4P](#)). The proportion of aeolian Kalahari sand reworked in river sediments is readily identified by commonly rounded to subrounded monocrystalline quartz and thus easily calculated in these cases. Overwhelming in the Caculuar, Mucope, Okavango, Cuando, and Rietfontein Rivers ([Figs. 4C and 4I](#)), reworked aeolian quartz represents more than 90% of bulk sand in the upper Zambezi ([Fig. 4K](#)) and still ~85% upstream of Lake Kariba despite progressively increasing volcanoclastic supply across the basaltic gorges downstream of Victoria Falls. In Zambezi tributaries of western Zimbabwe, aeolian quartz is estimated to range from a minimum of ~35% in Matetsi sand up to 80-85% in Upper Gwai and Shangani sands ([Garzanti et al., 2014a](#)). Recycled aeolian monocrystalline quartz with rounded outlines or abraded overgrowths accounts for a large majority of the sand in the Molopo River ([Fig. 4G](#)).

## 11. Paleoweathering in the Kalahari

791 The extent to which a sediment has been subjected to chemical weathering, integrated over a series  
 1  
 792 of sedimentary cycles, can be evaluated by combining evidence from petrographic, heavy-mineral,  
 3  
 793 clay-mineral, and geochemical data.  
 4  
 5  
 6

794 Distilled multicyclic sand of northern Kalahari dunes and of the Okavango, Cuando, and upper  
 8  
 795 Zambezi Rivers is composed dominantly of quartz with strongly depleted tHM suites including  
 9  
 10  
 11  
 12  
 13  
 14  
 15  
 16  
 17  
 18  
 19  
 20  
 21  
 22  
 23  
 24  
 25  
 26  
 27  
 28  
 29  
 30  
 31  
 32  
 33  
 34  
 35  
 36  
 37  
 38  
 39  
 40  
 41  
 42  
 43  
 44  
 45  
 46  
 47  
 48  
 49  
 50  
 51  
 52  
 53  
 54  
 55  
 56  
 57  
 58  
 59  
 60  
 61  
 62  
 63  
 64  
 65

796 zircon, tourmaline, rutile, staurolite, and kyanite but virtually no garnet or apatite (both invariably  $\leq$   
 797 1%tHM; [Table 1](#)). The scarcity of garnet relative to staurolite, kyanite, andalusite, and sillimanite  
 798 [ $G/(G+SKA) < 5\%$  in both dune and river sands; [Fig. 10](#)] is anomalous, because these minerals are  
 799 associated in amphibolite-facies metapelites and unweathered detritus derived from them, where  
 800 garnet is typically dominant [ $G/(G+SKA) = 70\pm 20\%$ ; [Garzanti et al., 2006, 2010](#)].  
 801 The Okavango and Zambezi Rivers carry mud containing ~40% kaolinite (i.e., more than in any  
 802 other river sourced in tropical southern Africa; [Garzanti et al., 2014b](#)). Northern Kalahari dunes are  
 803 strongly depleted in most chemical elements but Si. Even Zr and Hf are low in both dune and river  
 804 sands ( $83\pm 55$  and  $2\pm 1$  ppm *versus* 190 and ~6 ppm in the Upper Continental Crust standard; [Taylor](#)  
 805 [and McLennan, 1995](#)), suggesting that all minerals including zircon are depleted relative to most  
 806 durable quartz. Among chemical indices of weathering ([Garzanti et al., 2014a, 2014b](#)),  $\alpha_{Na}^{Al}$  is  $> 3$   
 807 in Okavango, Cuando, and upper Zambezi fluvial sands, reaches  $> 5$  in dune sand, and is ~20 in  
 808 mud. The traditional WIP and CIA indices ([Parker, 1970](#); [Nesbitt and Young, 1982](#)) reach down to  
 809 0 and up to  $\geq 80$  in dune sand (down to 1 and up to  $\geq 90$  in river sand), with consequently extreme  
 810 CIA/WIP ratio reflecting extensive recycling ([Garzanti et al., 2019b](#)).

811 Pure quartzose sand lacking garnet in presence of common staurolite and kyanite, abundance of  
 812 kaolinite in mud, and chemical indices pointing at high weathering intensity cannot be the product  
 813 of a single sedimentary cycle in the current climatic setting. They require widespread recycling of  
 814 sediments affected by extensive chemical weathering in chemically much more aggressive hot-  
 815 humid climates of the past. All these pieces of evidence combined cannot be explained with  
 816 breakdown of all but the most durable minerals by grain-to-grain aeolian impacts, which prove to be

817 effective enough to round sand-sized silicate grains but far from efficient enough to systematically  
 1  
 818 destroy them mechanically ([Garzanti et al., 2015b](#); [Rittner et al., 2016](#); [Resentini et al., 2018](#)).  
 3  
 4  
 819 Detrital components of northern Kalahari dune sand must have undergone very extensive  
 5  
 6  
 820 weathering in humid subequatorial climate before being recycled during repeated episodes of  
 7  
 8  
 9  
 821 alternating fluvial and wind erosion, leading to their accumulation in the erg. In other words, they  
 10  
 11  
 822 represent the echo of paleo-weathering stages passed on to the present landscape through multiple  
 12  
 13  
 14  
 823 recycling episodes.  
 15  
 16

## 825 **12. Drainage integration as a driver of provenance change**

826  
 827 Sand seas such as the Kalahari or the Great Nafud and Rub'Al Khali in Arabia are huge reservoirs  
 23  
 24  
 828 of quartz-rich polycyclic sand trapped in the continental interiors. In the hyperarid climate of the  
 25  
 26  
 829 tropics, precipitation and runoff can be so scarce that ephemeral rivers are unable to carry sediment  
 27  
 28  
 830 across and beyond these vast rift-related sags, where they are dumped and multiply reworked while  
 29  
 30  
 31  
 831 remaining largely untapped for tens or even hundreds of million years.  
 32  
 33

832 In Arabia, sand seas are dominated by aeolian processes that drag sand uphill for hundreds of  
 34  
 35  
 833 kilometers from the Gulf coast inland across the Rub' Al Khali ([Garzanti et al., 2003, 2017](#)). Only a  
 36  
 37  
 834 trivial amount of aeolian sand has started to escape towards the Indian Ocean *via* Wadi  
 38  
 39  
 40  
 835 Hadhramaut-Masila, since this ephemeral river broke through the carbonate tableland representing  
 41  
 42  
 43  
 836 the shoulder of the Gulf of Aden rift ([Garzanti et al., 2001](#)). In the case of the Sahara, the Nile is the  
 44  
 45  
 46  
 837 only river that, before closure of the Aswan High Dam in 1964, possessed sufficient discharge and  
 47  
 48  
 49  
 838 competence to carry Saharan sand and silt as far as the sea (estimated as ~10% of its total sediment  
 50  
 51  
 839 load, which used to vary between  $\leq 50$  and  $\geq 300$  million tons/year; [Inman and Jenkyns, 1984](#);  
 52  
 53  
 840 [Garzanti et al., 2015a](#)). This is between one and two orders of magnitude less than the volume of  
 54  
 55  
 841 dust blown off the Sahara towards and beyond the Atlantic Ocean and the Mediterranean Sea,  
 56  
 57  
 58  
 842 estimated to range between 130-460 and 1400 million tons/year overall ([Goudie and Middleton,](#)  
 59  
 60  
 843 [2006](#); [Stuut et al., 2009](#) and references therein).  
 61  
 62  
 63  
 64  
 65

844 The amount of dust emissions from the Kalahari is much lower than for the Sahara ([Bhattachan et](#)  
1 [al., 2013](#)) and sediment exported to the ocean notably less, although diverse major rivers draining  
245 3 the dryland reach the coast. To the west, Kalahari sand supply to the Atlantic coast cannot be  
4 846 5 the dryland reach the coast. To the west, Kalahari sand supply to the Atlantic coast cannot be  
6  
747 8 estimated with forward-mixing calculations for the Congo River because it carries sediment  
9  
848 10 overwhelmingly recycled from multiple quartzose sandstone units, may represent up to 30% of  
11  
1249 12 Cuanza River sand (annual sediment load  $0.6\pm 0.1$  million tons, 43% mostly fine sand; [Holisticos,](#)  
13 [2012](#)), but is very minor for the Cunene River (although recycled aeolian sand accounts for ~15%  
14 850 15 of Cunene sand at the western edge of the Kalahari) and negligible for the Orange River (based on  
16  
1851 17 petrographic and heavy-mineral data in [Garzanti et al., 2014a, 2018a](#)). To the east, Kalahari sand is  
18  
19 852 20 conveyed towards the Indian Ocean only by the Zambezi River (annual sediment flux between 20  
21  
2253 22 and 100 million tons; [Hay, 1998](#)). At present, aeolian quartz grains representing ~85% of upper  
23  
2454 24 and 100 million tons; [Hay, 1998](#)). At present, aeolian quartz grains representing ~85% of upper  
25  
26 855 26 Zambezi sand are all trapped in Lake Kariba, but even before dam construction Kalahari sand  
27  
2856 27 accounted for no more than 10% of total Zambezi bedload ([Garzanti et al., 2021a](#)). The total  
28  
29 857 29 volume of Kalahari sand exported towards the oceans is thus of the same order of magnitude as the  
30  
31 858 30 endorheic Okavango sediment flux (between 0.2 and 2 million tons of mostly bedload sand recycled  
31  
32 859 31 from Kalahari dunes; [Shaw and Thomas 1992](#)). Hence, less than half of the sand eroded from  
32  
33 860 32 Kalahari dunes is exported towards the ocean today.  
33  
34 861 33 This budget, however, may have changed drastically and repeatedly in the past and may change  
34  
35 862 34 again in the future, depending on climatic conditions as well as on the balance between rejuvenated  
35  
36 863 35 subsidence in the Okavango Graben *versus* rejuvenated uplift of the African superswell ([Kinabo et](#)  
36  
37 864 36 [al., 2007](#); [Al-Hajri et al., 2009](#)). River piracy plays a fundamental role too, as emblematically  
37  
38 865 37 documented on both flanks of the Kalahari Plateau by the recent capture of formerly endorheic  
38  
39 866 38 Cunene and Zambezi drainage by headward eroding coastal rivers. Capture of the upper Zambezi  
39  
40 867 39 by the middle Zambezi is generally held to have occurred around early Pleistocene times ([Moore et](#)  
40  
41 868 40 [al., 2007](#)) but the upper Zambezi returned to be at least partly endorheic in the mid-Pleistocene, as  
41  
42 869 41 inferred from diverse mega-lake Makgadikgadi phases through the late Pleistocene ([Burrough et al.,](#)  
42  
43 870 42  
43  
44  
45  
46  
47  
48  
49  
50  
51  
52  
53  
54  
55  
56  
57  
58  
59  
60  
61  
62  
63  
64  
65

870 2009b; Moore et al., 2012). During this period of partly endorheic Zambezi floods (Burrough et al.,  
 1  
 871 2008), repeated drainage changes were induced by the evolution of the Okavango Graben (Vainer et  
 3  
 872 al., 2021). This tectonic depression finally diverted the Cuando River towards the Zambezi and is  
 4  
 6  
 873 presently favoring the capture of the Okavango as well, conveyed eastward along the Selinda  
 8  
 874 spillway (Gumbrecht et al. 2001).

11  
 1875 In a deeper past, a marked increase in monocrystalline quartz grains with rounded to subrounded  
 13  
 14  
 1876 outline and abraded overgrowths is documented in post-Tortonian strata of the Zambezi Delta  
 15  
 1877 subsurface (Chanvry et al., 2018), pointing to a sudden flux of recycled quartz-rich Kalahari sand  
 18  
 1878 from the continental interiors. A similar episode may well be repeated in the near future if the  
 20  
 21  
 1879 capture of the entire Okavango by the Zambezi River will proceed to the point that most of recycled  
 23  
 1880 Kalahari sand is conveyed towards the Indian Ocean.

25  
 26  
 1881 This argument highlights how tapping of huge sand reservoirs in continental interiors represents —  
 27  
 28  
 1882 besides tectonic activity, climate-induced chemical weathering, or dissolution during diagenesis —  
 30  
 31  
 1883 an effective potential factor that can produce significant pulses of mineralogical change (e.g.,  
 32  
 33  
 1884 stepwise up-section increase of recycled quartz grains) in coastal passive-margin and continental-  
 35  
 1885 embankment successions.

### 38 39 40 1887 **13. Conclusions**

42  
 1888  
 43  
 44  
 1889 Kalahari dune sands are homogeneously pure quartzose in Angola, Zambia, and over much of  
 45  
 46  
 1890 Botswana and parts of Zimbabwe and Namibia, where they contain mainly K-feldspar grains and  
 48  
 49  
 1891 strongly depleted heavy-mineral assemblages dominated by ZTR minerals and including common  
 50  
 51  
 1892 staurolite in Botswana and kyanite in Zambia, but no garnet. Composition varies markedly only at  
 52  
 53  
 1893 the western and eastern edges of the erg, ranging from feldspar-rich feldspatho-quartzose and  
 55  
 56  
 1894 hornblende-rich in the Damara Belt of central Namibia to quartzo-feldspathic and hornblende-rich  
 57  
 58  
 1895 in the Zimbabwe Craton or litho-quartzo-feldspathic and clinopyroxene-rich beside the Zambezi  
 60  
 1896 basaltic gorges near Victoria Falls. Compositionally distinct is the partially active western Kalahari

897 dunefield of SE Namibia, where sand is quartzose to quartz-rich feldspatho-quartzose with common  
 1  
 898 epidote, indicating partly first-cycle but largely polycyclic provenance from Mesoproterozoic  
 3  
 899 crustal domains, Damara Belt, and Nama and Karoo Groups.

900 U-Pb age spectra of detrital zircons allow discrimination among protosources of different ages in  
 8  
 901 various parts of the erg. Damara ages (0.45-0.65 Ga) are widespread and most abundant in dunes of  
 10  
 902 central Namibia. Namaqua-Irumide ages (1.0-1.1 Ga), also widespread, are particularly common in  
 13  
 903 dunes along the Botswana/South Africa border, increasing southward towards the Namaqua Belt.  
 15  
 904 Sinclair ages (1.2-1.4 Ga) characterize dunes in the western Kalahari dunefield of SE Namibia.  
 18  
 905 Eburnean ages (1.8-2.05 Ga) are most frequent in Angola and northernmost Botswana. Neoproterozoic  
 20  
 906 ages characterize dunes at the edge of the Zimbabwe and Kaapvaal Cratons in SW Zimbabwe and  
 23  
 907 SE Botswana. Cretaceous to Paleocene ages sparsely occur.

908 The compositional fingerprints of dune sand and their variability reflect the degree of interaction  
 26  
 909 between fluvial and aeolian processes across the sand sea. In northern Kalahari dunefields adjacent  
 30  
 910 to humid subequatorial regions, widespread monocrystalline quartz commonly showing abraded  
 32  
 911 overgrowths combined with strongly depleted ZTR-rich heavy-mineral assemblages lacking garnet  
 35  
 912 but containing staurolite and kyanite, common kaolinite in river muds, and geochemical indices  
 37  
 913 reveal that the sand has undergone very extensive weathering in humid subequatorial climate before  
 40  
 914 being presently stored into the erg. Dune sand composition thus reverberates the echo of paleo-  
 42  
 915 weathering passed on to the present landscape through multiple recycling episodes.

916 Intracratonic sag basins such as the Kalahari, straddling the arid tropical belt, contain vast amounts  
 47  
 917 of quartz-rich polycyclic sand. Whenever tectonic or climatic conditions favor the development of  
 49  
 918 an integrated drainage system connecting the continental interiors with the coast, tapping into such  
 52  
 919 a huge sediment reservoir may induce a sudden pulse of quartz-rich sand to the oceans and thus a  
 54  
 920 significant mineralogical change in continental-embankment successions. Such an event, recorded  
 57  
 921 in post-Tortonian sediments of the Zambezi Delta, may occur again in the near future if



922 development of the Okavango rift will lead to the incorporation of the entire Okavango River to the  
 1  
 923 Zambezi drainage system.

924

925

926

8

## 927 **Acknowledgments**

10

928

929 Several samples from the Kalahari Basin were obtained thanks to the generosity of Sallie Burrough,

13

930 Tom Kemp, and Matt Telfer. Most petrographic and heavy-mineral analyses were made by Giuditta

16

931 Radeff, Marta Padoan, and Mara Limonta. Marta Padoan helped substantially with the compilation

18

932 of geochronological ages and Martin Rittner with geochronological analyses. Editor Chris Fielding

21

933 and reviewers \_\_\_\_\_ provided constructive critical advice. This study was supported by MIUR

23

934 – Dipartimenti di Eccellenza 2018–2022, Department of Earth and Environmental Sciences,

26

935 University of Milano-Bicocca.

28

936

30

## 937 **Appendices - Supplementary Data**

32

938

939 Supplementary data associated with this article include information on sampling sites ([Table A1](#)),

36

940 together with the complete bulk-sand petrography ([Table A2](#)), heavy mineral ([Table A3](#)), and

38

941 detrital-zircon geochronology datasets ([Appendix B](#)). [Appendix C](#) presents a compilation of

41

942 numerous radiometric ages from diverse literature sources on modern sands, ancient sandstones,

43

943 and crustal domains in the areas described in this article. The Google-Earth™ map of sampling sites

46

944 [Kalahari.kmz](#) is also provided.

48

49

50

51

52

53

54

55

56

57

58

59

60

61

62

63

64

65

## 945 FIGURE AND TABLE CAPTIONS

1

946

3

4

947

5

6

948

8

9

949

10

11

12

950

13

14

951

15

16

952

17

18

19

953

20

21

954

22

23

24

955

25

26

956

27

28

957

29

30

958

31

32

959

33

34

960

35

36

961

37

38

962

39

40

963

41

42

964

43

44

965

45

46

966

47

48

967

49

50

968

51

52

969

53

54

970

55

56

971

57

58

972

59

60

973

61

62

974

63

64

975

65

**Figure 1.** The vast Kalahari Basin in southern Africa. **A)** Main regions and river courses. **B)** Relief map with sampling sites.

**Figure 2.** The Kalahari sand sea. **A)** Dune types, wind directions, and sand flow patterns (compiled after [Thomas and Shaw, 1991](#), [Nicholson, 1996](#), and [Haddon, 2005](#)). NWK, NEK, EK, WK, SK = northwestern, northeastern, eastern, western, and southern Kalahari; **B)** Rainfall map, showing increase in precipitation from south to north and from west to east across southern Africa. **C)** Distribution of climatic zones (Köppen–Geiger classification; [Kottek et al., 2006](#)): A = equatorial; B = arid; C = warm temperate. Precipitation: W = desert; S = steppe; f = fully humid; s = summer dry; w = winter dry. Temperature: h = hot arid; k = cold arid; a = hot summer; and b = warm summer.

**Figure 3.** Geology of southern Africa (compiled after [Schlüter, 2008](#) and other sources cited in text).

**Figure 4.** Comparison between the petrographic composition of fluvial and nearby aeolian-dune sands in the Kalahari Basin (photos arranged in geographical order: **A** to **H** from NW to SE in the west; **I** to **P** from W to E in the east). **A, B:** feldspar-rich feldspatho-quartzose sands (S4364 and E4875). **C, D:** pure quartzose sands (S4309 and E4889). Feldspatho-quartzose (**E:** S4313) and quartz-rich feldspatho-quartzose sands (**F:** NAM6/4/2). Quartz-rich feldspatho-quartzose (**G:** S5145) and pure quartzose sands (**H:** E5540). Pure quartzose sands (**I:** S4299, note weathered quartz to the right; **J:** NKALB, note ooids). **K, L:** pure quartzose sands (S4297 and E5481). Quartzo-lithic volcanoclastic (**M:** S4287) and litho-quartzo-feldspathic volcanoclastic sands (**N:** E4881, note rounded clinopyroxene). **O, P:** feldspatho-quartzose sands (S4284 and E4882). All photos with crossed polars; blue bar for scale = 100  $\mu\text{m}$ .

969 **Figure 5.** Petrography and heavy minerals in river (circles, above) and aeolian-dune sands (squares,  
 1 below). Q = quartz; F = feldspars; L= lithic fragments; ZTR = zircon + tourmaline + rutile; SKA =  
 970 3 staurolite + kyanite + andalusite + sillimanite; AGE = amphibole + garnet+ epidote. Besides sand  
 4  
 971 6 largely derived from Karoo basalts in western Zimbabwe, samples plot along the Q/F leg of the  
 972 8 triangle, with compositions ranging from quartzo-feldspathic (QF) and feldspatho-quartzose (FQ),  
 973 10 to quartzose (Q) and pure quartzose (pQ) (compositional fields after [Garzanti, 2019](#)). The Q/F ratio  
 1974 13 and ZTR parameter are indicators of selective chemical breakdown of less durable feldspars  
 14  
 1975 15 (generally plagioclase) and heavy minerals (largely garnet, amphibole, and epidote) integrated  
 16  
 1976 18 through repeated sedimentary cycles. Symbols for upstream samples in the same river system are  
 1977 20 smaller.  
 21  
 978 22

23  
 24  
 979 26 **Figure 6.** U-Pb age spectra of detrital zircons (age vs. frequencies plotted as Kernel Density  
 27  
 980 28 Estimates using the *provenance* package of [Vermeesch et al., 2016](#); complete dataset presented in  
 29  
 981 31 [Appendix B](#)). Age fingerprints are homogenized in the northern and central Kalahari but distinct at  
 30  
 982 33 the edges of the erg, where prominent Damara peaks in central Namibia and Archean ages in SW  
 34  
 983 35 Zimbabwe to SE Botswana reflect the time structure of source rocks in southern Africa ([Hanson,](#)  
 36  
 984 38 [2003](#); [Gärtner et al., 2014](#)).  
 39

40  
 985 41 **Figure 7.** Multidimensional scaling maps based on U-Pb age spectra of detrital zircons highlight the  
 42  
 986 43 degree of sand homogenization across various parts of the Kalahari Basin (axes units are normalised  
 44  
 987 46 values based on Kolmogorov-Smirnov distance). **A)** Comparison among age spectra of aeolian-  
 45  
 988 48 dune and river sands presented in [Fig. 6](#). Distinct provenance signatures are documented locally  
 49  
 989 51 (69% of ages  $\geq 2$  Ga in western Zimbabwe dunes; 54% Orosirian-Rhyacian ages in Mucope sand;  
 50  
 990 53 55% Tonian ages in Qangwa dune; 67% of Cambrian-Ediacaran ages in Okahandja dune; 61% of  
 54  
 991 56 Stenian-Ectasian ages in Western and western Southern Kalahari). **B)** Comparison among age  
 55  
 992 58 spectra of aeolian-dune sands from this study and literature data compiled in [Table 2](#). **C)**  
 59  
 993 60 Comparison between the cumulative age spectrum of aeolian dunes analysed in this study and all  
 61  
 994 63 potential sources and protosources (data compiled in [Table 2](#)). Closest and second closest  
 62  
 63  
 64  
 65

995 neighbours are linked by solid and dashed lines, respectively. The goodness of fit is evaluated using  
 1  
 996 the “stress” value of the configuration (0.2 = poor; 0.1 = fair; 0.05 = good; table 1 in [Vermeesch,](#)  
 3  
 4  
 997 [2013](#)).

998 **Figure 8.** Mineralogy of Kalahari dune sands discriminated with the compositional biplot (drawn  
 9  
 10  
 999 with CoDaPack software by [Comas-Cufí and Thió-Henestrosa, 2011](#)). Pure quartzose sand strongly  
 11  
 12  
 1000 depleted in all detrital components besides durable ZTR minerals, staurolite, kyanite, and andalusite  
 13  
 14  
 1001 dominates through the northern Kalahari and across the central erg in Botswana. Detritus from  
 15  
 16  
 1002 Precambrian bedrocks, significant in SE Namibia, is locally dominant at opposite edges of the erg  
 17  
 18  
 1003 in central Namibia and western Zimbabwe. Detritus from Karoo basalts, abundant near Victoria  
 19  
 20  
 1004 Falls, is only locally significant elsewhere. Lvm = volcanic and metavolcanic lithics; Lsm =  
 21  
 22  
 1005 sedimentary and metasedimentary lithics; tHMC =transparent heavy-mineral concentration; ZTR =  
 23  
 24  
 1006 zircon + tourmaline + rutile.

1007 **Figure 9.** Comparison between the mineralogy of river (circles) and aeolian-dune (squares) sands.  
 28  
 29  
 1008 The correspondence between mineralogical signatures of fluvial and nearby aeolian-dune sands  
 30  
 31  
 1009 indicates that pure quartzose polycyclic Kalahari sand mixes locally with first-cycle detritus from  
 32  
 33  
 1010 Archean to Cambrian bedrocks, as in western Zimbabwe and central Namibia. Because of arid  
 34  
 35  
 1011 conditions and high-frequency climatic fluctuations, exchange of sediment from river channels to  
 36  
 37  
 1012 dunefields and back has taken place repeatedly across the erg throughout the Quaternary.  
 38  
 39  
 1013 Parameters as in [Figs. 5 and 8](#).

1014 **Figure 10.** Provenance maps of the Kalahari Basin. Across most of the erg, dune sand has  
 44  
 45  
 1015 homogenized pure quartzose composition with depleted tHM suites lacking garnet. Mixing with  
 46  
 47  
 1016 locally supplied detritus including significant amounts of feldspars, rock fragments and heavy  
 48  
 49  
 1017 minerals including garnet occurs in seven areas: 1) inland branch of the Damara Belt; 2) SE  
 50  
 51  
 1018 Namibia; 3) near Aha Hills; 4) near Karoo basalts; 5) near Magondi Belt; 6) Zimbabwe Craton; 7)  
 52  
 53  
 54  
 55  
 56  
 57  
 58  
 59  
 60  
 61  
 62  
 63  
 64  
 65

1019 near Kaapvaal Craton. Lack of garnet from north to south across the central erg indicates intense  
 1  
 1020 weathering inherited from previous climatic stages.  
 2  
 3  
 4

1021 **Table 1.** Petrography and heavy minerals in river and dune sands of the Kalahari. Q = quartz; F =  
 5  
 6  
 7  
 1022 feldspars (P = plagioclase); L = lithic grains (Lvm = volcanic to very low-rank metavolcanic; Lsm =  
 8  
 9  
 1023 sedimentary and metasedimentary); MI\* = Metamorphic Index ([Garzanti and Vezzoli, 2003](#)).  
 10  
 11  
 1024 tHMC = transparent heavy minerals; ZTR = zircon + tourmaline + rutile; Ap = apatite; Ep =  
 12  
 13  
 14  
 1025 epidote; Grt = garnet; St = staurolite; Ky = kyanite; Amp = amphibole; Px = pyroxene; &tHM =  
 15  
 16  
 17  
 1026 other transparent heavy minerals (mostly andalusite, titanite, anatase, sillimanite, and locally olivine  
 18  
 19  
 1027 or monazite).  
 20  
 21  
 22

1028 **Table 2.** Age spectra of modern sands, ancient sandstones, and crustal domains in southern Africa  
 23  
 24  
 1029 (full dataset including 4224 ages from 107 literature sources provided in [Appendix C](#)). Age peaks  
 25  
 26  
 27  
 1030 and relative frequencies calculated with Density Plotter ([Vermeesch, 2012](#)).  
 28  
 29  
 30  
 31  
 32  
 33  
 34  
 35  
 36  
 37  
 38  
 39  
 40  
 41  
 42  
 43  
 44  
 45  
 46  
 47  
 48  
 49  
 50  
 51  
 52  
 53  
 54  
 55  
 56  
 57  
 58  
 59  
 60  
 61  
 62  
 63  
 64  
 65

## 1031 REFERENCES

- 1032  
1033 Al-Hajri, Y., White, N., Fishwick, S., 2009. Scales of transient convective support beneath Africa. *Geology*,  
1034 37(10), 883-886.
- 1035  
1036 Allen, P.A., 2017. *Sediment Routing Systems. The Fate of Sediments from Source to Sink*. Cambridge  
1037 University Press, Cambridge, 407 p.
- 1038  
1039 Andersen, T., Kristoffersen, M., Elburg, M.A., 2016. How far can we trust provenance and crustal evolution  
1040 information from detrital zircons? A South African case study. *Gondwana Research*, 34, 129–148.
- 1041  
1042 Andersen, T., Elburg, M.A., van Niekerk, H.S., Ueckermann, H., 2018. Successive sedimentary recycling  
1043 regimes in southwestern Gondwana: Evidence from detrital zircons in Neoproterozoic to Cambrian  
1044 sedimentary rocks in southern Africa. *Earth-Science Reviews*, 181, 43-60.
- 1045  
1046 Andò, S., Morton, A., Garzanti, E., 2014. Metamorphic grade of source rocks revealed by chemical  
1047 fingerprints of detrital amphibole and garnet. In: Scott, R.A., Smyth, H.R., Morton, A.C., Richardson, N.  
1048 (Eds.), *Sediment provenance studies in hydrocarbon exploration and production*. Geological Society  
1049 London, Special Publication 386, 351-371.
- 1050  
1051 Baillieul, T.A., 1975. A reconnaissance survey of the cover sands in the Republic of Botswana. *Journal of*  
1052 *Sedimentary Petrology*, 45, 494-503.
- 1053  
1054 Bateman, M.D., Thomas, D.S.G., Singhvi, A.K., 2003. Extending the aridity record of the Southwest  
1055 Kalahari: current problems and future perspectives. *Quaternary International*, 111, 37-49.
- 1056  
1057 Becker, T., Schreiber, U., Kampunzu, A.B., Armstrong, R., 2006. Mesoproterozoic rocks of Namibia and  
1058 their plate tectonic setting. *Journal of African Earth Sciences*, 46, 112-140.
- 1059  
1060 Bhattachan, A., D'Odorico, P., Okin, G.S., Dintwe, K., 2013. Potential dust emissions from the southern  
1061 Kalahari's dunelands. *Journal of Geophysical Research: Earth Surface*, 118(1), 307-314.
- 1062  
1063 Blanco, G., Germs, G.J.B, Rajesh, H.M, Chemale, F., Dussin, I.A., Justino, D., 2011. Provenance and  
1064 paleogeography of the Nama Group (Ediacaran to early Palaeozoic, Namibia): petrography, geochemistry  
1065 and U–Pb detrital zircon geochronology. *Precambrian Research*, 187, 15-32.
- 1066  
1067 Blenkinsop, T., Moore, A., 2013. Tectonic geomorphology of passive margins and continental hinterlands.  
1068 In: Shroder, J.F. (Ed.), *Treatise on Geomorphology*. Academic Press, San Diego, vol. 5, pp. 71-92.
- 1069  
1070 Boocock, C., Van Straten, O.J., 1962. Notes on the geology and hydrogeology of the central Kalahari region,  
1071 Bechuanaland Protectorate. *South African Journal of Geology*, 65(1), 125-176.
- 1072  
1073 Botha, G.A., 2000. Paleosols and duricrusts. In: Partridge, T.C. and Maud, R.M. (Eds.) *Cenozoic of Southern*  
1074 *Africa*. Oxford University Press, New York, Oxford Monographs on Geology and Geophysics, 40,  
1075 pp.131-144,
- 1076  
1077 Brook, G.A., Cowart, J.B., Brandt, S.A., 1998. Comparison of Quaternary environmental change in eastern  
1078 and southern Africa using cave speleothem, tufa and rock shelter sediment data. In: Alsharhan, G.,  
1079 Whittle, Kendall (Eds.), *Quaternary Deserts and Climate Change*. Balkema, Rotterdam, pp. 239–250.
- 1080  
1081 Brook, G.A., Scott, L. Railsback, L.B., Goddard, E.A., 2010. A 35 ka pollen and isotope record of  
1082 environmental change along the southern margin of the Kalahari from a stalagmite and animal dung  
1083 deposits in Wonderwerk Cave, South Africa. *Journal of Arid Environments*, 74, 870-884.
- 1084  
1085 Bullard, J.E., Nash, D.J., 1998. Linear dune pattern variability in the vicinity of dry valleys in the south-west  
1086 Kalahari. *Geomorphology*, 23, 35-54.

- 1072 Bullard, J.E., Nash, D.J., 2000. Valley-marginal sand dunes in the south-west Kalahari: their nature,  
1073 classification and possible origins. *Journal of Arid Environments*, 45, 369-383.  
2
- 1074 Bullard, J.E., Thomas, D.S.G., Livingstone, I., Wiggs, G.F.S., 1995. Analysis of linear sand dune  
1075 morphological variability, southwestern Kalahari dunefield. *Geomorphology*, 11, 189-203.  
4  
5
- 1076 Bultot, F., Griffiths, J.W., 1972. The equatorial wet zone. In: Griffiths, J.W. (Ed.), *Climates of Africa*.  
1077 Elsevier, Amsterdam, World Survey of Climatology, vol. 10, pp. 259–311.  
6  
7  
8
- 1078 Burrough, S.L., Thomas, D.S.G., 2008. Late Quaternary lake-level fluctuations in the Mababe Depression:  
1079 Middle Kalahari palaeolakes and the role of Zambezi inflows. *Quaternary Research*, 69, 388–403.  
9  
10
- 1080 Burrough, S.L., Thomas, D.S., Bailey, R.M., 2009a. Mega-Lake in the Kalahari: a Late Pleistocene record of  
1081 the Palaeolake Makgadikgadi system. *Quaternary Science Reviews*, 28(15-16), 1392-1411.  
11  
12  
13
- 1082 Burrough, S.L., Thomas, D.S., Singarayer, J.S., 2009b. Late Quaternary hydrological dynamics in the  
1083 Middle Kalahari: forcing and feedbacks. *Earth-Science Reviews*, 96(4), 313-326.  
14  
15  
16  
17  
18
- 1084 Burrough, S.L., Thomas, D.S.G., Barham, L.S., 2019. Implications of a new chronology for the  
1085 interpretation of the Middle and Later Stone Age of the upper Zambezi Valley. *Journal of Archaeological  
1086 Science: Reports*, 23, 376-389.  
19  
20  
21  
22  
23
- 1087 Caracciolo, L., 2020. Sediment generation and sediment routing systems from a quantitative provenance  
1088 analysis perspective: Review, application and future development. *Earth-Science Reviews*, 209, 103226.  
24  
25  
26
- 1089 Catuneanu, O., Wopfner, H., Eriksson, P.G., Cairncross, B., Rubidge, B.S., Smith, R.M.H., Hancox, P.J.,  
1090 2005. The Karoo basins of south-central Africa. *Journal of Asian Earth Sciences*, 43, 211-253.  
27  
28  
29
- 1091 Chanvry, E., Ando, S., Garzanti, E., Guillocheau, F., Dall'Asta, M., Beaufort, D., Patrier, P., 2018. Impact of  
1092 hinterland evolution in mineralogy of clastics sediments: first results from mineralogical analysis focus on  
1093 the Zambezi system during Meso-Cenozoic times. *EGU General Assembly Conference Abstracts*, p.  
1094 18077.  
30  
31  
32  
33  
34  
35
- 1095 Comas-Cufí, M., Thió-Henestrosa, F.S., CoDaPack 2.0: a stand-alone, multi-platform compositional  
1096 software.  
36  
37  
38
- 1097 Cook, K., 2000. The South Indian convergence zone and interannual rainfall variability over southern  
1098 Africa. *Journal of Climate*, 13, 3789–3804.  
39  
40  
41
- 1099 De Carvalho, H., Tassinari, C., Alves, P.H., Guimarães, F., Simões, M.C., 2000. Geochronological review of  
1100 the Precambrian in western Angola: links with Brazil. *Journal of African Earth Sciences*, 31, 383–402.  
42  
43  
44  
45
- 1101 De Ploey, J., Lepersonne, J., Stopps, G., 1968. Sédimentologie et origine de sables de la Série des "Grès  
1102 polymorphes"(Système du Kalahari) au Congo occidental. *Musée royal de L'Afrique Centrale Tervuren,  
1103 Belgique*, 61, 72 p.  
46  
47  
48  
49
- 1104 De Wit, M., 2007. The Kalahari Epeirogeny and climate change: differentiating cause and effect from core to  
1105 space. *South African Journal of Geology*, 110(2-3), 367-392.  
50  
51  
52
- 1106 Dirks, P.H.G.M., Blenkinsop, T.G., Jelsma, H.A., 2009. The Geological Evolution of Africa. In: De Vito, B.,  
1107 Grasemann, B., Stuwe, K. (Eds.), *Geology. Encyclopedia of Life Support Systems*, vol. IV., EOLSS  
1108 Publishers, Paris, 978-1-84826-457-1, pp. 230-251.  
53  
54  
55  
56  
57
- 1109 Du Toit, A.L., 1954. *Geology of South Africa*. Oliver & Boyd, London, 611 p.  
58  
59  
60  
61  
62  
63  
64  
65

- 1110 East, A.E., Clift, P.D., Carter, A., Alizai, A., Van Laningham, S., 2015. Fluvial-eolian interactions in  
 1111 sediment routing and sedimentary signal buffering: an example from the Indus Basin and Thar Desert.  
 1112 Journal of Sedimentary Research, 85, 715-728.
- 1113 Eglinger, A., Vanderhaeghe, O., André-Mayer, A.S., Goncalves, P., Zeh, A., Durand, C., Deloule, E., 2016.  
 1114 Tectono-metamorphic evolution of the internal zone of the Pan-African Lufilian orogenic belt (Zambia):  
 1115 Implications for crustal reworking and syn-orogenic uranium mineralizations. *Lithos*, 240, 167-188.
- 1116 Eglington, B.M. 2006. Evolution of the Namaqua–Natal Belt, southern Africa—a geochronological and  
 1117 isotope geochemical review. *Journal of African Earth Sciences*, 46, 93-111.
- 1118 Eglington, B.M., Armstrong, R.A. 2004. The Kaapvaal Craton and adjacent orogens, Southern Africa: a  
 1119 geochronological database and overview of the geological development of the craton. *South African  
 1120 Journal of Geology*, 107, 13-32.
- 1121 Feller, W., 1948. On the Kolmogorov-Smirnov limit theorems for empirical distributions. *Annals of  
 1122 Mathematical Statistics*, 19, 177-189.
- 1123 Frimmel, H.E., Basei, M.S., Gaucher, C. 2011. Neoproterozoic geodynamic evolution of SW-Gondwana: a  
 1124 southern African perspective. *International Journal of Earth Sciences*, 100, 323-354.
- 1125 Gabriel, K.R., 1971. The biplot graphic display of matrices with application to principal component analysis.  
 1126 *Biometrika*, 58, 453-467.
- 1127 Galehouse, J.S., 1971. Point counting. In: Carver, R.E. (Ed.), *Procedures in sedimentary petrology*. Wiley,  
 1128 New York, pp. 385-407.
- 1129 Gärtner, A., Linnemann, U., Hofmann, M., 2014. The provenance of northern Kalahari Basin sediments and  
 1130 growth history of the southern Congo Craton reconstructed by U–Pb ages of zircons from recent river  
 1131 sands. *International Journal of Earth Sciences*, 103(2), 579-595.
- 1132 Garzanti, E., 2016. From static to dynamic provenance analysis – Sedimentary petrology upgraded. In:  
 1133 Caracciolo, L., Garzanti, E., von Eynatten, H., Weltje, G.J. (Eds.), *Sediment generation and provenance:  
 1134 processes and pathways*. *Sedimentary Geology*, 336, 3-13.
- 1135 Garzanti E., 2017. The maturity myth in sedimentology and provenance analysis. *Journal of Sedimentary  
 1136 Research*, 87, 353-365.
- 1137 Garzanti, E., 2019. Petrographic classification of sand and sandstone. *Earth-Science Reviews*, 192, 545-563.
- 1138 Garzanti, E., Andò, S., 2007. Heavy-mineral concentration in modern sands: implications for provenance  
 1139 interpretation. In: Mange, M.A., Wright, D.T. (Eds.), *Heavy minerals in use*. Elsevier, Amsterdam,  
 1140 *Developments in Sedimentology Series*, 58, pp. 517-545.
- 1141 Garzanti, E., Andò, S., 2019. Heavy Minerals for Junior Woodchucks. *Minerals*, 9(3), 148,  
 1142 doi:10.3390/min9030148.
- 1143 Garzanti, E., Vezzoli, G. 2003. A classification of metamorphic grains in sands based on their composition  
 1144 and grade. *Journal of Sedimentary Research*, 73, 830-837.
- 1145 Garzanti, E., Vezzoli, G., Ando, S., Castiglioni, G., 2001. Petrology of rifted-margin sand (Red Sea and Gulf  
 1146 of Aden, Yemen). *The Journal of Geology*, 109(3), 277-297.
- 1147 Garzanti, E., Ando, S., Vezzoli, G., Dell'Era, D., 2003. From rifted margins to foreland basins: investigating  
 1148 provenance and sediment dispersal across desert Arabia (Oman, UAE). *Journal of Sedimentary Research*,  
 1149 73(4), 572-588.



- 1150 Garzanti, E., Ando, S., Vezzoli, G., 2006. The continental crust as a source of sand (southern Alps cross  
1151 section, northern Italy). *The Journal of Geology*, 114(5), 533-554.  
2
- 1152 Garzanti, E., Resentini, A., Vezzoli, G., Ando, S., Malusa, M.G., Padoan, M., Paparella, P., 2010. Detrital  
1153 fingerprints of fossil continental-subduction zones (Axial Belt Provenance, European Alps). *The Journal*  
1154 *of Geology*, 118(4), 341-362.  
6
- 1155 Garzanti, E., Andò, S., Vezzoli, G., Lustrino, M., Boni, M., Vermeesch, P., 2012. Petrology of the Namib  
1156 sand sea: long-distance transport and compositional variability in the wind-displaced Orange Delta. *Earth-*  
1157 *Science Reviews*, 11, 173-189.  
11
- 1158 Garzanti, E., Vermeesch, P., Andò, S., Vezzoli, G., Valagussa, M., Allen, K., Kadi, K.A., Al-Juboury, A.I.,  
1159 2013. Provenance and recycling of Arabian desert sand. *Earth-Science Reviews*, 120, 1-19.  
13  
14
- 1160 Garzanti, E., Vermeesch, P., Padoan, M., Resentini, A., Vezzoli, G., Andò, S., 2014a. Provenance of passive-  
1161 margin sand (southern Africa). *The Journal of Geology*, 122, 17-42.  
15  
16
- 1162 Garzanti, E., Padoan, M., Setti, M., López-Galindo, A., Villa, I.M., 2014b. Provenance versus weathering  
1163 control on the composition of tropical river mud (southern Africa). *Chemical Geology*, 366, 61-74.  
18  
19
- 1164 Garzanti, E., Andò, S., Padoan, M., Vezzoli, G., El Kammar, A., 2015a. The modern Nile sediment  
1165 system: Processes and products. *Quaternary Science Reviews*, 130, 9-56.  
21  
22  
23  
24
- 1166 Garzanti, E., Resentini, A., Andò, S., Vezzoli, G., Vermeesch, P., 2015b. Physical controls on sand  
1167 composition and relative durability of detrital minerals during long-distance littoral and eolian transport  
1168 (coastal Namibia). *Sedimentology*, 62, 971-996.  
25  
26  
27  
28  
29
- 1169 Garzanti, E., Vermeesch, P., Al-Ramadan, K.A., Andò, S., Limonta, M., Rittner, M., Vezzoli, G., 2017.  
1170 Tracing transcontinental sand transport: from Anatolia–Zagros to the Rub'Al Khali Sand Sea. *Journal of*  
1171 *Sedimentary Research*, 87(11), 1196-1213.  
31  
32  
33
- 1172 Garzanti, E., Dinis, P., Vermeesch, P., Andò, S., Hahn, A., Huvi, J., Limonta, M., Padoan, M., Resentini, A.,  
1173 Rittner, M., Vezzoli, G., 2018a. Dynamic uplift, recycling, and climate control on the petrology of  
1174 passive-margin sand (Angola). *Sedimentary Geology*, 375, 86-104.  
34  
35  
36  
37  
38
- 1175 Garzanti, E., Vermeesch, P., Rittner, M., Simmons, M., 2018b. The zircon story of the Nile: Time- structure  
1176 maps of source rocks and discontinuous propagation of detrital signals. *Basin Research*, 30, 1098-1117.  
39  
40  
41
- 1177 Garzanti, E., Ghassemi, M.R., Limonta, M., Resentini, A., 2019a. Provenance of Karakum Desert sand  
1178 (Turkmenistan): lithic-rich orogenic signature of central Asian dune fields. *Rivista Italiana di*  
1179 *Paleontologia e Stratigrafia*, 125(1), 77-89.  
42  
43  
44  
45  
46
- 1180 Garzanti, E., Vermeesch, P., Vezzoli, G., Andò, S., Botti, E., Limonta, M., Dinis, P., Hahn, A., Baudet, D.,  
1181 De Grave, J., Yaya, N.K., 2019b. Congo River sand and the equatorial quartz factory. *Earth-Science*  
1182 *Reviews*, 197, 102918.  
47  
48  
49  
50
- 1183 Garzanti, E., Liang, W., Andò, S., Clift, P.D., Resentini, A., Vermeesch, P., Vezzoli, G., 2020. Provenance  
1184 of Thal Desert sand: Focused erosion in the western Himalayan syntaxis and foreland-basin deposition  
1185 driven by latest Quaternary climate change. *Earth-Science Reviews*, 207, 103220.  
51  
52  
53  
54  
55
- 1186 Garzanti, E., Pastore, G., Resentini, A., Vezzoli, G., Vermeesch, P., Ngube, L., Van Niekerk, E., Jouet, G.,  
1187 Dall'Asta, M., 2021a. The segmented Zambezi sedimentary system from source to sink 1. Sand petrology  
1188 and heavy minerals. *The Journal of Geology*, <https://doi.org/10.1086/715792>.  
56  
57  
58  
59

- 1189 Garzanti, E., Capaldi, T., Vezzoli, G., Limonta, M., Vezzoli, G., Sosa, N., 2021b. Transcontinental retroarc  
 1190 sediment routing controlled by subduction geometry and climate change (Central and Southern Andes,  
 1191 Argentina). *Basin Research*, <https://doi.org/10.1111/bre.12607>.
- 1192 Glynn, S.M., Master, S., Frei, D., Wiedenbeck, M., 2020. U-Pb zircon geochronology of the Dete-Kamativi  
 1193 Inlier, NW Zimbabwe, with implications for the western margin of the Archaean Zimbabwe Craton.  
 1194 *Precambrian Research*, 346, 105824.
- 1195 Goscombe, B., Foster, D.A., Gray, D., Wade, B., 2020. Assembly of central Gondwana along the Zambezi  
 1196 Belt: Metamorphic response and basement reactivation during the Kuunga Orogeny. *Gondwana Research*,  
 1197 80, 410-465.
- 1198 Goudie, A.S., 2020. Duricrusts and landforms. In: Richards, K.S., Arnett, R.R., Ellis, S. (Eds.),  
 1199 *Geomorphology and soils*. Routledge, Milton Park (UK), ch. 2, pp. 37-57.
- 1200 Goudie, A.S., Middleton, N.J., 2006. Desert dust in the global system. Springer Science & Business Media.  
 1201 Berlin, 286 p.
- 1202 Goudie A.S., Thomas, D.S.G., 1985. Pans in southern Africa with particular reference to South Africa and  
 1203 Zimbabwe. *Zeitschrift für Geomorphologie N.F.*, 29(1), 1-19.
- 1204 Goudie, A., Viles, H., 2015. *Landscapes and Landforms of Namibia*. Springer Netherlands, 173 p.
- 1205 Greber, N.D., Davies, J.H., Gaynor, S.P., Jourdan, F., Bertrand, H., Schaltegger, U., 2020. New high  
 1206 precision U-Pb ages and Hf isotope data from the Karoo large igneous province; implications for pulsed  
 1207 magmatism and early Toarcian environmental perturbations. *Results in Geochemistry*, 1, 100005.
- 1208 Griffin, W.L., Powell, W.J., Pearson, N.J., O'Reilly, S.Y., 2008. GLITTER: data reduction software for laser  
 1209 ablation ICP-MS. *Laser Ablation-ICP-MS in the earth sciences*. Mineralogical association of Canada  
 1210 short course series, 40, 204-207.
- 1211 Gumbrecht, T., McCarthy, T.S., Merry, C.L., 2001. The topography of the Okavango Delta, Botswana, and  
 1212 its tectonic and sedimentological implications. *South African Journal of Geology*, 104(3), 243-264.
- 1213 Haddon, I.G., 2005. The sub-Kalahari geology and tectonic evolution of the Kalahari Basin, southern Africa.  
 1214 Unpublished Ph. D. thesis, University of the Witwatersrand, Johannesburg, 346 p.
- 1215 Haddon, I.G., McCarthy, T.S., 2005. The Mesozoic–Cenozoic interior sag basins of Central Africa: the Late-  
 1216 Cretaceous–Cenozoic Kalahari and Okavango basins. *Journal of African Earth Sciences*, 43, 316-333.
- 1217 Hall, W.S., Hitzman, M.W., Kuiper, Y.D., Kylander-Clark, A.R., Holm-Denoma, C.S., Moscati, R.J., Plink-  
 1218 Björklund, P., Enders, M.S., 2018. Igneous and detrital zircon U-Pb and Lu-Hf geochronology of the late  
 1219 Meso-to Neoproterozoic northwest Botswana rift: Maximum depositional age and provenance of the  
 1220 Ghanzi Group, Kalahari Copperbelt, Botswana and Namibia. *Precambrian Research*, 318, 133-155.
- 1221 Hanson, R.E. 2003. Proterozoic geochronology and tectonic evolution of southern Africa. In: Yoshida, M.;  
 1222 Windley, B.F.; and Dasgupta, S. eds. *Proterozoic East Gondwana: supercontinent assembly and breakup*.  
 1223 Geological Society, London, Special Publications, 206, 427-463.
- 1224 Hanson, R.E., Harmer, R.E., Blenkinsop, T.G., Bullen, D.S., Dalziel, I.W.D., Gose, W.A., Hall, R.P.,  
 1225 Kampunzu, A.B., Key, R.M., Mukwakwami, J., Munyanyiwa, H., Pancake, J.A., Seidel, E.K., Ward, S.E.,  
 1226 2006. Mesoproterozoic intraplate magmatism in the Kalahari Craton: a review. *Journal of African Earth  
 1227 Sciences*, 46, 141-167.

- 1228 Hargrove, U.S., Hanson, R.E., Martin, M.W., Blenkinsop, T.G., Bowring, S.A., Walker, N., Munyanyiwa,  
1229 H., 2003. Tectonic evolution of the Zambezi orogenic belt: geochronological, structural, and petrological  
1230 constraints from northern Zimbabwe. *Precambrian Research*, 123(2-4), 159-186.
- 1231 Hay, W.W., 1998. Detrital sediment fluxes from continents to oceans. *Chemical geology*, 145(3-4), 287-323.
- 1232 Hipondoka, M.H.T., Mauz, B., Kempf, J., Packman, S., Chiverrell, R.C., Bloemendal, J., 2014. Chronology  
1233 of sand ridges and the Late Quaternary evolution of Etosha Pan, Namibia. *Geomorphology*, 204, 553-563.
- 1234 Holisticos, 2012. Environmental Impact Study for the Rehabilitation and Expansion of the Cambambe  
1235 Hydroelectric Power Plant. <https://www.miga.org/documents/Angola> Cambambe\_HPP\_EIS.pdf.
- 1236 Holmgren, K., Karlén, W., Shaw, P. A., 1995. Paleoclimatic significance of the stable isotopic composition  
1237 and petrology of a Late Pleistocene stalagmite from Botswana. *Quaternary Research*, 32, 320-328.
- 1238 Holmgren, K., Lee-Thorp, J.A., Cooper, G.R., Lundblad, K., Partridge, T.C., Scott, L., Sithaldeen, R.,  
1239 Talma, A.S., Tyson, P.D., 2003. Persistent millennial-scale climatic variability over the past 25,000 years  
1240 in Southern Africa. *Quaternary Science Reviews*, 22(21-22), 2311-2326.
- 1241 Holzkämper, S., Holmgren, K., Lee-Thorp, J. L., Talma, S., Mangini, A., Partridge, T., 2009. Late  
1242 Pleistocene stalagmite growth in Wolkberg Cave, South Africa. *Earth and Planetary Science Letters*, 282,  
1243 212-221.
- 1244 Houben, G.J., Kaufhold, S., Miller, R.M., Lohe, C., Hinderer, M., Noll, M., Hornung, J., Joseph, R., Gerdes,  
1245 A., Sitnikova, M., Quinger, M., 2020. Stacked megafans of the Kalahari Basin as archives of  
1246 paleogeography, river capture, and Cenozoic paleoclimate of southwestern Africa. *Journal of*  
1247 *Sedimentary Research*, 90(9), 980-1010.
- 1248 Hubert, J.F., 1962. A zircon–tourmaline–rutile maturity index and the interdependence of the composition of  
1249 heavy mineral assemblages with the gross composition and texture of sandstones. *Journal of Sedimentary*  
1250 *Petrology*, 32, 440-450.
- 1251 Huntsman-Mapila, P., Kampunzu, A.B., Vink, B., Ringrose, S., 2005. Cryptic indicators of provenance from  
1252 the geochemistry of the Okavango Delta sediments, Botswana. *Sedimentary Geology*, 174(1-2), 123-148.
- 1253 Hürkamp, K., Völkel, J., Heine, K., Bens, O., Leopold, M., Winkelbauer, J., 2011. Late Quaternary  
1254 environmental changes from aeolian and fluvial geoarchives in the southwestern Kalahari, South Africa:  
1255 implications for past African climate dynamics. *South African Journal of Geology*, 114 (3–4), 459–474.
- 1256 Ingersoll, R.V., Bullard, T.F., Ford, R.L., Grimm, J.P., Pickle, J.D., Sares, S.W., 1984. The effect of grain  
1257 size on detrital modes: a test of the Gazzi-Dickinson point-counting method. *Journal of Sedimentary*  
1258 *Petrology*, 54, 103-116.
- 1259 Inman, D.L., Jenkins, S.A., 1984. The Nile littoral cell and man's impact on the coastal zone of the  
1260 southeastern Mediterranean. *Coastal Engineering*, ch. 109, 1600-1617.
- 1261 Jackson, S.E., Pearson, N.J., Griffin, W.L., Belousova, E.A., 2004. The application of laser ablation-  
1262 inductively coupled plasma-mass spectrometry to in situ U–Pb zircon geochronology. *Chemical Geology*,  
1263 211, 47-69.
- 1264 Jacobs, J., Pisarevsky, S., Thomas, R.J., Becker, T. 2008. The Kalahari Craton during the assembly and  
1265 dispersal of Rodinia. *Precambrian Research*, 160, 142-158.
- 1266 Jelsma, H.A., Dirks, P.H.G.M., 2002. Neoarchean tectonic evolution of the Zimbabwe Craton. In: Fowler, C.  
1267 M.R., Ebinger, C.J., Hawkesworth, C.J. (Eds), *The early Earth: physical, chemical and biological*  
1268 *development*. Geological Society London, Special Publication 199, 183-211.

- 1269 Jelsma, H.A., McCourt, S., Perritt, S.H., Armstrong R.A., 2018. The Geology and Evolution of the Angolan  
1270 Shield, Congo Craton. In Siegesmund, S., Basei, M., Oyhantçabal, P., Oriolo, S. (Eds.), *Geology of*  
1271 *Southwest Gondwana. Regional Geology Reviews.* Springer, Cham, pp. 217-239.  
1272 [https://doi.org/10.1007/978-3-319-68920-3\\_9](https://doi.org/10.1007/978-3-319-68920-3_9).
- 1273 John, T., Schenk, V., Mezger, K., Tembo, F., 2004. Timing and PT evolution of whiteschist metamorphism  
1274 in the Lufilian Arc–Zambezi Belt orogen (Zambia): implications for the assembly of Gondwana. *The*  
1275 *Journal of Geology*, 112(1), 71-90.
- 1276 Johnson, M.R., 1991. Sandstone petrography, provenance and plate tectonic setting in Gondwana context of  
1277 the southeastern Cape-Karoo Basin. *South African Journal of Geology*, 94(2), 137-154.
- 1278 Johnson, M.R., van Vuuren, C.J., Hegenberger, W.F., Key, R., Shoko, U. 1996. Stratigraphy in the Karoo  
1279 Supergroup in southern Africa: an overview. *Journal of African Earth Sciences*, 23, 3-15.
- 1280 Jung, S., Hoffer, E., Hoernes, S., 2007. Neo-Proterozoic rift-related syenites (Northern Damara Belt,  
1281 Namibia): Geochemical and Nd–Sr–Pb–O isotope constraints for mantle sources and petrogenesis. *Lithos*,  
1282 96, 415-435.
- 1283 Kampunzu, A.B., Cailteux, J., 1999. Tectonic evolution of the Lufilian Arc (Central Africa Copper Belt)  
1284 during Neoproterozoic Pan African orogenesis. *Gondwana Research*, 2(3), 401-421.
- 1285 Kampunzu, A.B., Ringrose, S., Huntsman-Mapila, P., Harris, C., Vink, B. W., Matheson, W., 2007. Origins  
1286 and palaeo-environments of Kalahari duricrusts in the Moshaweng dry valleys (Botswana) as detected  
1287 by major and trace element composition. *Journal of African Earth Sciences*, 48(2-3), 199-221.
- 1288 Kinabo, B.D., Atakwana, E.A., Hogan, J.P., Modisi, M.P., Wheaton, D.D., Kampunzu, A.B., 2007. Early  
1289 structural development of the Okavango rift zone, NW Botswana. *Journal of African Earth Sciences*, 48,  
1290 125–136.
- 1291 Kiss, T., Sipos, G., Kovács, F., 2009. Human impact on fixed sand dunes revealed by morphometric analysis.  
1292 *Earth Surface Processes and Landforms*. 34(5), 700-711.
- 1293 Klöcking M., Hoggard, M.J., Tribaldos, V.R., Richards, F.D., Guimarães, A.R., MacLennan, J., White, N.J.,  
1294 2020. A tale of two domes: Neogene to recent volcanism and dynamic uplift of northeast Brazil and  
1295 southwest Africa. *Earth and Planetary Science Letters*, 547, 116464.
- 1296 Kottek, M., Grieser, J., Beck, C., Rudolf, B., Rubel, F., 2006. World map of the Köppen–Geiger climate  
1297 classification updated. *Meteorologische Zeitschrift*, 15, 259–263.
- 1298 Kruskal, J.B., Wish, M., 1978. *Multidimensional scaling.* Sage Publications, Newbury Park (CA),  
1299 *Quantitative applications in the social sciences*, Sage University Paper Series 07-011, 92 p.
- 1300 Kulongoski, J.T., Hilton, D.R., Selaolo, E.T., 2004. Climate variability in the Botswana Kalahari from the  
1301 late Pleistocene to the present day. *Geophysical Research Letters*, 31, L10204.
- 1302 Kusky, T.M. 1998. Tectonic setting and terrane accretion of the Archean Zimbabwe craton. *Geology*, 26,  
1303 163-166.
- 1304 Lancaster, N., 1978. The Pans of the southern Kalahari, Botswana. *The Geographical Journal*, 144, 81-98.
- 1305 Lancaster, N., 1979. Quaternary environments in the arid zone of southern Africa, Dept. Geogr. and Envir.  
1306 *Studies, Occ. Pap. 22*, pp. 73, Univ. Witswatersrand, Johannesburg
- 1307 Lancaster, N., 1981. Palaeoenvironmental implications of fixed dune systems in southern Africa.  
1308 *Palaeogeography, Palaeoclimatology, Palaeoecology*, 33(4), 327-346.

- 1309 Lancaster, N., 1986. Pans in the southwestern Kalahari: a preliminary report. In: Southern African society for  
1310 Quaternary research. Biennial conference, 7, pp. 59-67.  
2
- 1311 Lanci, L., Tohver, E., Wilson, A., Flint, S., 2013. Upper Permian magnetic stratigraphy of the lower Beaufort  
1312 group, Karoo basin. *Earth and Planetary Science Letters*, 375, 123-134.  
4  
5
- 1313 Lehmann, J., Saalman, K., Naydenov, K.V., Milani, L., Belyanin, G.A., Zwingmann, H., Charlesworth, G.,  
1314 Kinnaird, J.A., 2016. Structural and geochronological constraints on the Pan- African tectonic evolution  
1315 of the northern Damara Belt, Namibia. *Tectonics*, 35(1), 103-135.  
6  
7
- 1316 Ludwig, K.R., 1998. On the treatment of concordant uranium-lead ages. *Geochimica et Cosmochimica Acta*,  
1317 62, 665-676.  
8  
9
- 1318 Lukich, V., Porat, N., Faershtein, G., Cowling, S., Chazan, M., 2019. New chronology and stratigraphy for  
1319 Kathu Pan 6, South Africa. *Journal of Palaeolithic Archaeology*, 2, 235-257.  
10  
11
- 1320 Lukich, V., Cowling, S., Chazan, M., 2020. Palaeoenvironmental reconstruction of Kathu Pan, South Africa,  
1321 based on sedimentological data. *Quaternary Science Reviews*, 230, 106153.  
12  
13
- 1322 Lutjeharms, J.R.E., Van Ballegooyen, R.C., 1988. The retroflection of the Agulhas Current. *Journal of*  
1323 *Physical Oceanography*, 18(11), 1570-1583.  
14  
15
- 1324 Matmon, A., Hidy, A.J., Vainer, S., Crouvi, O., Fink, D., Erel, Y., Arnold, M., Aumaître, G., Bourlès, D.,  
1325 Keddadouche, K., Horwitz, L.K., Chazan, M., 2015. New chronology for the southern Kalahari Group  
1326 sediments with implications for sediment-cycle dynamics and early hominin occupation. *Quaternary*  
1327 *Research*, 84, 118-132.  
16  
17
- 1328 Matmon, A., Enzel, Y., Vainer, S., Grodek, T., Mushkin, A., and ASTER Team, 2018. The near steady state  
1329 landscape of western Namibia. *Geomorphology*, 313, 72-87.  
18  
19
- 1330 Mayaud, J.R., Bailey, R.M., Wiggs, G.F., 2017. Modelled responses of the Kalahari Desert to 21<sup>st</sup> century  
1331 climate and land use change. *Scientific reports*, 7(1), 3887, doi:10.1038/s41598-017-04341-0.  
20  
21
- 1332 McCarthy, T.S., Ellery, W.N., 1995. Sedimentation on the distal reaches of the Okavango Fan, Botswana,  
1333 and its bearing on calcrete and silcrete (ganister) formation. *Journal of Sedimentary Research*, 65(1a),  
1334 77-90.  
22  
23
- 1335 McCarthy, T.S., Ellery, W.N., 1998. The Okavango delta. *Transactions of the Royal Society of South Africa*,  
1336 53(2), 157-182.  
24  
25
- 1337 McCarthy, T.S., Metcalfe, J., 1990. Chemical sedimentation in the semi-arid environment of the Okavango  
1338 Delta, Botswana. *Chemical Geology*, 89, 157-178.  
26  
27
- 1339 McCourt, S., Armstrong, R.A., Jelsma, H., Mapeo, R.B.M., 2013. New U–Pb SHRIMP ages from the  
1340 Lubango region, SW Angola: insights into the Palaeoproterozoic evolution of the Angolan Shield,  
1341 southern Congo Craton, Africa. *Journal of the Geological Society London*, 170, 353–363.  
28  
29
- 1342 McFarlane, M.J., Eckardt, F.D., 2007. Palaeodune morphology associated with the Gumare fault of the  
1343 Okavango graben in the Botswana/Namibia borderland: a new model of tectonic influence. *South African*  
1344 *Journal of Geology*, 110(4), 535-542.  
30  
31
- 1345 McFarlane, M.J., Long, C.W., 2015. Pan floor ‘barchan’ mounds, Ntwetwe Pan, Makgadikgadi, Botswana:  
1346 Their origin and palaeoclimatic implications. *Quaternary International*, 372, 108-119.  
32  
33
- 1347 McFarlane, M.J., Segadika, P., 2001. Archaeological evidence for the reassessment of the ages of the  
1348 Makgadikgadi paleolakes. *Botswana Notes & Records*, 33(1), 83-89.  
34  
35  
36  
37  
38  
39  
40  
41  
42  
43  
44  
45  
46  
47  
48  
49  
50  
51  
52  
53  
54  
55  
56  
57  
58  
59  
60  
61  
62  
63  
64  
65

- 1349 McFarlane, M.J., Eckardt, F.D., Ringrose, S., Coetzee, S.H., Kuhn, J.R., 2005. Degradation of linear dunes  
1350 in Northwest Ngamiland, Botswana and the implications for luminescence dating of periods of aridity.  
1351 Quaternary International, 135(1), 83-90.
- 1352 McFarlane, M.J., Eckardt, F.D., Coetzee, S.H., Ringrose, S., 2010. An African surface weathering profile in  
1353 the Kalahari of North West Ngamiland, Botswana: processes and products. *Zeitschrift für*  
1354 *Geomorphologie*, 54(3), 273-303.
- 1355 McKay, M.P., Coble, M.A., Hessler, A.M., Weislogel, A.L., Fildani, A., 2016. Petrogenesis and provenance  
1356 of distal volcanic tuffs from the Permian–Triassic Karoo Basin, South Africa: A window into a dissected  
1357 magmatic province. *Geosphere*, 12(1), 1-14.
- 1358 Miller, R.M. 2008, *The geology of Namibia*. Ministry of Mines and Energy, Windhoek (3 vol.).
- 1359 Miller, R.M., 2014. Evidence for the evolution of the Kalahari dunes from the Auob River, southeastern  
1360 Namibia. *Transactions of the Royal Society of South Africa*, 69(3), 195-204.
- 1361 Miller, R.M., Pickford, M., Senut, B., 2010. The geology, palaeontology and evolution of the Etosha Pan,  
1362 Namibia: Implications for terminal Kalahari deposition. *South African Journal of Geology*, 113(3), 307-  
1363 334.
- 1364 Modisi, M.P., Atekwana, E.A., Kampunzu, A.B., Ngwisanyi, T.H., 2000. Rift kinematics during the  
1365 incipient stages of continental extension: Evidence from the nascent Okavango rift basin, northwest  
1366 Botswana. *Geology*, 28(10), 939-942.
- 1367 Moore, A.E., Dingle, R.V., 1998. Evidence for fluvial sediment transport of Kalahari sands in central  
1368 Botswana. *South African Journal of Geology*, 101(2), 143-153.
- 1369 Moore, A.E., Larkin, P.A., 2001. Drainage evolution in south-central Africa since the breakup of Gondwana.  
1370 *South African Journal of Geology*, 104, 47-68.
- 1371 Moore, A.E., Cotterill, F., Main, M.P.L., Williams, H.B., 2007. The Zambesi River. In: Gupta, A. (Ed.),  
1372 *Large Rivers: Geomorphology and Management*. Chichester, Wiley, pp. 311-332.
- 1373 Moore, A.E., Blenkinsop, T., Cotterill, F., 2008. Controls on post-Gondwana alkaline volcanism in Southern  
1374 Africa. *Earth and Planetary Science Letters*, 268(1-2), 151-164.
- 1375 Moore, A.E., Cotterill, F.P.D., Eckardt, F.D., 2012. The evolution and ages of Makgadikgadi palaeo-lakes:  
1376 consilient evidence from Kalahari drainage evolution south-central Africa. *South African Journal of*  
1377 *Geology*, 115(3), 385-413.
- 1378 Moucha, R., Forte, A.M. 2011. Changes in African topography driven by mantle convection. *Nature*  
1379 *Geosciences*, 4, 707-712.
- 1380 Nash, D.J., 2015. Of dunes, depressions and dry valleys: the arid landscapes of the Kalahari desert. In: Grab,  
1381 S., Knight, J. (Eds.), *Landscapes and Landforms of South Africa*. Springer, Berlin, pp.129-137.
- 1382 Nash, D.J., Endfield, G.H., 2002. Historical flows in the dry valleys of the Kalahari identified from  
1383 missionary correspondence. *South African Journal of Science*, 98, 244–248.
- 1384 Nash, D.J., Shaw, P.A., 1998. Silica and carbonate relationships in silcrete-calcrete intergrade duricrusts from  
1385 the Kalahari desert of Botswana and Namibia. *Journal of African Earth Sciences*, 27, 11–25.
- 1386 Nash, D.J., McLaren, S.J., 2003. Kalahari valley calcretes: their nature, origins, and environmental  
1387 significance. *Quaternary International*, 111(1), 3-22.

- 1388 Nash, D.J., McLaren, S.J., Webb, J.A., 2004. Petrology, geochemistry and environmental significance of  
1389 silcrete- calcrete intergrade duricrusts at Kang Pan and Tswaane, central Kalahari, Botswana. *Earth*  
1390 *Surface Processes and Landforms*, 29(12), 1559-1586.
- 1391 Nesbitt, H.W., Young, G.M., 1982. Early Proterozoic climates and plate motions inferred from major  
1392 element chemistry of lutites. *Nature*, 299, 715-717.
- 1393 Nicholson, S.E., 1996. A review of climate dynamics and climate variability in eastern Africa. In: Johnson,  
1394 T.C., Odada, E.O. (Eds.), *The Limnology, Climatology and Palaeoclimatology of the East African Lakes*.  
1395 Gordon and Breach, Amsterdam, pp. 25–56.
- 1396 Nikulin, G., Hewitson, B., 2019. A simple set of indices describing the Tropical Rain Belt over central and  
1397 southern Africa. *Atmospheric Science Letters*, 20(12), e946.
- 1398 O'Connor, P.W., Thomas, D.S.G., 1999. The timing and environmental significance of Late Quaternary  
1399 linear dune development in western Zambia. *Quaternary Research*, 52, 44-55.
- 1400 Parker, A. 1970. An index of weathering for silicate rocks. *Geological Magazine*, 107, 501-504.
- 1401 Partridge, T.C., 1993. The evidence for Cainozoic aridification in southern Africa. *Quaternary International*,  
1402 17, 105-110.
- 1403 Pastore, G., Baird, T., Vermeesch, P., Resentini, A., Garzanti, E., 2021. Provenance and recycling of Sahara  
1404 Desert sand. *Earth-Science Reviews*, 216, 103606.
- 1405 Pickering, R., Hanock, P. J., Lee-Thopr, J.A., Grün, R., Mortimer, G.E., McCulloch, M., Berger, L.R., 2007.  
1406 Stratigraphy, U-Th chronology, and paleoenvironments at Gladysvale Cave: insights into the climatic  
1407 control of South African hominin-bearing cave deposits. *Journal of Human Evolution*, 53, 602-619.
- 1408 Poldervaart, A., 1957. Kalahari sands. In: Clark, J.D. (Ed.), *The 3<sup>rd</sup> Pan-African Congress on Prehistory*,  
1409 Livingstone 1955. Chatto & Windus, London, pp. 106–119.
- 1410 Reason, C.J.C., 2001. Evidence for the influence of the Agulhas current on regional atmospheric circulation  
1411 patterns. *Journal of Climate*, 14, 2769–2778.
- 1412 Resentini, A., Andò, S., Garzanti, E., 2018. Quantifying roundness of detrital minerals by image analysis:  
1413 Sediment transport, shape effects, and provenance implications. *Journal of Sedimentary Research*, 88(2),  
1414 276-289.
- 1415 Ringrose, S., Kampunzu, A.B., Vink, B.W., Matheson, W., Downey, W.S., 2002. Origin and  
1416 palaeo- environments of calcareous sediments in the Moshaweng dry valley, southeast Botswana. *Earth*  
1417 *Surface Processes and Landforms*, 27(6), 591-611.
- 1418 Ringrose, S., Harris, C., Huntsman-Mapila, P., Vink, B.W., Diskins, S., Vanderpost, C., Matheson, W., 2009.  
1419 Origins of strandline duricrusts around the Makgadikgadi Pans (Botswana Kalahari) as deduced from  
1420 their chemical and isotope composition. *Sedimentary Geology*, 219(1-4), 262-279.
- 1421 Rittner, M., Vermeesch, P., Carter, A., Bird, A., Stevens, T., Garzanti, E., Andò, S., Vezzoli, G., Dutt, R.,  
1422 Xu, Z., Lu, H., 2016. The provenance of Taklamakan desert sand. *Earth and Planetary Science Letters*,  
1423 437, 127-137.
- 1424 Rogers, J., Bremner, J.M., 1991. The Benguela Ecosystem. Part VII. Marine-geological aspects. In: Barnes,  
1425 M. (Ed.), *Oceanography and marine biology, an annual review*, vol. 29. Aberdeen University Press, pp.  
1426 1–86.

- 1427 Romans, B.W., Castelltort, S., Covault, J.A., Fildani, A., Walsh, J.P., 2016. Environmental signal  
1428 propagation in sedimentary systems across timescales. *Earth-Science Reviews*, 153, 7-29.  
2
- 1429 Schlegel, G.C.J., von Harmse, H.J.M., Brunke, O., 1989. Granulometric and mineralogical characteristics of  
1430 the Kalahari sands of southern Africa. *South African Journal of Geology*, 92(3), 207-222.  
4  
5
- 1431 Schlüter, T. 2008. *Geological Atlas of Africa*. Springer, Heidelberg, 307 p.  
7
- 1432 Schüller, I., Blez, L., Wilkes, H., Wehrmann, A., 2018. Late Quaternary shift in southern African rainfall  
1433 zones: sedimentary and geochemical data from Kalahari pans. *Zeitschrift für Geomorphologie*, 61(4),  
1434 339-362.  
8  
9  
10
- 1435 Schulze, B. (1972). South Africa. In: Griffiths, J.W. (Ed.), *Climates of Africa*. Elsevier, Amsterdam, World  
1436 Survey of Climatology, vol. 10, pp. 501–586.  
15
- 1437 Shaw, P.A., de Vries, J.J., 1988. Duricrust, groundwater and valley development in the Kalahari of south-  
1438 east Botswana. *Journal of Arid Environments*, 14, 245-254.  
17  
18
- 1439 Shaw, A.I., Goudie, A.S., 2002. Geomorphological evidence for the extension of the Mega-Kalahari into  
1440 south-central Angola. *South African Geographical Journal*, 84, 182-194.  
19  
20  
21
- 1441 Shaw, P.A., Nash, D.J., 1998. Dual mechanisms for the formation of fluvial silcretes in the distal reaches of  
1442 the Okavango Delta Fan, Botswana. *Earth Surface Processes and Landforms*, 23(8), 705-714.  
22  
23  
24
- 1443 Shaw, P., Thomas, D.S.G. 1992. Geomorphology, sedimentation and tectonics in the Kalahari Rift. *Israel  
1444 Journal of Earth Sciences*, 41, 87–94.  
27  
28
- 1445 Shaw, P.A., Thomas, D.S.G., 1988. Lake Caprivi: a late Quaternary link between the Zambezi and middle  
1446 Kalahari drainage systems. *Zeitschrift für Geomorphologie*, 32(3), 329-337.  
29  
30  
31
- 1447 Shaw, P.A., Thomas, D.S., Nash, D.J., 1992. Late Quaternary fluvial activity in the dry valleys (mekgacha)  
1448 of the Middle and Southern Kalahari, southern Africa. *Journal of Quaternary Science*, 7(4), 273-281.  
32  
33  
34
- 1449 Sláma, J., Košler, J., Condon, D.J., Crowley, J.L., Gerdes, A., Hanchar, J.M., Horstwood, M.S., Morris,  
1450 G.A., Nasdala, L., Norberg, N., Schaltegger, U., 2008. Plešovice zircon—a new natural reference material  
1451 for U–Pb and Hf isotopic microanalysis. *Chemical Geology*, 249, 1-35.  
37  
38  
39
- 1452 Stokes, S., Haynes, G., Thomas, D.S.G., Horrocks, J.L., Higginson, M., Malifa, M., 1998. Punctuated aridity  
1453 in southern Africa during the last glacial cycle: the chronology of linear dune construction in the  
1454 northeastern Kalahari. *Palaeogeography Palaeoclimatology Palaeoecology*, 137, 305-322.  
40  
41  
42  
43  
44
- 1455 Stone, A., 2021a. Landscape evolution of the Stampriet Transboundary Basin and relation to the  
1456 groundwater system: the land of duricrusts, pans, dry valleys and dunes, and the relation to the  
1457 groundwater system. In Eckardt, F. (Ed.) *Landscapes and Landforms of Botswana*. Springer, Berlin, Part  
1458 of the World Geomorphological Landscapes series, Springer Nature Switzerland, pp.9-10, ISBN/EAN  
1459 3030861015/9783030861018.  
46  
47  
48  
49
- 1460 Stone, A., 2021b. Dryland dunes and other dryland environmental archives as proxies for Late Quaternary  
1461 stratigraphy and environmental and climate change in southern Africa. *South African Journal of Geology*,  
1462 **in press**  
53  
54  
55
- 1463 Stone, A.E.C., Thomas, D.S.G., 2008. Linear dune accumulation chronologies from the southwest Kalahari,  
1464 Namibia: challenges of reconstructing late Quaternary palaeoenvironments from aeolian landforms.  
1465 *Quaternary Science Reviews*, 27(17-18), 1667-1681.  
56  
57  
60  
61  
62  
63  
64  
65

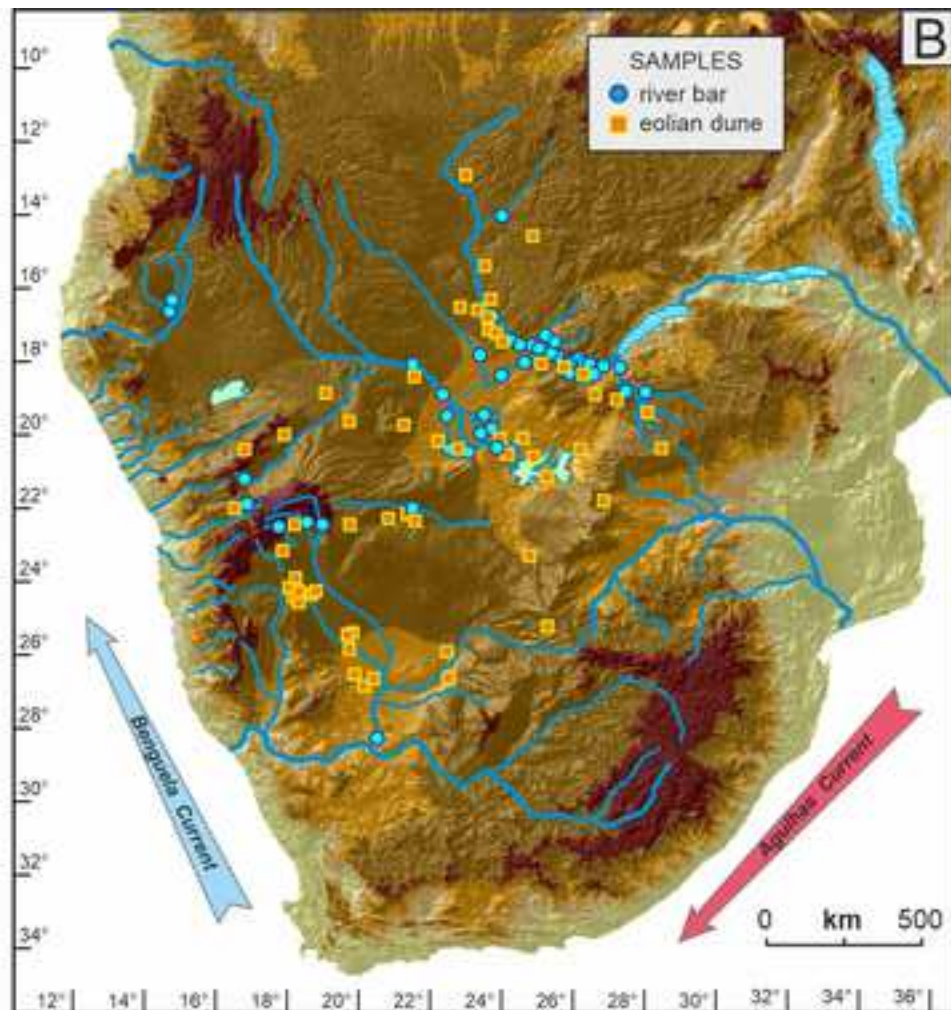
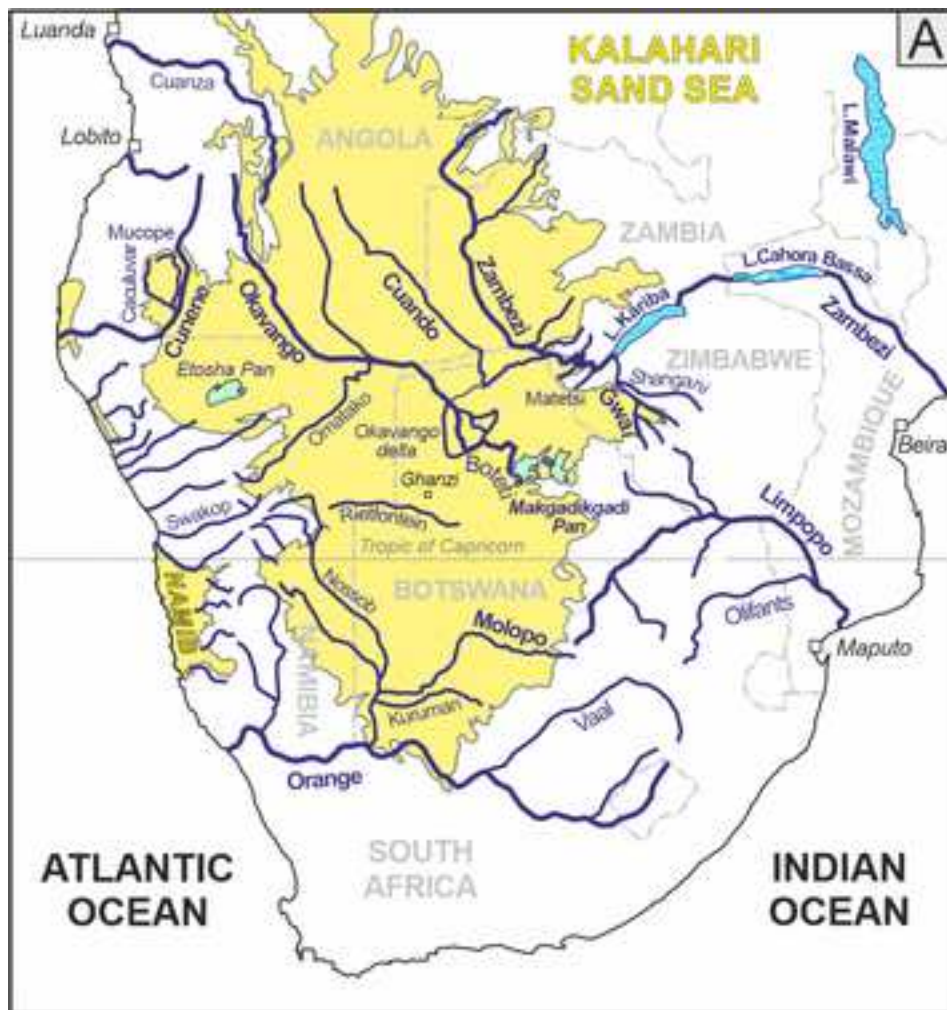


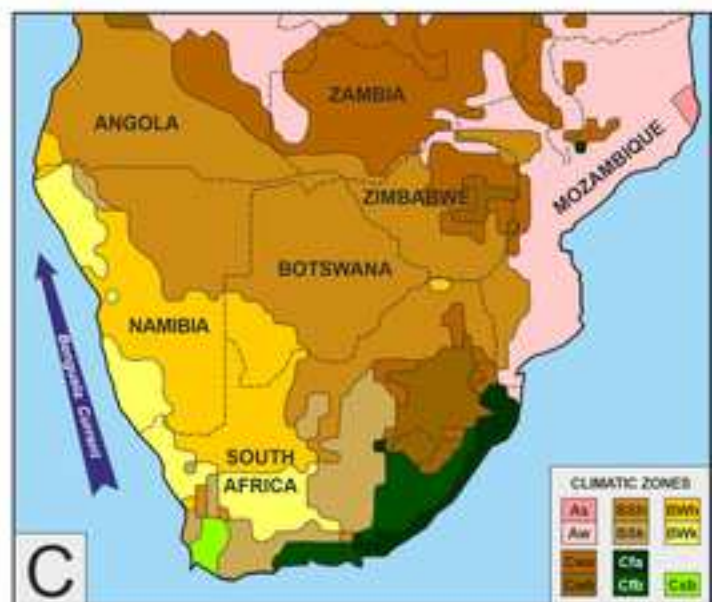
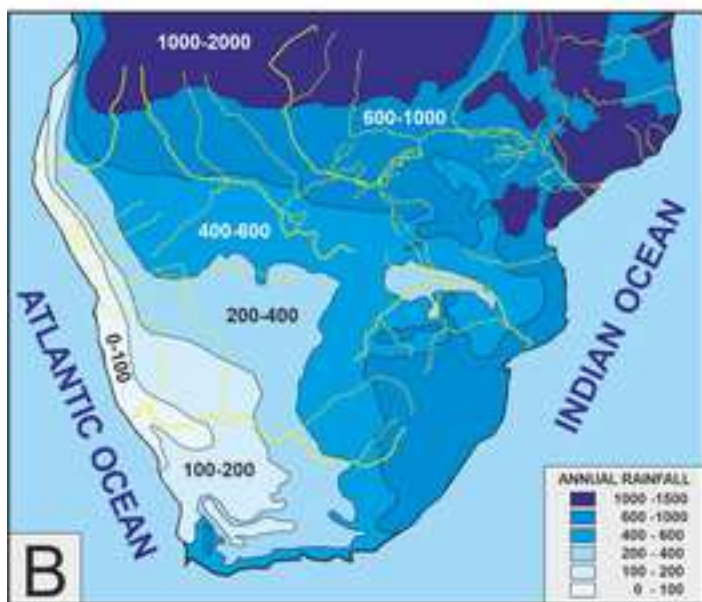
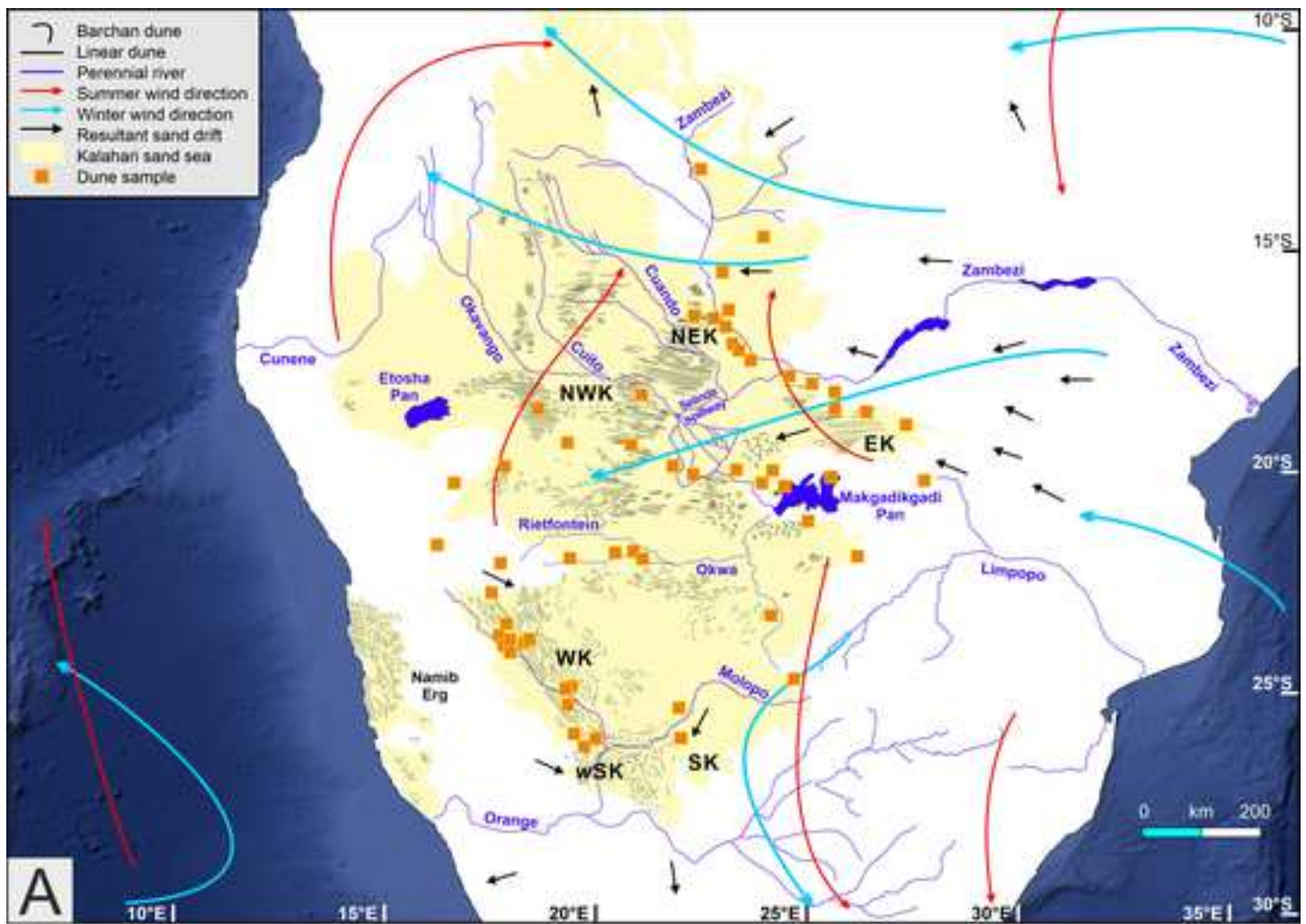
- 1466 Stone, A., Bateman, M.D., Burrough, S.L., Garzanti, E., Limonta, M., Radeff, G., Telfer, M.W., 2019. Using  
 1467 a portable luminescence reader for rapid age assessment of aeolian sediments for reconstructing dunefield  
 1468 landscape evolution in southern Africa. *Quaternary Geochronology*, 49, 57-64.  
 3
- 1469 Stute, M., Talma, A.S., 1998. Glacial temperatures and moisture transport regimes reconstructed from noble  
 1470 gases and  $\delta^{18}\text{O}$ , Stampriet aquifer, Namibia. *Isotope techniques in the study of environmental change.*  
 1471 *Proceedings of the International symposium on applications of isotope techniques in studying past and*  
 1472 *current environmental changes in the hydrosphere and the atmosphere, Vienna (Austria), 14/18 April*  
 1473 *1997, pp. 307-318.*  
 10
- 1474 Stuut, J.B., Smalley, I., O'Hara-Dhand, K., 2009. Aeolian dust in Europe: African sources and European  
 1475 deposits. *Quaternary International*, 198(1-2), 234-245.  
 13
- 1476 Summerfield, M.A., 1983. Silcrete as a palaeoclimatic indicator: evidence from southern Africa  
 1477 *Palaeogeography, Palaeoclimatology and Palaeoecology*, 41, 65-79.  
 17
- 1478 Svensen, H., Corfu, F., Polteau, S., Hammer, Ø., Planke, S., 2012. Rapid magma emplacement in the Karoo  
 1479 Large Igneous Province. *Earth Planetary Science Letters*, 325/326, 1-9.  
 20
- 1480 Taylor, S.R., McLennan, S.M., 1995. The geochemical evolution of the continental crust. *Reviews of*  
 1481 *Geophysics*, 33, 241-265.  
 23
- 1482 Telfer, M.W., Thomas, D.S.G., 2006. Complex Holocene lunette dune development, South Africa:  
 1483 Implications for palaeoclimate and models of pan development in arid regions. *Geology*, 34(10), 853-856.  
 27
- 1484 Telfer, M.W., Thomas, D.S.G., Parker, A.G., Walkington, H., Finch, A.A., 2009. Optically Stimulated  
 1485 Luminescence (OSL) dating and palaeoenvironmental studies of pan (playa) sediment from Witpan,  
 1486 South Africa. *Palaeogeography, Palaeoclimatology, Palaeoecology*, 273, 50-60.  
 31
- 1487 Thomas, D.S., 1984. Ancient ergs of the former arid zones of Zimbabwe, Zambia, and Angola. *Transactions*  
 1488 *of the Institute of British Geographers*, 9(1), 75-88.  
 34
- 1489 Thomas, D.S.G., 1987. Discrimination of depositional environments using sedimentary characteristics in the  
 1490 Mega Kalahari, central southern Africa. In: Frostick, L., Reid, I. (Eds.), *Desert Sediments: Ancient and*  
 1491 *Modern*. Geological Society, London, Special Publications 35, pp. 293-306.  
 39
- 1492 Thomas, D.S.G., Burrough, S.L., 2016. Luminescence-based chronologies in southern Africa: Analysis and  
 1493 interpretation of dune database records across the subcontinent. *Quaternary International*, 410(B), 30-45.  
 42
- 1494 Thomas, D.S.G., Shaw, P.A. 1988. Late Cainozoic drainage evolution in the Zambezi basin: evidence from  
 1495 the Kalahari rim. *Journal of African Earth Sciences*, 7, 611-618.  
 45
- 1496 Thomas, D.S.G., Shaw, P.A., 1990. The deposition and development of the Kalahari Group sediments,  
 1497 Central Southern Africa. *Journal of African Earth Sciences (and the Middle East)*, 10(1-2), 187-197.  
 49
- 1498 Thomas D.S.G., Shaw, P.A., 1991. *The Kalahari Environment*. Cambridge University Press, Cambridge, 287  
 1499 p.  
 52
- 1500 Thomas, D.S.G., Brook, G., Shaw, P., Bateman, M., Haberyan, K., Appleton, C., Nash, D., McLaren, S.,  
 1501 Davies, F., 2003. Late Pleistocene wetting and drying in the NW Kalahari: an integrated study from the  
 1502 Tsodilo Hills, Botswana. *Quaternary International*, 104, 53-67.  
 57
- 1503 Thomas, D.S., Knight, M., Wiggs, G.F., 2005. Remobilization of southern African desert dune systems by  
 1504 twenty-first century global warming. *Nature*, 435(7046), 1218-1221.  
 60  
 61  
 62  
 63  
 64  
 65

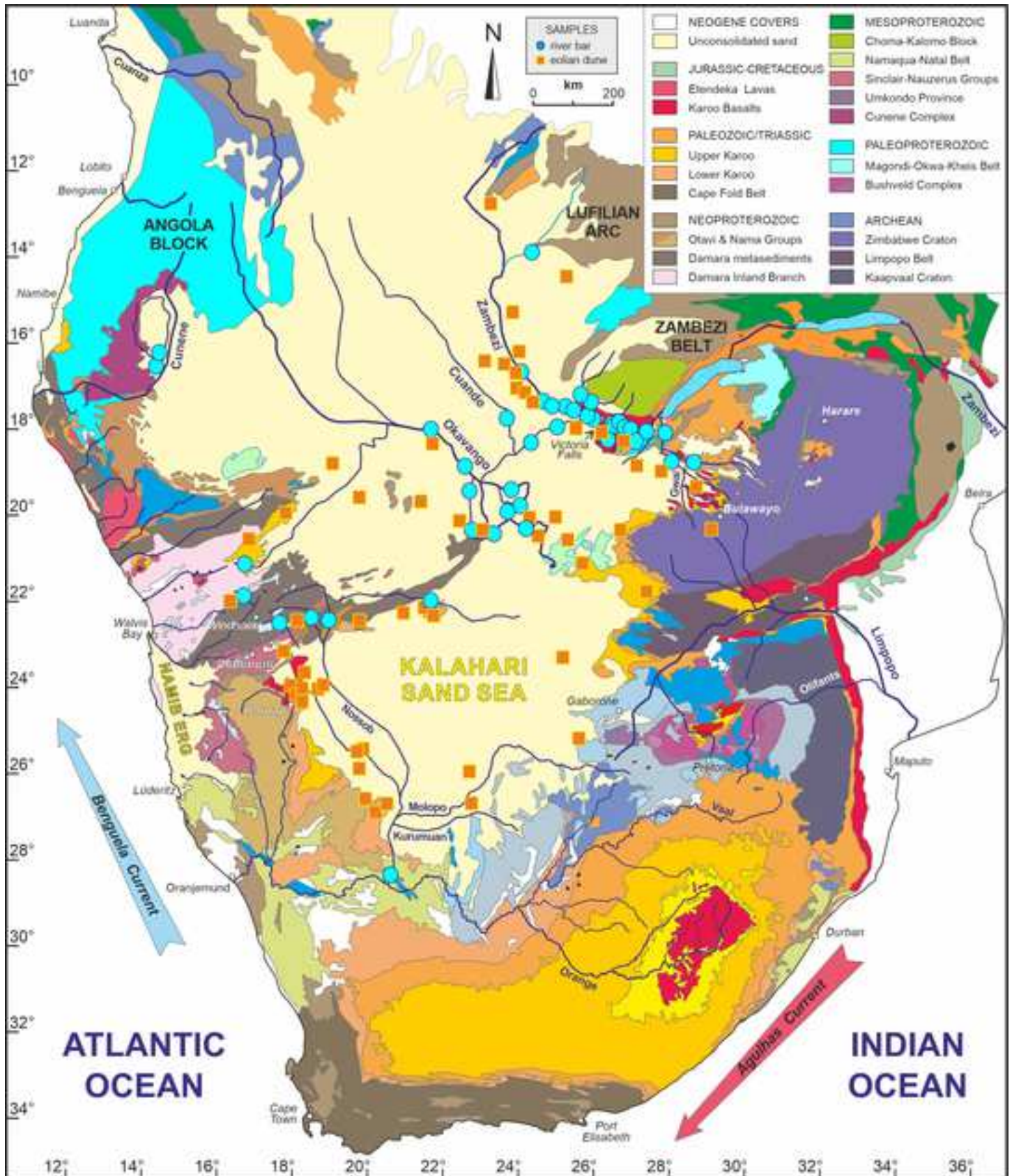
- 1505 Todd, M.C., Washington, R., Palmer, P.I., 2002. Water vapour transport associated with tropical-temperate  
1506 trough systems over southern Africa and the Southwest Indian Ocean. *Journal of Climate*, 24, 555–568.  
2
- 1507 Trumbull, R.B., Harris, C., Frindt, S., Wigand, M., 2004. Oxygen and neodymium isotope evidence for  
1508 source diversity in Cretaceous anorogenic granites from Namibia and implications for A-type granite  
1509 genesis. *Lithos*, 73, 21–40.  
7
- 1510 Tyson, S.J., 1999. Sand ramps or climbing dunes? Identification and palaeoenvironmental significance of  
1511 aeolian deposits in the southern Kalahari and Breede River Valley, South Africa. MSc Dissertation,  
1512 University of Cape Town, 136 p.  
11
- 1513 Tyson, P.D., Preston-Whyte, R.A., 2000. *The Weather and Climate of Southern Africa*, 2<sup>nd</sup> edition. Oxford  
1514 University Press, Cape Town, 396 p.  
13
- 1515 Vainer, S., Ben Dor, Y., 2021. The Cosmolian program for simulating aeolian dynamics and its application  
1516 to central Australia. *Earth Surface Processes and Landforms*, 46(9), 1631-1639.  
16
- 1517 Vainer, S., Ben Dor, Y., Matmon, A., 2018a. Coupling cosmogenic nuclides and luminescence dating into a  
1518 unified accumulation model of aeolian landforms age and dynamics: The case study of the Kalahari Erg.  
1519 *Quaternary Geochronology*, 48, 133-144.  
21
- 1520 Vainer, S., Erel, Y., Matmon, A., 2018b. Provenance and depositional environments of Quaternary sediments  
1521 in the southern Kalahari Basin. *Chemical Geology*, 476, 352-369.  
24
- 1522 Vainer, S., Matmon, A., Erel, Y., Hidy, A.J., Crouvi, O., De Wit, M., Geller, Y., and ASTER Team, 2021.  
1523 Landscape responses to intraplate deformation in the Kalahari constrained by sediment provenance and  
1524 chronology in the Okavango Basin. *Basin Research*, 33(2), 1170-1193.  
26
- 1525 Van Rensburg, H.J., 1971. Range ecology in Botswana. Vegetation studies in connection with vegetation/soil  
1526 correlation and bush encroachment investigations. FAO Technical Document, n<sup>o</sup> 2,  
1527 UNDP/SF/359/(BOT.1), Rome.  
32
- 1528 Van Veelen, M., Baker, T., Mulale, K., Bron, A., Fanta, A., Jonker, V., Mullins, W., Shoeman, H., 2009.  
1529 Feasibility Study of the Potential for Sustainable Water Resources Development in the Molopo-Nossob  
1530 Watercourse. ILISO Consulting LTD Project no 700192, 106 p.  
35
- 1531 Verboom, W.C., 1974. The Barotse loose sands of Western Province, Zambia. *Zambian Geographical  
1532 Magazine*, 27, 13-17.  
41
- 1533 Vermeesch, P., 2012. On the visualisation of detrital age distributions. *Chemical Geology*, 312, 190-194.  
43
- 1534 Vermeesch, P., 2013. Multi-sample comparison of detrital age distributions. *Chemical Geology*, 341, 140-  
1535 146.  
45
- 1536 Vermeesch, P., 2018. IsoplotR: A free and open toolbox for geochronology. *Geoscience Frontiers*, 9, 1479-  
1537 1493.  
48
- 1538 Vermeesch, P., 2021. On the treatment of discordant detrital zircon U–Pb data. *Geochronology Discussions*,  
1539 1-19.  
53
- 1540 Vermeesch, P., Resentini, A., Garzanti, E., 2016. An R package for statistical provenance analysis.  
1541 *Sedimentary Geology*, 336, 14-25.  
55
- 1542 Vermeesch, P., Rittner, M., Petrou, E., Omma, J., Mattinson, C., Garzanti, E., 2017. High throughput  
1543 petrochronology and sedimentary provenance analysis by automated phase mapping and LAICPMS.  
1544 *Geochemistry, Geophysics, Geosystems*, 18, doi:10.1002/2017GC007109.  
62

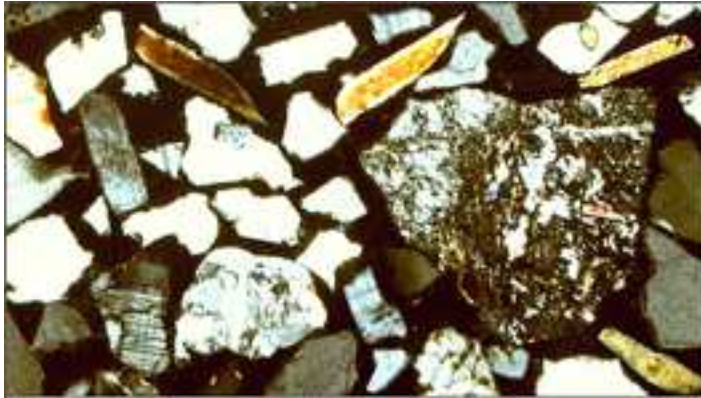
- 1545 Vigaud, N., Richard, Y., Rouault, M., Fauchereau, N., 2009. Moisture transport between the South Atlantic  
 1546 Ocean and southern Africa: relationships with summer rainfall and associated dynamics. *Climate*  
 1547 *Dynamics*, 32, 113-123.
- 1548 Walker, N., 1990. Links between South African summer rainfall and temperature variability of the Agulhas  
 1549 and Benguela current systems. *Journal of Geophysical Research*, 95, 3297–3319.
- 1550 Washington, R., Preston, A., 2006. Extreme wet years over southern Africa: role of Indian Ocean sea surface  
 1551 temperatures. *Journal of Geophysical Research*, 111, doi:10.1029/2005JD006724
- 1552 Watts, N.L., 1980. Quaternary pedogenic calcretes from the Kalahari (southern Africa): mineralogy, genesis  
 1553 and diagenesis. *Sedimentology*, 27(6), 661-686.
- 1554 White, K., Bullard, J., Livingstone, I., Moran, L., 2015. A morphometric comparison of the Namib and  
 1555 southwest Kalahari dunefields using ASTER GDEM data. *Aeolian Reserch*, 19, part A, 87-95.
- 1556 Wiggs, G.F.S., Livingstone, I., Thomas, D.S.G., Bullard, J.E., 1995. Dune mobility and vegetation cover in  
 1557 the southwest Kalahari Desert. *Earth Surface Processes Landforms*, 20, 515-529.
- 1558 Wiggs, G.F., Livingstone, I., Thomas, D.S., Bullard, J.E., 1996. Airflow and roughness characteristics over  
 1559 partially vegetated linear dunes in the southwest Kalahari Desert. *Earth Surface Processes and Landforms*,  
 1560 21(1), 19-34.
- 1561 Wittmann, H., Oelze, M., Gaillardet, J., Garzanti, E., von Blanckenburg, F., 2020. A global rate of  
 1562 denudation from cosmogenic nuclides in the Earth's largest rivers. *Earth-Science Reviews*, 204, 103147.
- 1563 Zeh, A., Gerdes, A., Klemd, R., Barton, J.M. 2007. Archaean to Proterozoic crustal evolution in the Central  
 1564 Zone of the Limpopo Belt (South Africa-Botswana): constraints from combined U-Pb and Lu-Hf Isotope  
 1565 analyses of zircon. *Journal of Petrology*, 48, 1605-1639.

1566  
 34  
 35  
 36  
 37  
 38  
 39  
 40  
 41  
 42  
 43  
 44  
 45  
 46  
 47  
 48  
 49  
 50  
 51  
 52  
 53  
 54  
 55  
 56  
 57  
 58  
 59  
 60  
 61  
 62  
 63  
 64  
 65

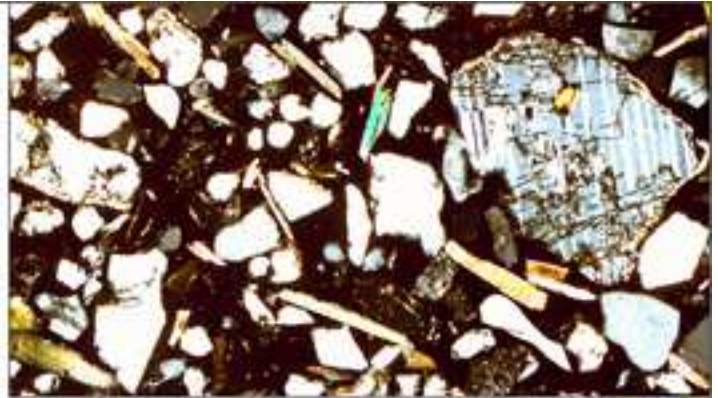




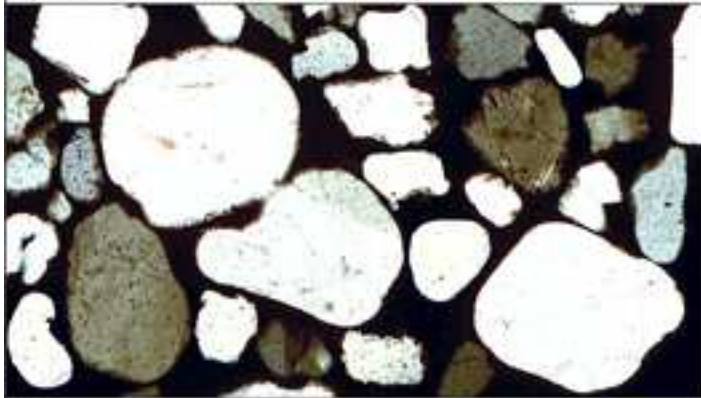




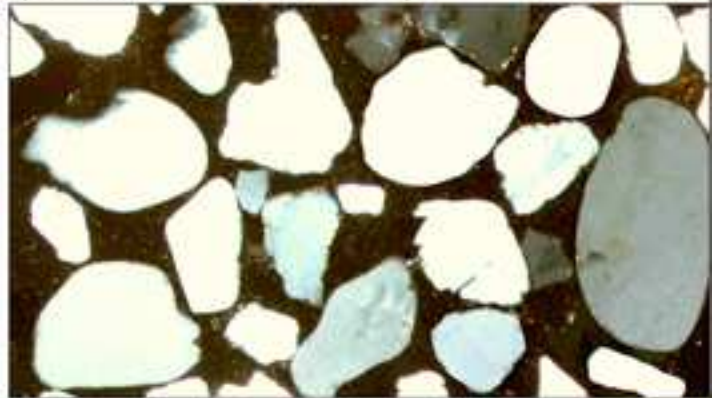
A) OKAKONGO RIVER (central Namibia)



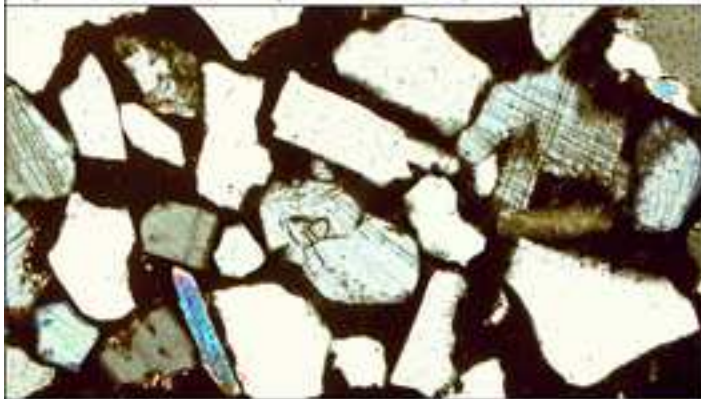
B) OKAHANDJA DUNE (central Namibia)



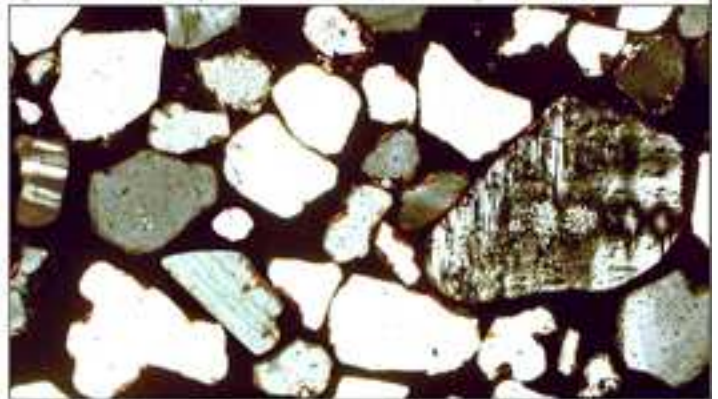
C) RIETFONTEIN RIVER (western Botswana)



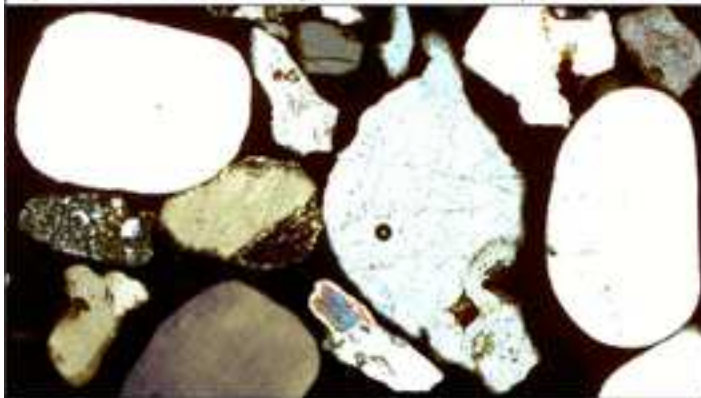
D) GHANZI DUNE (western Kalahari, Botswana)



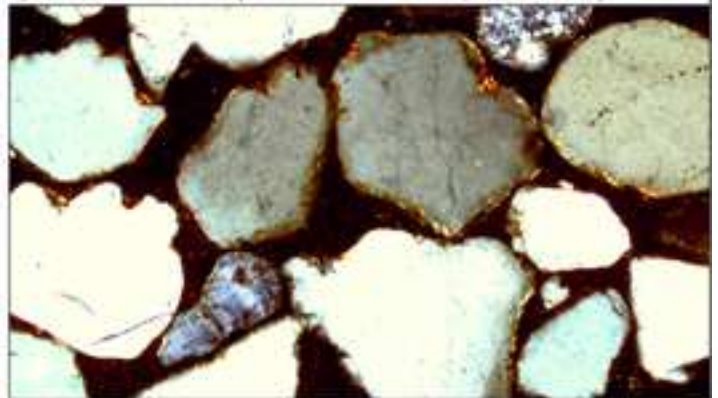
E) WHITE NOSSOB RIVER (southeastern Namibia)



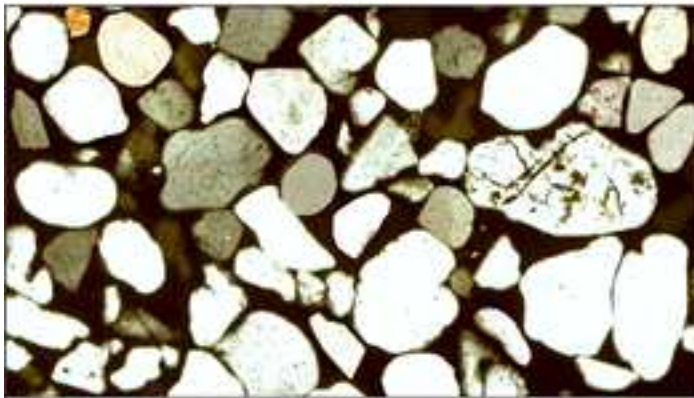
F) BAGATELLE DUNE (southwestern Kalahari, SW Namibia)



G) MOLOPO RIVER (southern Botswana)



H) BELLA VISTA DUNE (southern Kalahari, South Africa)



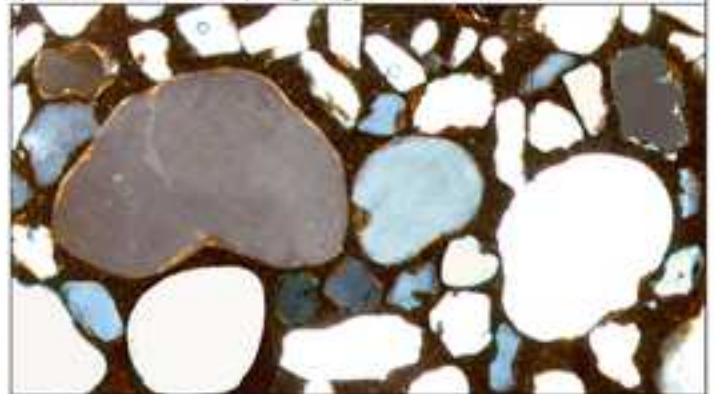
I) OKAVANGO RIVER (Caprivi Strip)



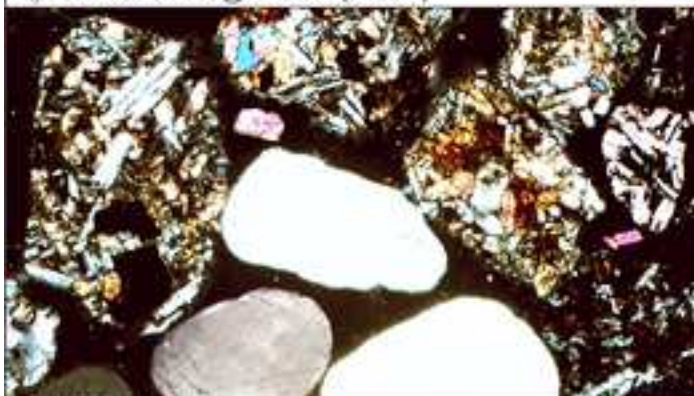
J) NTWETWE MOUND (Makgadikgadi Pan, Botswana)



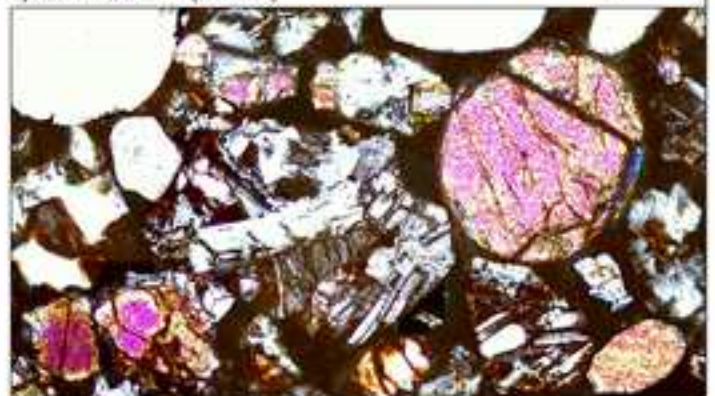
K) ZAMBEZI RIVER @ Sesheke (Zambia)



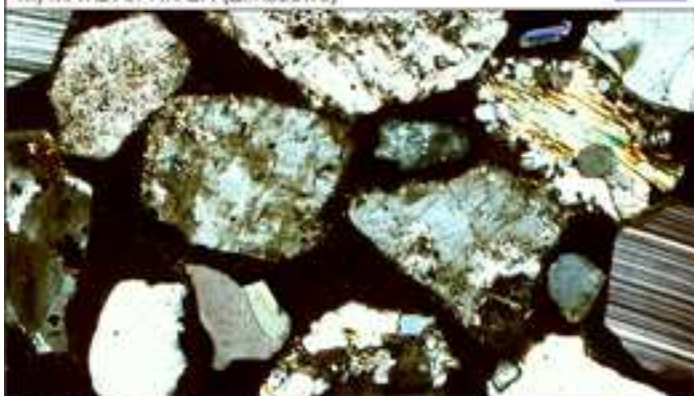
L) NZIMBA DUNE (Zambia)



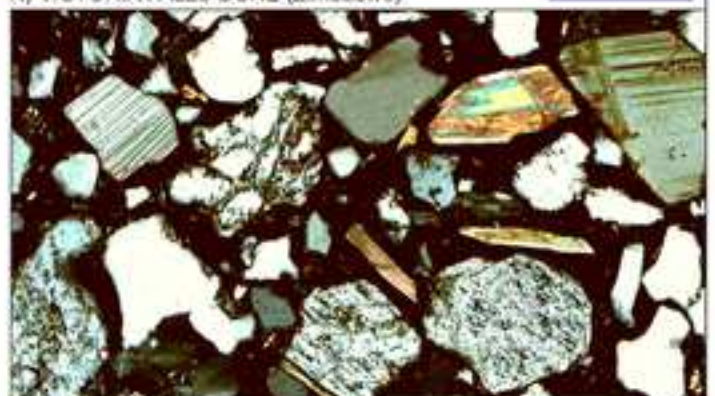
M) MATETSI RIVER (Zimbabwe)



N) VICTORIA FALLS DUNE (Zimbabwe)



O) GWAI RIVER (Zimbabwe)



P) MASUMA DUNE (Zimbabwe)



Figure 5

[Click here to access/download;Figure;Figure 5 Kalahari QFL ZTR SKA AGE.jpg](#)

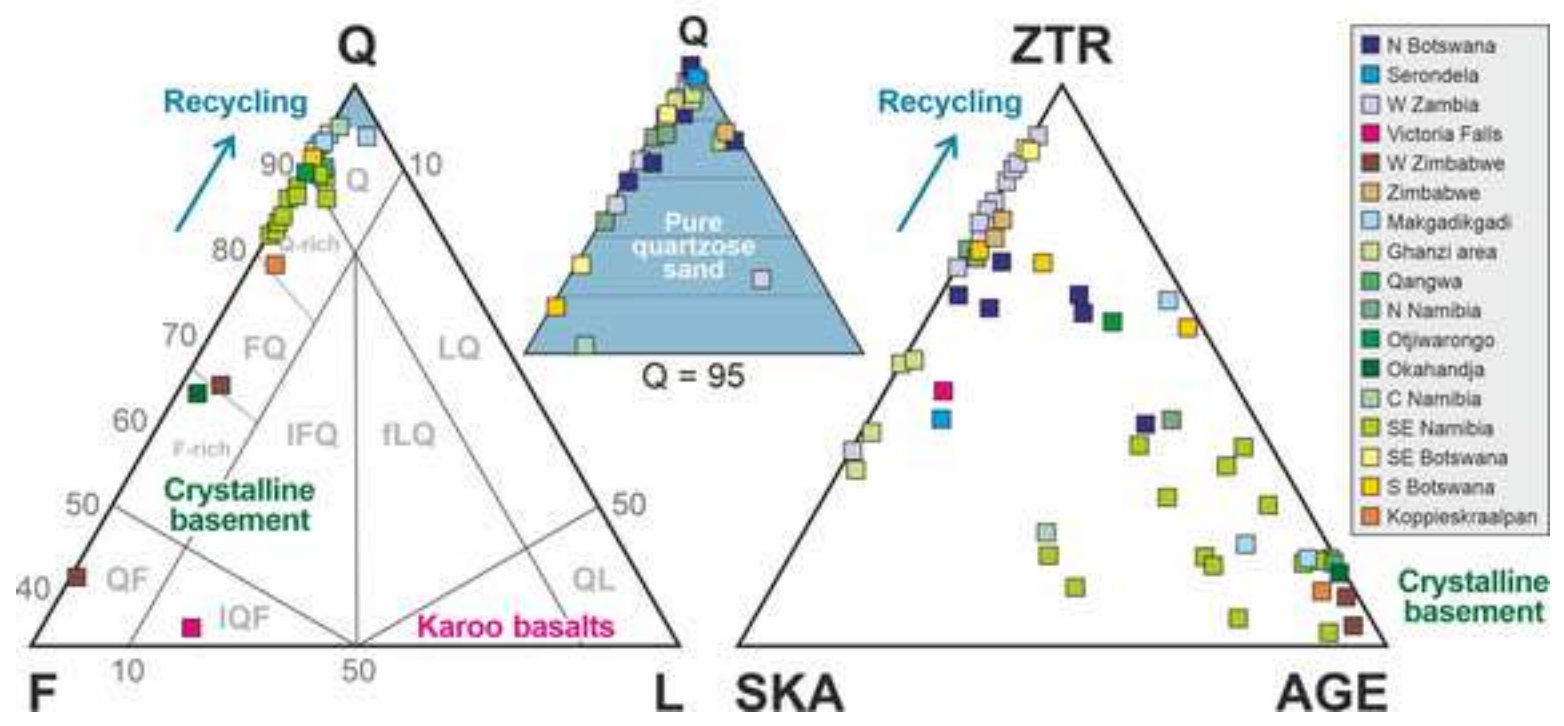
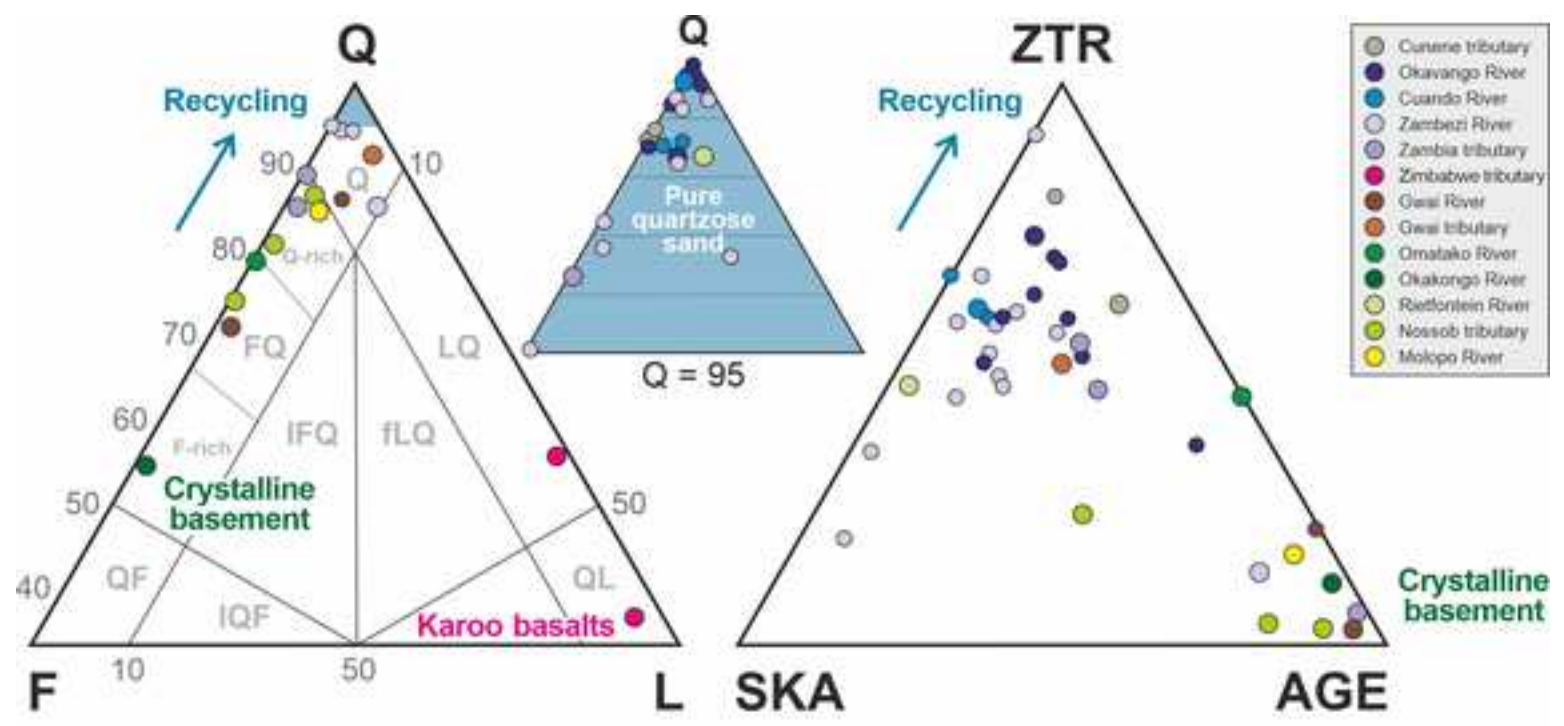
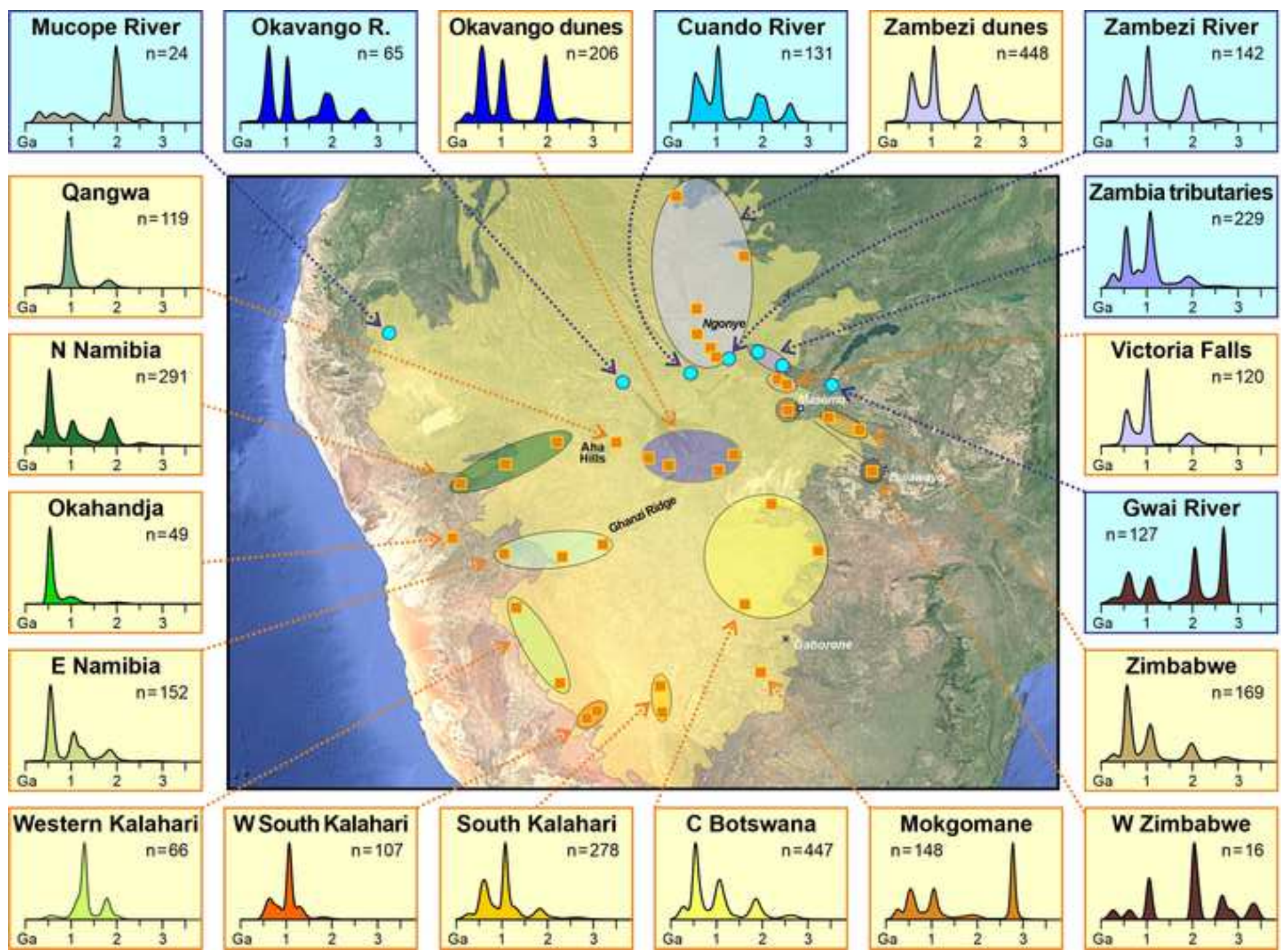


Figure 6



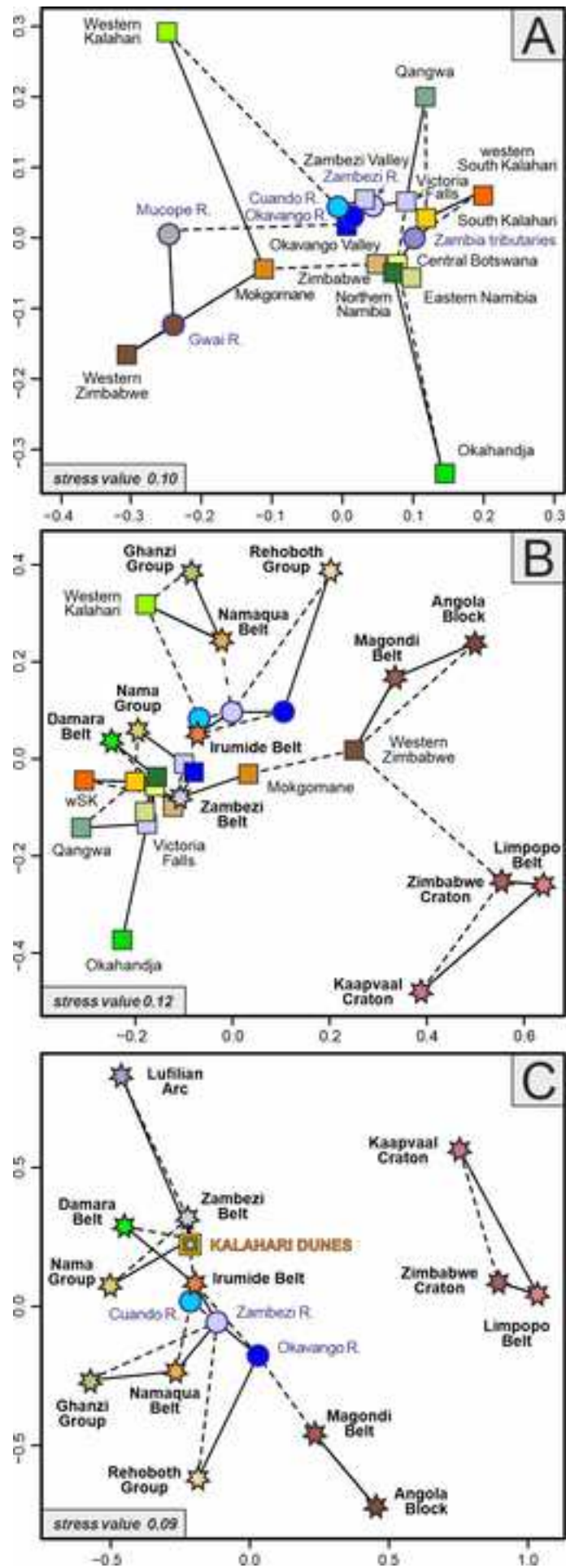


Figure 8

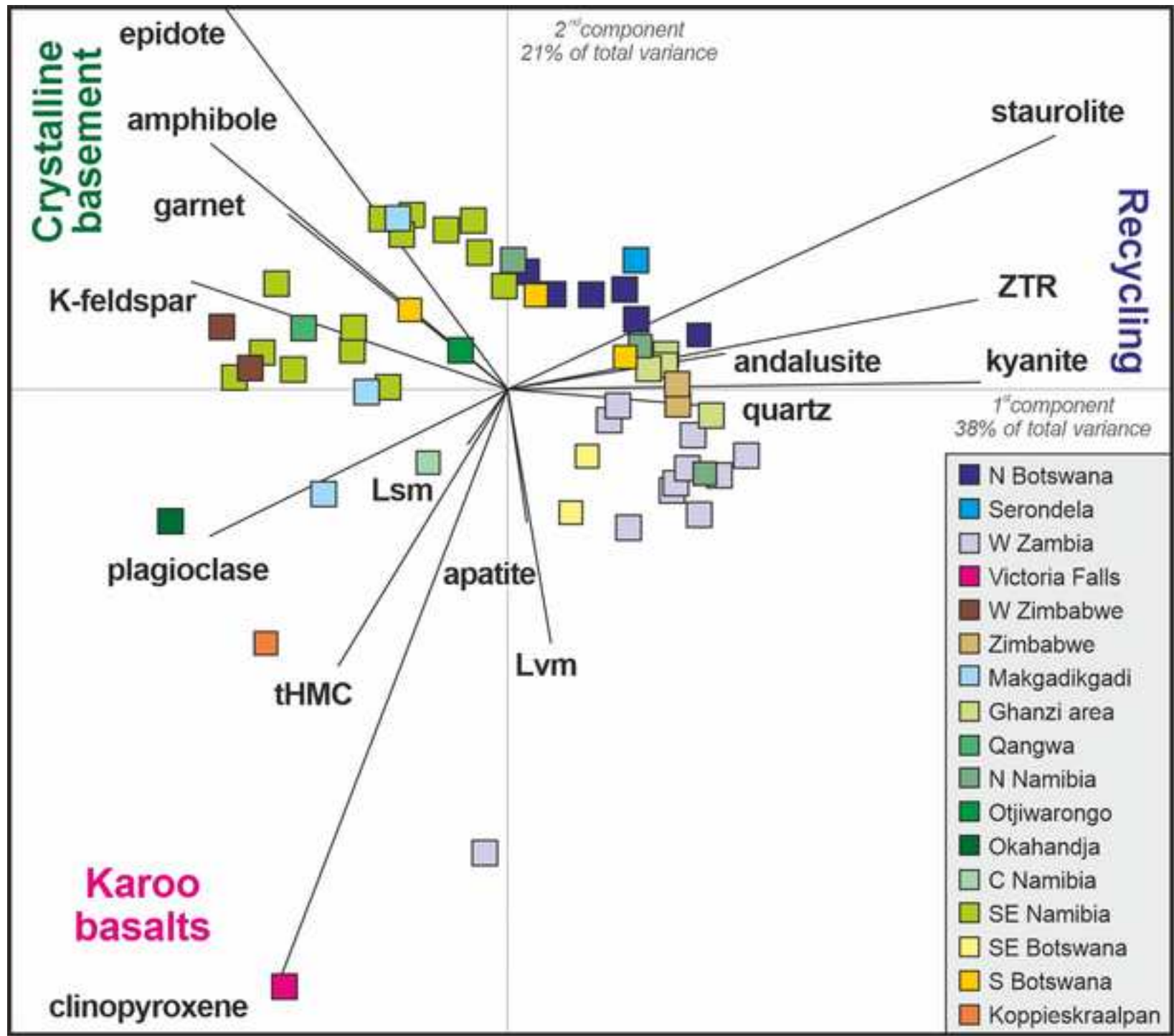


Figure 9

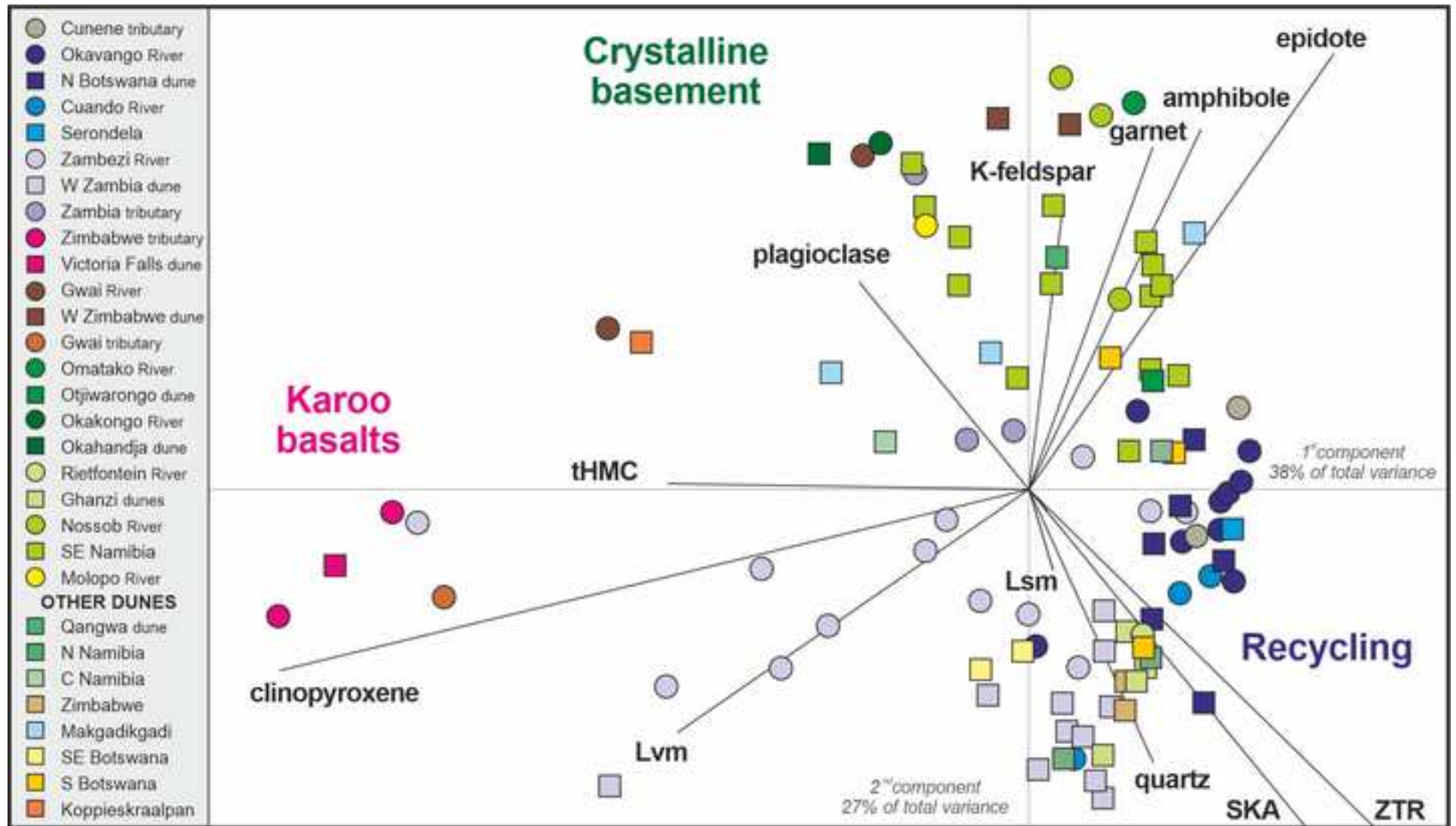
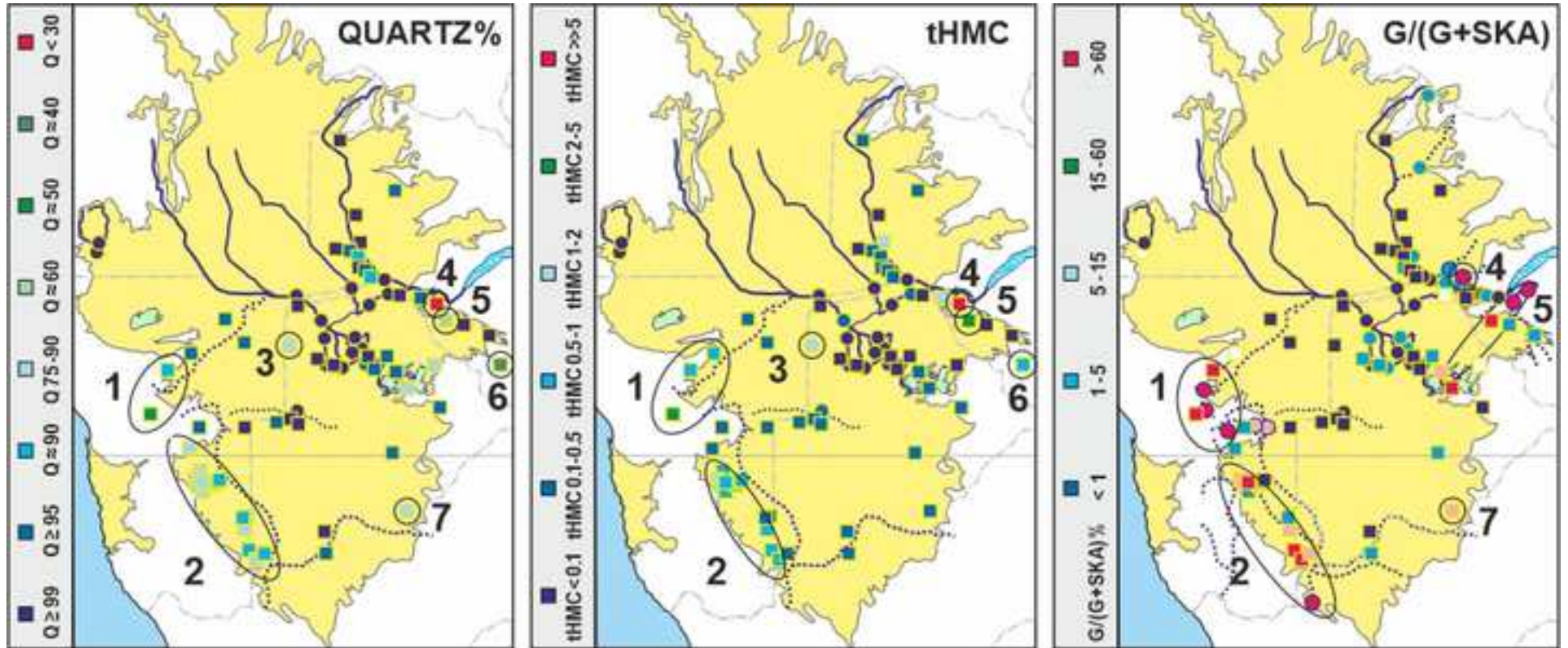


Figure 10

[Click here to access/download;Figure;Figure 10 Kalahari Mineralogical Maps.jpg](#)



	n°	Q	F	Lvm	Lsm	P/F%	MI*	tHMC	ZTR	Ap	Ep	Gr	St	Ky	Amp	Px	&tHM		
<b>RIVERS</b>																			
Cunene tributaries	2	99	1	0	0	100.0	13	n.d.	0.04	69	2	16	1	4	2	1	0	6	100.0
Okavango	9	99	0.5	0.1	0	100.0	n.d.	n.d.	0.06	57	0.4	15	0.3	14	6	5	0.2	2	100.0
Cuando	3	99	0.6	0.1	0	100.0	n.d.	n.d.	0.08	61	0.3	3	0	16	16	2	0	1	100.0
Upper Zambezi	7	97	3	0	0.1	100.0	32	n.d.	0.2	58	0.1	6	0.4	7	21	2	4	2	100.0
Zambezi	1	85	5	9	0.3	100.0	50	n.d.	2.7	0	0.6	0	0	0	0	0.6	96	3	100.0
Matetsi	1	37	3	60	0.3	100.0	100	n.d.	33.3	0	0	0	0	0	0	0	100	0	100.0
Shangani	1	91	2	6	0	100.0	86	n.d.	4.7	1	0	0	0	0.5	0	0.5	98	0	100.0
Gwai	1	71	27	1	0.7	100.0	54	414	0.5	2	2	17	17	0	3	48	8	3	100.0
Omatoko	1	79	21	0	0.3	100.0	21	n.d.	0.1	44	0	9	22	0	0	26	0	0	100.0
Okakongo	1	55	44	0	1	100.0	53	419	3.0	10	5	4	13	0.5	0	61	4	2	100.0
Rietfontein	1	98	0.7	0	1	100.0	n.d.	n.d.	0.2	46	0	1	0	43	8	3	0	0	100.0
Nossob	3	81	18	0	1	100.0	56	333	2.8	10	2	21	19	14	5	28	0	0.7	100.0
Molopo	1	85	11	0.3	4	100.0	69	200	0.9	14	2	28	14	4	2	28	8	0	100.0
<b>DUNES</b>																			
N Botswana	6	99	1	0.1	0.2	100.0	29	n.d.	0.1	58	1	16	0.3	16	7	1	0	1	100.0
Serondela	1	100	0	0	0.3	100.0	n.d.	n.d.	0.1	40	0	5	4	11	35	1	0	2.4	100.0
W Zambia	11	98	2	0.3	0	100.0	22	n.d.	0.4	72	0.3	0.1	0.1	10	10	0	7	0.2	100.0
Victoria Falls	1	35	49	15	0.4	100.0	99	n.d.	24.3	0.5	1	0	0	0	0.5	0	98	0	100.0
Masuma	1	64	32	0	4	100.0	71	296	3.0	3	5	24	64	0.5	2	1	0	0	100.0
Bulawayo	1	41	58	0	0.6	100.0	37	400	0.6	9	1	37	0	0	2	51	0	0.4	100.0
Zimbabwe	2	99	0	0.7	0	100.0	n.d.	n.d.	0.1	74	0.3	1	0.6	17	6	1	0	0.2	100.0
Makgadikgadi	3	93	6	0.6	0.2	100.0	25	143	0.2	28	0.6	40	2	2	4	8	13	2.1	100.0
Ghanzi area	4	99	0.4	0.1	0.3	100.0	n.d.	n.d.	0.2	43	0.2	1	0	48	7	0.5	0	0.3	100.0
N Namibia	3	98	2	0.1	0	100.0	0	n.d.	0.3	60	0	16	0.5	17	6	0	0	0.3	100.0
Qangwa	1	90	10	0	0	100.0	60	n.d.	1.6	15	3	78	0	1	0	2	0	0.5	100.0
Otiwarongo	1	90	8	0	2	100.0	6	n.d.	0.7	55	1	3	24	1	11	1	0	3.9	100.0
Okahandja	1	63	34	0	2	100.0	60	367	3.0	11	9	7	2	0.5	0	60	10	0.5	100.0
C Namibia	1	95	4	1	0	100.0	21	n.d.	1.0	16	0.5	24	1	14	20	5	20	0	100.0
SE Namibia	14	86	13	0.4	0.5	100.0	10	250	0.7	18	0.3	54	4	12	3	5	2	0.6	100.0
SE Botswana	2	98	2	0	0	100.0	17	n.d.	0.1	87	0.2	0.7	0.2	9	1	0	1	0.2	100.0
Mokgomane	1	91	9	0	0	100.0	31	n.d.	0.3	57	0	40	1	0.5	1	0	0	0.5	100.0
S Botswana	2	97	3	0	0	100.0	43	n.d.	0.1	69	0.5	7	0.5	19	3	0.2	0	0.5	100.0
Koppieskraalpan	1	79	19	1	1	100.0	62	125	3.4	4	0	6	27	1	1	0	61	0.5	100.0

	<b>peak 1</b>	<i>frequency</i>	<b>peak 2</b>	<i>frequency</i>	<b>peak 3</b>	<i>frequency</i>	<b>peak 4</b>	<i>frequency</i>	<b>peak 5</b>	<i>frequency</i>
MODERN SANDS										
<b>Cunene River</b>	<b>1394 ± 5</b>	28.6%	<b>1746 ± 4</b>	31.9%	<b>1948 ± 4</b>	36.7%	<b>2456 ± 10</b>	2.8%		
<b>Okavango River</b>	<b>96 ± 1</b>	2.1%	<b>545 ± 2</b>	23.8%	<b>1040 ± 4</b>	13.3%	<b>1971 ± 2</b>	49.6%	<b>2607 ± 5</b>	11.2%
<b>Cuando River</b>	<b>29 ± 2</b>	0.8%	<b>590 ± 2</b>	23.7%	<b>1024 ± 3</b>	30.9%	<b>1902 ± 3</b>	38.8%	<b>2648 ± 6</b>	5.8%
<b>Zambezi River</b>	<b>646 ± 5</b>	19.2%	<b>1023 ± 6</b>	27.4%	<b>1193 ± 5</b>	45.2%	<b>2570 ± 8</b>	8.2%		
ANCIENT SANDSTONES										
<b>Nama Group</b>	<b>616 ± 1</b>	20.8%	<b>1010 ± 1</b>	26.0%	<b>1181 ± 1</b>	38.3%	<b>1891 ± 2</b>	14.9%		
<b>Ghanzi Group</b>	<b>1118 ± 1</b>	50.3%	<b>1259 ± 1</b>	32.4%	<b>1881 ± 1</b>	17.3%				
<b>Rehoboth Group</b> (Langberg and Billstein Fms.)	<b>1221 ± 2</b>	22.5%	<b>1858 ± 2</b>	61.0%	<b>2023 ± 3</b>	16.5%				
CRUSTAL DOMAINS										
<b>Damara Belt</b> (+ Cretaceous granite)	<b>131 ± 1</b>	3.2%	<b>523 ± 1</b>	33.6%	<b>794 ± 1</b>	16.6%	<b>1464 ± 1</b>	35.8%	<b>2096 ± 2</b>	10.8%
<b>Lufilian Arc</b>	<b>555 ± 1</b>	41.6%	<b>826 ± 1</b>	43.1%	<b>1125 ± 6</b>	15.3%				
<b>Zambesi Belt</b>	<b>485 ± 2</b>	16.8%	<b>827 ± 5</b>	26.1%	<b>1104 ± 1</b>	34.1%	<b>1794 ± 16</b>	15.4%	<b>2860 ± 4</b>	8.0%
<b>Irumide Belt</b> (+ Pan-African rejuvenation)	<b>597 ± 1</b>	20.4%	<b>1065 ± 1</b>	28.7%	<b>1140 ± 1</b>	5.6%	<b>1958 ± 1</b>	27.7%	<b>2354 ± 2</b>	17.5%
<b>Namaqua Belt</b>	<b>1119 ± 1</b>	47.8%	<b>1662 ± 1</b>	30.3%	<b>2003 ± 7</b>	11.9%	<b>23608 ± 1</b>	9.9%		
<b>Magondi Belt</b> (+ Pan-African rejuvenation)	<b>569 ± 7</b>	7.1%	<b>2080 ± 93</b>	92.9%						
<b>Angola Block</b>	<b>1935 ± 1</b>	100.0%								
<b>Limpopo Belt</b> (+ PPz tectono-thermal event)	<b>1953 ± 1</b>	54.0%	<b>2594 ± 1</b>	29.1%	<b>3284 ± 2</b>	16.9%				
<b>Zimbabwe Craton</b> (+ PPz tectono-thermal event)	<b>1881 ± 1</b>	11.7%	<b>2411 ± 1</b>	44.8%	<b>2580 ± 1</b>	43.6%				
<b>Kaapvaal Craton</b> (+ Vredefort magmatic rocks)	<b>977 ± 4</b>	8.8%	<b>2845 ± 1</b>	7.3%	<b>3467 ± 2</b>	83.9%				



**Declaration of interests**

The authors declare that they have no known competing financial interests or personal relationships that could have appeared to influence the work reported in this paper.

The authors declare the following financial interests/personal relationships which may be considered as potential competing interests: